Spaceborne monitoring of Arctic lake ice in a changing climate

by

Cristina M. Surdu

A thesis
presented to the University of Waterloo
in fulfillment of the
thesis requirement for the degree of
Doctor of Philosophy
in
Geography

Waterloo, Ontario, Canada, 2015

AUTHOR'S DECLARATION

I hereby declare that I am the sole author of this thesis. This is a true copy of the thesis, including any required final revisions, as accepted by my examiners.

I understand that my thesis may be made electronically available to the public.

Cristina M. Surdu

January, 2015

Abstract

Lake ice phenology (timing of ice-on and ice-off) and thickness are changing in response to generally warmer climate conditions at high northern latitudes observed during recent decades. Monitoring changes in the lake ice cover provides valuable evidence in assessing climate variability in the Arctic. To enhance our understanding of the role of lake ice in the Arctic cryosphere and to evaluate the extent to which Arctic lakes have been impacted by the contemporary changing climate, development of a lake ice monitoring system at pan-Arctic scale is needed. While large lakes across the Arctic are currently being monitored through satellite observations, there are extremely sparse and mostly non-existent records tracking the changes in small high-latitude lakes.

Employing a combination of spaceborne observations from synthetic aperture radar (SAR) and optical sensors, and simulations from the Canadian Lake Ice Model (CLIMo), this researched aimed to investigate changes in winter ice growth and ice phenology of lakes across the Arctic, focus being given to smaller lakes on the North Slope of Alaska (NSA) and lakes of various sizes in the Canadian Arctic Archipelago (CAA).

To determine the changes in the fraction of lakes that freeze to bed (grounded ice) in late winter on the NSA from 1991 to 2011, a time series of ERS-1/2 was analysed. Results show a trend toward increasing floating ice fractions from 1991 to 2011, with the greatest change occurring in April, when the grounded ice fraction declined by 22% ($\alpha = 0.01$). This finding is in good agreement with the decrease in ice thickness simulated with CLIMo, a lower fraction of lakes frozen to the bed corresponding to a thinner ice cover. Model simulations over the same period as SAR acquisitions (1991-2011) indicate a trend toward thinner ice covers by 18-22 cm (no-snow and 53% snow depth scenarios, $\alpha = 0.01$). The results emphasize the regime shifts that these lakes are currently undergoing, including shorter ice seasons. The longer-term trends (1950-2011) derived from model simulations show a decrease in the ice cover duration by ~ 24 days consequent to later freeze-up dates by 5.9 days ($\alpha = 0.1$) and earlier break-up dates by 17.7-18.6 days ($\alpha = 0.001$).

The temporal evolution of backscatter (σ^0) from two C-band SAR sensors – Advanced Synthetic Aperture Radar (ASAR) Wide Swath and RADARSAT-2 ScanSAR Wide Swath – was then used to investigate the potential of high temporal-frequency SAR for determining lake ice phenological events (e.g. freeze onset, melt onset and water-clear-of-ice). Results show that combined SAR observations are generally suitable for detection of important lake ice events timing. However, the wide range of incidence angles and to a certain extent the orbit differences between the observations, the wind effect, particularly during fall freeze-up, the low differences in σ^0 during transition from a grounded-ice cover to melt onset of ice in early spring, complicate the detection of lake ice phenological events.

In order to order to document the response of ice cover of lakes in the Canadian High Arctic to climate conditions during recent years, a 15-year time series (1997-2011) of RADARSAT-1/2 ScanSAR Wide Swath, ASAR Wide Swath and Landsat acquisitions were analyzed. Results show that earlier melt onset occurred earlier for all 11 polar-desert and polar-oasis lakes that were investigated. With the exception of Lower Murray Lake, all lakes experienced earlier ice-minimum and water-clear-of-ice dates, with greater changes being observed for polar-oasis lakes (9-23.6 days earlier water-clear-of-ice for lakes located in polar oases and 1.6-20 days earlier water-clear-of-ice for polar-desert lakes). Additionally, results suggest that some lakes may be transitioning from a perennial to a seasonal ice regime, with only a few lakes maintaining a perennial ice cover on occasional years. Aside Lake Hazen and Murray Lakes that preserved their ice cover during the summer of 2009, no residual ice was observed on any of the other lakes from 2007 to 2011.

This research provides the foundation of a lake-ice monitoring network that can be built on with the newly launched and future SAR and multispectral missions. Additionally, this study shows that in response to warmer climate conditions, Arctic lakes are experiencing regime shifts with overall shorter ice seasons, thinner ice covers, fewer lakes that freeze to the bottom and more lakes that lose the perennial ice cover and experience a seasonal ice regime.

Acknowledgements

My sincerest appreciation and gratitude goes out to my supervisor, Claude Duguay, for his continuous and unlimited support, mentorship, guidance, encouragement, patience, and likely most important, his inspiration and enthusiasm, which undoubtedly motivated me through the more challenging parts during these years. Claude, it was amazing being part of 'The Duguay research Group'! I am also incredibly grateful to Claude for giving me the opportunity to study and visit the Arctic – an amazing, mind-blowing place in so many ways – a gift I will forever treasure and hold as an extremely dear memory.

I would like to extend my appreciation to Dr. Richard Kelly (GEM, University of Waterloo), Dr. Stephen Howell (Environment Canada), and Dr. Roland Hall (Department of Biology, University of Waterloo) for their continuous support and advice, and for serving as my committee members on this thesis.

The European Space Agency (the STSE North Hydrology project) and the University of Waterloo are also gratefully acknowledged for their financial support. This work was also supported by a Discovery Grant from the Natural Sciences and Engineering Research Council of Canada (NSERC) to Claude Duguay.

I would like to sincerely thank all of my family and close friends for their genuine interest in my research and for their support during these four years. This thesis is as much yours as it is mine. I am extremely grateful to my husband, Stefan, for being by my side throughout this seemingly endless period. He tremendously supported me, encouraged me and showed his support in my ability to accomplish my PhD during this four-year long journey. Thank you also to my father who helped with many of the daily routines and made sure that my son was properly cared for when I worked extended hours. I also want to thank my son, Noah, for keeping me grounded and reminding me daily of what truly matters.

I am also grateful to my extended academic family and fellow members of 'Team Duguay' that collectively guided and supported me through these years, in particular Laura Brown, Kevin Kang, Homa Keyrolalh Pour, and Grant Gunn. I would also like to express my

gratitude and appreciation to the staff and many faculty members in the Department of Geography and Environmental Management at University of Waterloo who provided administrative and technical support during this process. A special ‘thank you’ to Mike Lackner and Scott McFarlane (MAD helpdesk) for always promptly helping with technical and software issues.

Lastly, I would like to also thank David Clausi (University of Waterloo) and Fan Li (University of Waterloo) for providing access and helping with the MAGIC software.

Dedication

I would like to dedicate this manuscript to my amazing, loving and happy son, Noah. Your loud giggles, large smiles, and tight hugs have motivated me to keep going. Without you in my life, this achievement would not have had the same savour. You are my rock.

Table of Contents

List of Figures

List of Tables

List of Abbreviations

ACP	Arctic Coastal Plain
AMAP	Arctic Monitoring and Assessment Programme
AO	Arctic Oscillation
ASAR	Advanced Synthetic Aperture Radar
ASF	Alaska Satellite Facility
AVHRR	Advanced Very High Resolution Radiometer
BU	Break-up
CAA	Canadian Arctic Archipelago
CIS	Canadian Ice Service
CLIMo	Canadian Lake Ice Model
CRCM	Canadian Regional Climate Model
CSA	Canadian Space Agency
CTDD	Cumulative thawing degree days
DOY	Day of the year
ECMWF	European Centre for Medium-range Weather Forecast
ENSO	El Niño/Southern Oscillation
ERS-1/2	European Remote-Sensing Satellite 2
ESA	The European Space Agency
FLake	Freshwater lake model
FO	Freeze onset
FU	Freeze-up
GCOS	Global Climate Observing System
GPOD	Grid processing on demand
HIRLAM	High Resolution Limited Area Model
ICD	Ice cover duration
IPCC	Intergovernmental Panel on Climate Change
IRGS	Iterative Region Growing with Semantics

LIST	Lake Ice Surface Temperature
LSWT	Lake Surface Water Temperature
MAGIC	Map-Guided Ice Classification System
MO	Melt onset
MODIS	Moderate Resolution Imaging Spectrometer
NAO	North Atlantic Oscillation
NCDC	National Climatic Data Centre
NDVI	Normalized Difference Vegetation Index
NEST	Next ESA SAR toolbox
NOAA	National Oceanic and Atmospheric Administration
NP	North Pacific index
NSA	North Slope of Alaska
NWP	Numerical Weather Prediction
PDO	Pacific Decadal Oscillation
PNA	Pacific North American
ROI	Region of interest
SAR	Synthetic Aperture Radar
SSM/I	The Special Sensor Microwave Imager
SWE	Snow water equivalent
SWOT	Surface Water Ocean Topography
TAC	Total accumulated ice coverage
WCI	Water clear of ice

Preface

In addition to introductory chapters, this thesis contains three articles that are collaborative efforts, which have been published or submitted for publication. The first paper on "Response of ice cover on shallow lakes of the North Slope of Alaska to contemporary climate conditions (1950–2011): radar remote-sensing and numerical modeling data analysis" was published in *The Cryosphere* and is presented as chapter three of this thesis. The second paper, entitled "Ice freeze-up and break-up detection of shallow lakes in Northern Alaska with spaceborne SAR", was submitted to *Remote Sensing* and is presented as chapter four of this thesis. The third manuscript, entitled "Evidence of recent changes in the ice regime of High Arctic lakes from spaceborne satellite observations", was submitted to *Limnology and Oceanography* and is presented as chapter five of this thesis.

Materials constituting each of the included manuscripts were created in their original format by the author of this thesis in the capacity of the primary investigator. The final format of each paper is a result of collaboration with all listed co-authors. All work presented in this thesis is the result of a close collaboration with Professor Claude Duguay who aided greatly with the initial proposal of each article and provided continuous support, advice and valuable comments through the duration of the research. Assistance with the MAGIC software used in processing the ERS-1/2 data in chapter three was provided by Fan Li (University of Waterloo). CLIMo data and outputs used in chapters three and four, and prompt assistance with model results were provided by Dr. Laura Brown (University of Toronto). Radiometric calibration, geocoding and speckle filtering of ASAR images used in chapters four and five was performed by ESA's Grid Processing on Demand (GPOD) team, led by Roberto Cuccu and Giovanni Sabatini. The collaboration with Luis Veci (Array Systems) and Chris Stewart (ESA) was extremely helpful in processing of the raw RADARSAT-2 images used in the fourth chapter. Kevin Kang's (University of Waterloo) help with sorting the ~20,000 RADARSAT-1/2 acquisitions used in chapter five significantly reduced the pre-processing times. Image

segmentation of the numerous RADARSAT-2 scenes used in chapter five was performed with the valuable help of Andrew Wong (University of Waterloo).

Chapter 1

General Introduction

1.1 Motivation

Climate-driven changes have significantly altered the high-latitude environments during recent decades, changes that are predicted to continue or even accelerate in the near future as projected by global climate models (Prowse et al., 2009). In response to warmer climate conditions, the Arctic lake ice cover is expected to continue reducing in thickness, duration and extent. Thinning ice covers, shorter ice seasons and an increasing fraction of water under the ice (for shallow lakes that partially or completely freeze to bed in winter, particulalrly for lakes on the North Slope of Alaska) may affect a complex web of physical, chemical and ecological linkages, such as energy exchanges between the lakes and the atmosphere, shifts in lake algal productivity, habitat availability, thawing permafrost under lake beds, and methane releases to the atmosphere. Similarly, consequent to higher air temperatures, the lakes in the Canadian High Arctic are expected to transition from a perennial to a seasonal ice regime, with lakes being ice free during most summer seasons.

Past changes in lake ice cover have mostly been identified only through non-spatially representative point *in situ* measurements, which have been almost unavailable over the last two decades consequent to the declining global and Canadian terrestrial monitoring network for lakes and lake ice (Lenormand et al., 2002; Duguay et al., 2006; Prowse et al., 2011) (Figure 1.1). Recent studies have shown that satellite remote sensing provides a viable alternative to detecting and monitoring changes within the ice cover of high-latitude lakes (Latifovic and Pouliot, 2007; Arp et al., 2012; Duguay et al., 2012). Without the limitations of the optical sensors related to polar darkness and/or cloud coverage, spaceborne synthetic aperture radar (SAR) has been shown to be an efficient tool for detecting changes of the Arctic lake ice cover (Jeffries et al., 1994; Morris et al., 1995; Duguay et al., 2002; Jeffries et al., 2005; Cook and Bradley, 2010; Arp et al., 2012; Surdu et al., 2014).

While large lakes across the northern hemisphere, including the Arctic, are now being monitored through satellite observations (e.g., Duguay et al., 2014), no systematic approach or network exists for tracking changes in the ice cover of small (shallow) lakes that cover vast areas of the Arctic (e.g., coastal areas of Alaska, northern Canada and Siberia). Moreover, only a few past investigations monitored the changes in the ice cover of lakes in the Canadian High Arctic, lakes of different depths and many with unknown bathymetry.

Change detection in the ice cover of small Arctic lakes must consider spatial resolution as a key sensor characteristic. Additionally, a temporal resolution of the order of 1-2 days is needed for an accurate detection of important lake ice events for the purpose of climate monitoring (IGOS, 2007).

The paucity of *in situ* observations in the Arctic emphasizes the need to revitalize the monitoring network of Arctic lakes.

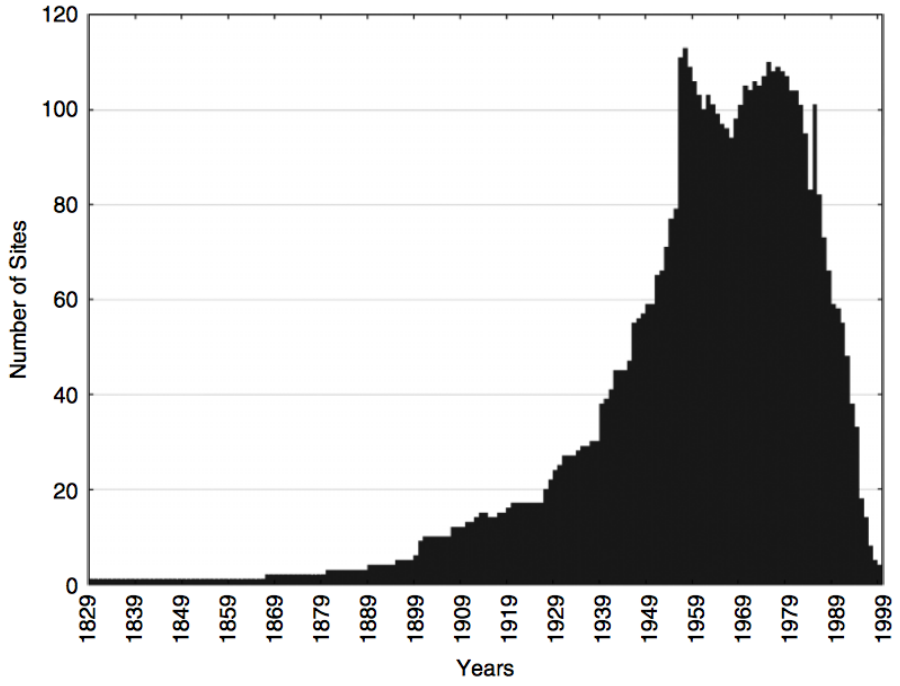

Figure 1.1: Lake ice observation sites from *in situ* observations from the Canadian Ice Database (1829-1999). From: Duguay et al. (2006).

Monitoring Arctic lakes and their ice covers is critical in improving our understanding of the complex interactions between lakes and the land-ocean-atmosphere system, and requires consistent, long-term observations of a large number of lakes.

1.2 Objectives

The overall goal of this research is to further our understanding of the response of Arctic lakes and their ice covers to recent high-latitude climate conditions and to provide the groundwork of a monitoring network for Arctic lake ice.

Specifically, the three primary objectives are: 1) to analyze the winter ice regimes, phenology and thickness of shallow lakes on the North Slope of Alaska; 2) to employ SAR observations in ice freeze-up and break-up detection of lakes on the North Slope; 3) to monitor and analyze changes in ice regimes of lakes in the Canadian High Arctic using a multi-sensor approach.

1.3 Thesis Structure

This manuscript-based thesis consists of six chapters in order to provide relevant background information and to address each of the identified study objectives. The preliminary chapter presents the rationale and objectives of the thesis, outlining the need for monitoring of Arctic lakes.

Chapter two provides a review of lake ice thermodynamics, available SAR sensors for lake ice monitoring, and introduces the thermodynamic lake ice model that was used as a complement to the spaceborne-observed lake ice conditions presented in chapters three and four.

Chapter three addresses the first objective of this thesis and examines the changes in the grounded ice cover of the Alaskan thermokarst lakes through historical (1991-2011) C-band SAR observations and compares them with model simulations.

> Surdu, C. M., Duguay, C. R., Brown, L. C., and Fernández Prieto, D. (2014). Response of ice cover on shallow lakes of the North Slope of Alaska to contemporary climate conditions (1950-2011): Radar remote sensing and numerical modeling data analysis. *The Cryosphere, 8*(1), 167-180.

Chapter four addresses the second objective of this thesis by examining the temporal evolution of C-band backscatter from two different SAR sensors in order to detect freeze onset, melt onset and ice-off dates for lakes on the North Slope of Alaska. This was submitted to *Remote Sensing*.

> Surdu, C. M., Duguay, C. R., Kheyrollah Pour, H., and Brown, L. C. (2014). Ice freeze-up and break-up detection of shallow lakes in Northern Alaska with spaceborne SAR.

Chapter five addresses the final objective of this thesis presenting observed changes in the timing of the melt onset, summer ice minimum and ice-off date for 11 lakes in the Canadian High Arctic between 1997-2011, using both spaceborne SAR and optical observations. This manuscript was submitted to *Limnology and Oceanography*.

> Surdu, C. M., Duguay, C. R., and Fernández Prieto, D. (2014). Evidence of recent changes in the ice regime of High Arctic lakes from spaceborne satellite observations.

The final chapter provides a summary of findings and limitations, and suggests future research directions.

Chapter 2

Research Context

2.1 Lakes and Lake Ice in a Changing Arctic

Lakes of different sizes comprise 2% of the Earth's land surface, the majority being located in the northern hemisphere. Depending on the location, vast surface areas of the Arctic and Subarctic regions are covered up to 15-40% by lakes (Duguay et al., 2003, Riordan et al., 2006). For instance, lakes cover up to 40% of the Alaskan Arctic Coastal Plain (Sellman et al., 1975). With such an extended areal coverage, lakes and their ice regimes represent an important component of the cryosphere.

While surface area of these lakes is known, bathymetry knowledge is extremely limited for most lakes and it only includes depth information for larger lakes and a few smaller lakes that have been previously investigated. Existing bathymetric measurements indicate that mean depth ranges from 1.4-2.2 m for the shallower lakes on the North Slope of Alaska to 3-10 m for lakes in the Canadian High Arctic. Lake Hazen, the largest lake north of 66°N reaches a maximum depth of 280 m. All lakes investigated in this study are located in continuous permafrost regions (Figure 2.1).

In areas where lakes cover an extended surface area such as the North Slope of Alaska, changes in the underlying permafrost have major implications for the physical and biogeochemical processes of lakes. In these areas, shallow thermokarst are also associated with methane release into the atmosphere consequent to permafrost thaw underneath the water or ice surface and lake expansion (Walter et al., 2006). The shift from a grounded-ice regime (ice frozen to lakebed) to a floating ice regimes observed during the last two decades (Surdu et al., 2014), has implications for ecology, winter water use and ice transportation.

In the Canadian High Arctic, small areas develop that are sheltered by mountains from the cold Arctic air currents. These areas, also known as polar oases, are controlled by a local

warmer microclimate, and have longer growing seasons and higher biodiversity. An hypothesis is that lakes located in polar oases have experienced greater changes than lakes located in polar desert environments. Moreover, consequent to recent warmer climate conditions at high latitudes, High Arctic lakes may be transitioning from a perennial ice cover to a seasonal ice regime.

Figure 2.1: Distribution of glaciers and permafrost zones in the Canadian Arctic and Alaska (USA). Modified from Brown and Duguay (2011b).

Lakes play a fundamental role within regional and local climate acting as regional climate controllers and influencing seasonal evaporation patterns (Rouse et al., 2008; Vincent et al., 2008). Lakes also provide habitat for various species of phytoplankton (Smol and Douglas, 2007), fish and wildlife. In addition, lakes supply fresh water in areas where availability is limited (Jeffries et al., 1994) and support winter transportation functions (Adams and Prowse, 1981; Leconte and Klassen, 1991; Prowse, 2009). As all components of the cryosphere are closely interrelated, sea ice loss contributes to warming of the adjacent land (and vice versa), thawing permafrost (Smith et al., 2005, 2010; Romanovsky et al., 2010; Rowland et al., 2010), increased photosynthetic production of tundra terrestrial vegetation and longer growing seasons indicated by high Normalized Difference Vegetation Index (NDVI) values (Reed et al., 2009; Bhatt et al., 2010), and shorter ice seasons in northern lakes (Magnuson et al., 2000; Bonsal et al., 2006; Duguay et al., 2006; Latifovic and Pouliot, 2007; Mishra et al., 2011).

Forthcoming decades are predicted to result in climatic shifts, mainly as a consequence of increased mean air temperatures (Morris et al., 2005), and lakes are expected to respond to these changes and undergo physical and ecological regime shifts. Rising air temperatures are hypothesized to result in a shift towards an open-water regime for 3.7% of Earth's lakes with areas over 0.1 km^2 (Weyhenmeyer et al., 2011). Ice-cover changes of Arctic lakes have comparable trends to those of lower latitude lakes but several Arctic regions display trends that are more evident. The timing of ice-on and ice-off date, mean ice duration, and ice thickness has a demonstrated considerable seasonal, interannual and interdecadal variability. However, significant trends for later freeze-up dates, earlier ice-off dates and an overall shorter ice seasons have occured during recent decades (Magnuson et al., 2000; Duguay et al., 2006; Latifovic and Pouliot, 2007; Benson et al., 2011).

2.1.1 Lake ice linkages to the atmosphere-ocean system

The impact of a changing climate is reflected both by ocean and inland waters (Petoukhov and Semenov, 2010). In a complex system such as the Arctic, anomalies in the coupled ocean-atmosphere circulation may result in extreme weather conditions, with warm events being more severe and frequent over the last 30 years (Benson et al., 2011; Guirguis et al., 2011) and further leading to extreme ice conditions (i.e. extremely late freeze-up, extremely early break-up or extremely short ice duration). The robustness of this relationship is also supported by the strong correlation between ice phenology trends and the autumn/spring 0°C isotherm dates (Bonsal and Prowse, 2003; Duguay et al., 2006). Albeit considerable interdecadal and interannual variability is noted, the lakes of the northern hemisphere have experienced changes in ice phenology (0.3-1.6 later for freeze-up, 0.5-1.9 earlier for break-up) and overall shorter ice seasons by 0.7-4.3 days, with a steeper trend during the last decades - 1975-2005 (Benson et al., 2011).

Previous ice phenology trend analyses established strong lake ice-air temperature interdependence whereby air temperatures (1-3 months) prior to lake ice events (Palecki and Barry, 1986; Robertson et al., 1992; Livingstone 1997, 1999; Duguay et al., 2006) is a useful indicator of freeze-up and break-up dates, often explaining 60-70 % of the variability in the ice timing (Livingstone, 1997). Whereas October and November climate drives lake ice onset of sub-Arctic lakes (e.g., Lake Kallavesi, Finland; Magnuson et al., 2000), April temperatures drive the break-up of Alaskan ponds (Jeffries and Morris, 2007).

However, Weyhenmeyer et al. (2004) advanced a non-linear relationship between ice-off dates and temperature. Warmer temperatures in the Arctic lower troposphere have often been associated with horizontal air advection from lower latitudes (Comiso et al., 2008) by sub-polar air masses. For instance, over recent decades, Alaska has experienced frequent and strong warm air advection from the North Pacific Ocean (Overland et al., 1997) highly noticeable in the western part (Trenberth, 1990). Likewise, central Arctic temperatures are mainly controlled by warm air advection and diabatic cooling (Serreze et al., 2011). These

highly synoptic/seasonal events partially explain air temperature anomalies (Turner et al., 2007) and consequent later freeze-up and break-up (Todd and Mackay, 2003). As surface air temperature rises, sea ice area reduces, a greater fraction of open ocean, with a much lower albedo is exposed to radiative warming, thus increasing the amount of sensible heat within the ocean (Serreze et al., 2009). As a result, insulating ice cover forms later in the season, and so exchanges of energy between the atmosphere and the ocean are extended past the summer season (Serreze et al., 2009). The stored heat is released back into the atmosphere during late fall and early winter and promotes strong warming of the adjacent land within ~50 km (e.g., increased photosynthetic activity of vegetation measured by the NDVI) but its effects extend far inland – Figure 2.2; Bhatt et al., 2010).

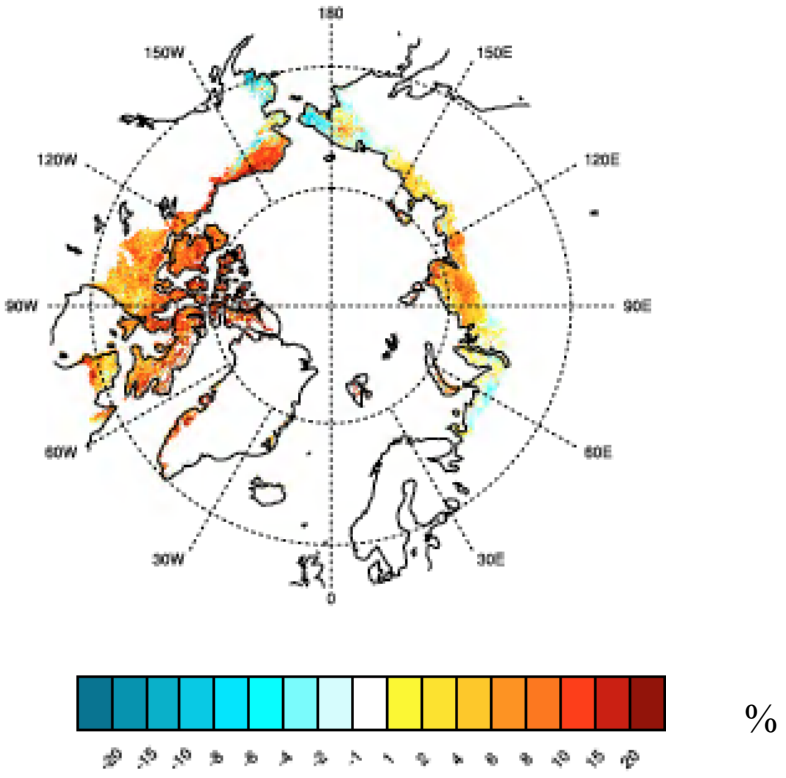

Figure 2.2: A 27-year trend (1982-2008) of maximum Arctic NDVI – change shown in percentage (%). From Bhatt et al. (2010).

A wide array of proxy records such as pollen assemblages, marine molluscs, oxygen isotopes of ice cores, diatoms (Smol et al., 2005; Keatley et al., 2008; Ruhland et al., 2008; Paul et al., 2010) and lake varved sediments (Stewart et al., 2008; Thomas and Briner, 2009; Tomkins et al., 2009) support the occurrence of shorter ice seasons in association with recent warmer temperature at high latitudes. The great sensitivity of small lakes and ponds is also illustrated by changes in the water balance between precipitation and evaporation (P – E) that further affects lakes' physical, biological and chemical properties (Smol and Douglas, 2007; Paul et. al., 2010). For example, shorter ice seasons promote a longer growing period followed by the development of more complex and abundant periphytic diatoms in shallow water bodies (Smol et al., 2005; Paul et al., 2010), a diversified planktonic flora (Keatley et al., 2008) and an overall increased rate of primary production (Smol et al., 2005) consequent to warmer water temperatures and additional light availability. Paleolimnological proxies also support the hypothesis that shorter ice seasons also lead to changes in the chemical properties of High Arctic lakes (e.g., iron-rich sediments extracted from a meromictic lake on Ellesmere Island, Tomkins et al., 2009 or concentration changes in organic matter, Schindler and Smol, 2006).

The Arctic region is dominated by the overwhelming presence of snow-covered sea ice that largely controls the surrounding environment with effects extending beyond its geographical area (Serreze and Barry, 2011). Recent temperature anomalies during the non-summer months have led to Arctic temperature amplification at the surface boundary layer, closely followed by decrease of the sea ice extent (Comiso et al., 2008; Serreze et al., 2007, 2009; Deser et al., 2010; Tivy et al., 2011). The sea ice-albedo feedback mechanism is the main controller of climate at high latitudes and is directly impacted by changes within the ice cover that imminently responds to changes in temperature, large-scale atmospheric and ocean circulation patterns and/or snowfall extent and depth.

Due to the proximity of the Arctic Ocean, high latitude lakes are highly sensitive to seasonal, interannual and decadal/interdecadal variations in temperature and winter precipitation patterns. Sensitivity of lake systems and their ice cover to climate forcings arises as a result

of complex interactions between ocean, land and atmosphere. In conjunction with the coastal location of many of the Arctic lakes, lake ice phenology is also associated with regime shifts in atmospheric conditions and teleconnection indices (Bonsal et al., 2006; Ghanbari et al., 2009; Wang et al., 2009) such as the Arctic Oscillation (AO), North Atlantic Oscillation (NAO), Pacific Decadal Oscillation (PDO), North Pacific (NP) and El Niño Southern Oscillation (ENSO).

Past ice phenology of northern hemisphere lakes displayed a greater response to extreme phases of teleconnections. Changes in the coupled Pacific atmosphere-ocean system have the potential to affect climate conditions at higher latitudes (Trenberth and Hurrell, 1994), with a shift towards a deeper Aleutian low in the late 1970s explaining the milder conditions over Alaska related to a positive PNA/PDO phase and a strong El Niño (Trenberth, 1990; Hartmann and Wendler, 2005) and the later freeze-up and earlier break-up dates over western Canada (Bonsal et al., 2006). Longer open water seasons over western Canada are also associated with negative phases of ENSO and NP (Bonsal et al., 2006). Future changes within the NP circulation will likely be confined to regions south of 65°N since NP is only dominant south of the Bering Strait (Dickson et al., 2000). Conversely, positive NAO values resulted in later ice decay in northeastern Canada (Bonsal et al., 2006).

Under projected amplified warming of polar regions, ice break-up timing of inland lakes may be prone to a greater change (i.e. advanced spring melt) than ice duration as ice decay responds to large-scale circulation forcings (Assel et al., 2003; Bonsal et al., 2006).

2.1.2 Lake ice and snow

The high-albedo of fresh snow (0.80-0.90) was shown to be a major driver of lake ice phenology, oscillations in snow duration, depth and extent having direct implications for the thermal regime, winter energy balance and ecology (Sturm and Liston, 2003) of lakes. Snow supports formation of snow ice, a unique feature of water surfaces (Sturm and Liston, 2003) by contributing to the thickening of the ice cover (Korhonen, 2006). Additionally, snow also

reduces the growth rate of the underlying lake ice because of its lower thermal conductivity (0.08-0.54 versus 2.24 Wm^{-2} K^{-1} for ice; Sturm, 1997) and insulating properties (half than that of terrestrial snow; Sturm and Liston, 2003). A thinner and denser snow layer provides less insulation and allows higher rates of heat flow from the lake surface to the atmosphere in spring (Sturm and Liston, 2003). Knowledge of the current state of Arctic snow can be used to predict lake ice-off dates, as break-up trends closely follow those of number of snow days (Jensen et al., 2007). Changes in the amount of snowfall in a certain region can also explain lake ice thickness and variability in the break-up date timing (Duguay et al., 2003).

Over the past five decades, the annual pan-Arctic snow-cover extent has experienced a continuous decline (10% per decade since 1972; Karlsson et al., 2011) with most abrupt changes occurring in spring and over continental coastal regions. For the North American Arctic, from 1967 to 2007, the snow cover extent has declined by 12% in May (Brown et al., 2010) and by 19.9% $decade^{-1}$ (1979-2013) in June (Derksen et al., 2013). The continental coastal regions experienced an increased reduction in the snow cover extent (Radionov et al., 2004). The variability of pan-Arctic snow extent in May and June is partially explained by temperature (49% and 56%), whereas a positive AO phase since the late 1980s is responsible for 21% of the variability in the snow cover extent (only 10% for North America, Brown et al., 2010). Reduced snow duration since the 1970s is also associated with earlier melting (Brown et al., 2010). Tedesco et al. (2009) also detected earlier snowmelt for the pan-Arctic region of 0.6 days $decade^{-1}$ from 1978 to 2008.

Whilst most regions across the Arctic experience changes that are more detectable within the spring snow cover, Alaska and the Canadian Arctic Archipelago undergo reduced duration of both autumn and spring snow cover (Brown et al., 2010). Figure 2.3 shows changes in the June snow cover extent between 1967-2012.

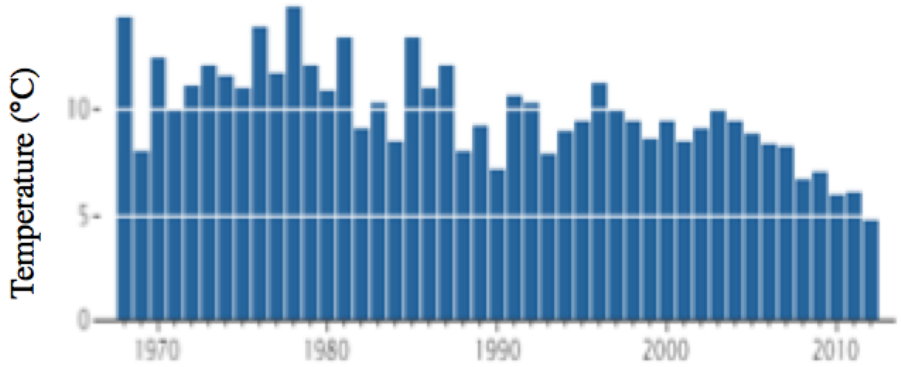

Figure 2.3: Anomalies in the Arctic June snow cover extent (1967-2012) shown in millions of square kilometers. The graph is based on data from the Rutgers University Global Snow Lab and was published at http://earthobservatory.nasa.gov.

Consequent to more precipitation at high latitudes during recent decades (Callaghan et al., 2011) as a result of increasing air temperatures, snow depth has increased in most northern regions, with significant changes in northern Canada and the Alaskan North Slope (Duguay et al., 2006; Tedesco et al., 2009). Snow depth changes have been related to earlier break-up dates (Vavrus et al., 1996; Morris et al., 2005).

2.1.3 High Arctic polar-desert and polar-oasis lakes

The High Arctic is in its majority a polar desert area with mostly barren land surfaces, intense and persistent coldness, and low amounts of precipitation (Woo et al., 2006). Mean annual temperature (1950-2011) at Alert, Nunavut (82°30’ N, 62°20’ W) is -19°C, at Eureka, Nunavut (79°59’ N, 85°56’ W) is -18°C, and at Resolute, Nunavut (74°41’ N, 94°49’ W) is -15°C. For the same period, mean total precipitation fall is 158 mm at Alert, 161 mm at Resolute and 79 mm at Eureka (Environment Canada, 2011). The majority of High Arctic lakes are situated in polar desert environments.

Within the dominant polar desert environment, small warmer areas have been identified. These fairly small regions (with surface areas ranging from 10^{-2} to 10^{2} km^2), called polar or High Arctic oases (Woo and Young, 1996), are of relatively great biological production and diversity, with warmer soil and longer growing season (Courtin and Labine, 1977), discretely localized from the surrounding arid landscape of polar deserts (Svoboda & Freedman, 1981). Lakes with longer frost-free seasons are associated with higher primary productivity and more rapid nutrient cycling (Perren et al., 2003; Keatley et al., 2007; Callaghan et al., 2012). They are characterized by a milder microclimate (Woo and Young, 1997) that is mainly attributed to higher incoming radiation given by the fact that most frequently they develop in relatively flat coastal lowlands, exception being the thermal oasis surrounding Lake Hazen (France, 1993). Lake Hazen is situated in a trough, and is sheltered from the cold Arctic Ocean air by the Grant Land Mountains (> 2000 m) in the north and a plateau (400-900 m) in the south.

Ellesmere Island contains some of the largest polar oases in the Queen Elisabeth Islands of Arctic Canada, including Eureka, Tanquary Fiord and Lake Hazen (Edlund and Alt, 1989). Other High Arctic oases have been identified on Devon Island *(*Bliss, 1977), Alexandra Fiord (Freedman et al., 1994), Polar Bear Pass (Bathurst Island), at Sherard Bay (Melville Island), and Mould Bay on Prince Patrick Island (Aiken et al., 1999). Given that the current analysis is limited by the low spatial resolution of the SAR sensors (150 m for ASAR, and 200 m for RADARSAT-1/2), Lake Hazen, Buchanan Lake, lake L6 on Devon Island and lake L7 on Bathurst Island were the only investigated lakes located in polar oases environments.

2.2 Lake Ice Thermodynamics

Energy exchanges between the various components of the cryosphere and atmosphere drive the overall Arctic climate. Lake ice plays an integrating role within this complex system as it actively interacts with the surrounding ocean and the overlying atmosphere. Since the net radiation F_{rad} at the top of the atmosphere (TOA) is

$$F_{rad} = (1 - A)\, K - L$$

where A is the planetary albedo, K the incoming shortwave radiation and L the emitted longwave energy (Serreze, 2005), this can be further integrated into the energy balance of the northern polar cap expressed as

$$\frac{\Delta E}{\Delta t} = F_{rad} + F_{wall} + F_{sfc}$$

where $\Delta E / \Delta t$ is the time change in the storage of moist static energy (the sum of sensible heat, latent heat and potential energy), F_{wall} is the net poleward energy from north of 70°, and F_{sfc} represents the net energy flux at the Earth's surface. If the result is negative, the atmosphere is losing heat versus heat gain indicated by positive values (Serreze, 2005 from Nakamura and Ort, 1988). In light of the above energy flux exchanges, it can be further stated that energy deficit or excess within a lake is highly influenced by the albedo of lake ice, which brings further contributions to the overall energy of the Arctic system. Lake ice albedo values range from 0.10 for black ice (Bolsenga, 1969) to 0.39-0.46 for white ice, 0.35-0.58 for refrozen slush (Bolsenga, 1977) and 0.70-0.90 for ice covered by freshly fallen snow (Brown and Duguay, 2010). Lower lake ice albedo values can contribute to energy surplus contrasted by the opposite situation of higher albedo values possibly associated with lake energy deficit.

The energy balance of ice integrates all the above-mentioned energy exchanges but becomes even more intricate since it also incorporates additional heat fluxes that one needs to consider when analyzing the response of lake ice cover to climate conditions. The energy balance of ice is described as

$$(1 - \alpha)\, K\downarrow - I_0 + L\downarrow - L\uparrow + Q_H + Q_E + Q_G + Q_M + Q_W + Q_P^{*} = 0$$

where, α is the ice surface albedo, $K\downarrow$ is the incoming solar radiation at the surface, I_0 is the energy flux that penetrates the ice surface, $L\downarrow$ and $L\uparrow$ are the incoming and outgoing longwave energy, Q_E and Q_H are the latent and sensible heat fluxes, Q_G is the conductive

heat, Q_M is the flux resulting from melting/freezing and Q_W is the contributing energy of water at the ice-water interface. The addition of Q_P (heat added by precipitation) to the formula depends on the climatic scenario (adapted from Heron and Woo, 1994).

2.2.1 Freeze-up

Lake ice starts forming following the decrease in the seasonal air temperatures. Ice onset is also driven by lake morphometry as different amounts of heat are being accumulated during the summer months depending on lake depth, area and volume. Once lake water reaches its utmost density at 3.98°C consequent to heat loss at the air-water interface, deeper warmer waters replace the denser surface ones (turnover) and additional cooling continues until a solid ice cover develops (Brown and Duguay, 2010). Without snowfall during freeze up, clear congelation ice starts forming (Figure 2.4a) and growth persists. Conversely, if snowfall occurs, ice development is either delayed (Adams, 1976) or snow ice (Figure 2.4b) forms.

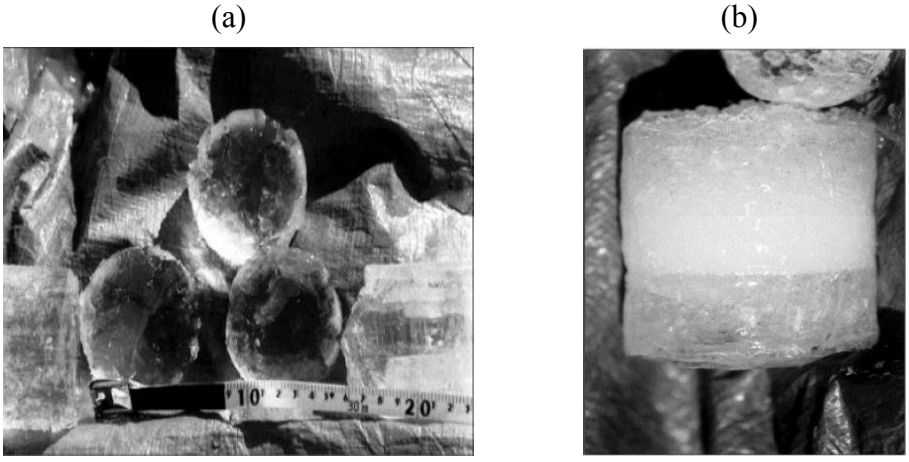

Figure 2.4: Types of ice present on shallow sub-Arctic lakes, Churchill, Manitoba: (a) clear (bubble-free) ice; (b) snow (white) ice. From Duguay et al. (2002).

Snow ice only develops if the ice sheet cannot support the weight of overlying snow (snow submerges the ice below the water hydrostatic level); then the flooded bottom snow saturates

(Sturm and Liston, 2003) and forms a slush layer that later freezes as white ice (Bengtsson, 1986; Liston and Hall, 1995). Rain infiltrations within the snow/ice cover or partial melt during the winter (Brown and Duguay, 2010) can also lead to white ice formation.

2.2.2 Break-up

Lake ice break-up follows increasing spring solar radiation and air temperatures above freezing. Further combination with wind stress, warmer inflows and runoff (Williams, 1965) can accelerate the process. The ice type (black or snow ice) and the presence/absence of a snow layer on the ice surface influences the ice decay process, with snow ice and snow increasing the surface albedo and thus resulting in delayed ice break-up (Jeffries and Morris, 2007). The presence of snow also delays ice melt onset as solar radiation will melt snow prior to disintegrating the internal structure of ice crystals (Ashton 1986). Melt gradually accelerates as soon as snow melts and more ice is exposed to radiative warming.

2.3 Data and Methods

2.3.1 Optical imagery

Optical imaging of Arctic lakes started with the launch of the first Landsat Multispectral Scanner (MSS) in 1972 and has continued to date through multiple Landsat sensors, Landsat 8 being launched in February 2013 at a spatial resolution of 30 m. Monitoring ice cover can also be performed with the Terra/Aqua Moderate-Resolution Imaging Spectroradiometer (MODIS) but is limited to larger lakes given the 250-500 m spatial resolution of the sensor (Arp et al., 2013). The presence of clouds, prolonged darkness or low sun elevation at northern latitudes limits the use of optical sensors during key months for lake ice phenology, particularly during freeze-up. Nevertheless, optical imagery is essential for validating and complimenting the SAR observations whenever is available.

2.3.2 Synthetic Aperture Radar

With day and night observations in all weather conditions at spatial resolutions raging from a few meters to 150 m, SAR sensors provide year-round acquisitions, critical for lake ice regimes monitoring.

Airborne X-band and C-band SAR images acquired over shallow lake regions have been shown to be useful for determining the presence of floating or grounded ice (Weeks et al., 1978; Mellor, 1982) and timing of lakes that freeze to their bed in winter (Elachi et al., 1976). The first analysis of ERS-1 SAR data over lakes on the North Slope of Alaska was performed by Jeffries et al. (1994) during the ice season of 1991/1992. The study shows that monitoring the evolution of radar return, also referred to as radar backscatter intensity or sigma-nought (σ°), is useful for detecting ice onset and melt, as well as floating or grounded ice (ice frozen to lakebed).

Methods developed in these earlier investigations have more recently been applied to map fish overwintering habitat in channels of the Sagavanirktok River, Alaska (Brown et al., 2010), to estimate methane sources (Walter et al., 2008) or to determine winter water availability in Alaska (White et al., 2008). C-band SAR has been shown to be the most useful frequency for distinguishing floating ice from grounded ice as discrimination between the two different ice covers is facilitated by the high contrast displayed in SAR images (Kozlenko and Jeffries, 2000). Detection and analysis of Arctic lake ice conditions between 1991-2011 from spaceborne SAR observations presented in this research used data from a combination of C-band SAR sensors that were in orbit during this period (Table 2.1).

Table 2.1: Characteristics of the SAR sensors used in this study's lake ice cover investigations (1991-2011).

	ERS-1	ERS-2	RADARSAT-1	RADARSAT-2	ASAR (Envisat)
Launch date	17-Jul-91	21-Apr-95	04-Nov-95	14-Dec-07	30-Oct-02
End of mission	10-Mar-00	05-Sep-11	29-Mar-13	still in orbit	08-Apr-12
Spatial resolution	240 m	240 m	100 m	100 m	150 m
Pixel spacing	100 m	100 m	50 m	50 m	75 m
Polarization	VV	VV	HH, HV	HH, VV, HV, VH	VV or HH
Revisit time	35 days	35 days	24 days	24 days	35 days
Swath width	400 km	400 km	500 km	500 km	406 km
Incidence angles	18-47°	19-26°	19-49°	20-46°	15-42°

Generally, low radar returns (-17 to -12 dB) in C-band ERS-1/2, VV polarized SAR imagery indicate the presence of a thin, relatively uniform ice cover at the beginning of the ice season, associated with specular reflection off the ice surface away from the sensor (Duguay et al., 2002). Low radar backscatter also attests the existence of grounded ice later into the growing season, explained by the low dielectric contrast at the ice-lake bottom interface and the absorption of the radar signal into the substrate (Jeffries et al., 1994). Steady increase in σ° persists during the ice season, from November to April, as ice continues to grow and remains afloat. Maximum returns (-11 to -2 dB) or brighter (white and dark/light grey) signatures are associated with the presence of floating ice. Higher backscatter from floating ice is a combination of high difference in dielectric properties between the ice and the underlying liquid water, and the presence of air inclusions in the ice layer, with bubbles mainly resulting in volume scattering (Duguay et al., 2002). Ice decay at the end of the season is characterized by low radar return from the melting ice and snow, and/or ponding water that reflects the radar signal (Duguay et al., 2002).

Detection of the start of ice formation, melt onset and end of the ice season can also be derived from analysis of the backscatter temporal evolution. At C-band, the start of ice

formation over lakes is indicated by the first considerable increase in σ°. When ice has formed as a thin, continuous layer, the σ° intensity decreases (Duguay and others, 2002). Conversely, melt onset is identified by the first significant decrease in σ°, given by the presence of water from internal melting of ice and/or a melting snow cover, and thus resulting in increased absorption of the radar signal (Duguay and others, 2002). Lower σ° is observed during the open-water season but may vary depending on wind speed.

2.3.3 Image segmentation

Segmentation of the SAR images used in this research was performed with two the MAp-Guided Ice Classification System (MAGIC) and the unsupervised K-means algorithm.

2.3.3.1 MAGIC

In order to map lakes/lake areas frozen to the bed (grounded ice) and those with ice afloat (floating ice) in the Barrow region of the Arctic Coastal Plain, image segmentation was performed for ERS-1/2 acquisitions extending over a 20-year period (1991-2011).

The automated segmentation combines graduated increased edge penalty and region growing techniques, both incorporated in the Iterative Region Growing with Semantics (IRGS) algorithm and implemented in the MAp-Guided Ice Classification System (MAGIC) software (Clausi et al., 2010). IRGS encompasses edge strength between regions in order to ensure that true class boundaries are preserved. Being an unsupervised algorithm, no training data is required prior to segmentation and classification (Yu et al., 2012). The method, proved to be robust, has been fully validated and is being successfully used by Environment Canada's Canadian Ice Service (CIS) for sea ice classification. The statistical and spatial characteristics of pixels in SAR images have been effectively modeled with IRGS and successfully used in a recent study to map and monitor ice cover on large northern lakes (Ochilov et al., 2010). Given that different ice types are present on lakes, a three-cluster segmentation (two floating ice classes and one grounded ice class) was used and in order to further verify the performance of the three-cluster segmentation, a five-cluster segmentation

was at times performed. Following the input of each individual SAR image and the corresponding vector file of lakes included in the study area, automated image segmentation is performed with IRGS, and the output is a file that includes fractions for all three classes that were initially selected by the operator. In order to determine the total fraction of grounded and floating ice, visual assessment of each segmentation result against the original SAR image is performed, and all resulting ice classes are merged into two classes (grounded and floating ice) by a human operator. Once merging was completed, a two-class map was generated for each date of SAR imagery included in the analysis. Low-resolution (100-m pixels) images were segmented with IRGS and further classified as floating and grounded ice, respectively. The current study extends the use of IRGS in documenting and analyzing changes in ice cover on shallow lakes.

The use of MAGIC at an operational level is limited by the lack of automatic labeling of the ice and open-water classes in the IRGS algorithm. Class labeling requires visual inspection of the original SAR image, assessment of initial observations against segmentation results and manual class merging of same-type classes.

2.3.3.2 The unsupervised K-means

The most common clustering method, the unsupervised K-means classification algorithm, has proved to be a suitable method to discriminate between ice and open water and thus monitor the lake ice break-up using SAR data (Sobiech and Dierking, 2013). Considering the large number of images analyzed in this study, the K-means algorithm was preferred over a fixed threshold method as it performs better given the changing ice conditions (Sobiech et al., 2013) during the melt season. The unsupervised K-means classification is an iterative process in which image intensity values are divided into ‘k’ classes or clusters. Throughout the 20 iterations performed for each segmentation, the K-means classification assigned each intensity value to the class with the nearest arithmetic mean (minimum-distance technique).

In order to reduce the inherent speckle present in SAR images, a Lee filter (Lee, 1980) with a kernel size of 3x3 was applied to all geocoded images. After the speckle was removed, regions of interest (ROIs) covering the lake areas were selected. Following ROI designation, image segmentation of each ROI was performed. The classification only included the pixels inside the ROI, all other pixels being excluded from analysis. The segmentation was set to five clusters that were further merged into two classes, one for open water and one for ice, that were next represented on a two-class map generated for each segmented image. Text files showing the percentage (%) or fraction of open water and ice were extracted for each ROI of the classified maps to quantify the amount of ice present on lakes from the start of the break-up process until the end of the melt season.

2.3.4 MODIS Land/Ice Surface Temperature

Moderate Resolution Imaging Spectroradiometer (MODIS) land/lake surface temperature data were acquired from 2006 to 2011. MODIS pixels were identified for each of the 14 ROIs (lakes) shown in Figure 1 and listed in Table 1, and used in the analysis of σ^0 values in relation to lake surface "skin" temperature. Selection of MODIS pixels was carefully performed in order to avoid land contamination and included MODIS pixels closer to the lake areas of interest. The pixels were selected based on two criteria: first – the proximity to the selected SAR ROIs, and second – each 1-km MODIS pixel had to be 95% over lake.

In this study, the MODIS UW-L3 Lake Surface Water Temperature/Lake Ice Surface Temperature (LSWT/LIST) product was used (Kheyrollah Pour et al., 2012, 2014). The product is generated from Aqua and Terra MYD/MOD 11- L2 data, at a spatial resolution of 1 km. A new algorithm was developed to create products at various temporal resolutions from the combination of MODIS data from the Aqua and Terra satellites, which were not available otherwise (see Duguay et al., 2012 and Soliman et al., 2012 for details). The Aqua and Terra satellite platforms follow the same orbit within 3 hours of each other. However, at higher latitudes, it is possible to monitor the same location from both sensors within an hour,

considering different viewing angles. In such case, it is feasible to combine observations from both sensors in each pixel during an hour. The MODIS UW-L3 LSWT/LIST product has been evaluated against *in situ* temperature measurements over Finnish lakes (Cheng et al., 2014; Kheyrollah Pour et al., 2014) as well as one-dimensional lake models over two large Canadian lakes (Kheyrollah Pour et al., 2012).

2.3.5 The Canadian Lake Ice Model (CLIMo)

Performance of lake ice models was previously evaluated for large and small lakes. Comparison of two 1-D lake ice models, Hostetler (Hostetler et al., 1993) and FLake, showed that models simulated well ice conditions for small lakes (Martynov et al., 2010). The use the FLake model as a parameterization scheme in investigating the performance of the High Resolution Limited Area Model (HIRLAM) Numerical Weather Prediction (NWP) model revealed model's limitations to simulate accurate ice conditions, freeze-up in particular. Assimilation of lake surface temperature (LST) would provide more reliable outputs (Eerola et al., 2010). Evaluation of the 1-D Freshwater Lake model (FLake) and the Canadian Lake ice Model (CLIMo) for Great Slave Lake and Great Bear Lake indicated that CLIMo outputs for ice thickness and break-up dates were generally in better agreement with *in situ* observations than the Flake simulations (Kheyrollah Pour et al., 2012). This is explained by the fact that unlike FLake, CLIMo considers the presence of snow on lake ice. The one-dimensional thermodynamic ice model CLIMo was extensively tested over various lakes across the Arctic, such as lakes on the North Slope of Alaska (Duguay et al., 2003), a shallow sub-Arctic lake near Churchill, Manitoba (Brown et al., 2011a) or at the pan-Arctic scale for lakes of different depths (Brown and Duguay, 2011b). Overall, it was demonstrated that CLIMo is capable of simulating well the seasonal and interannual changes in ice thickness, on-ice snow depth as well as changes in freeze-up and break-up dates (Ménard et al., 2002; Jeffries et al., 2005; Brown and Duguay, 2011a, b).

CLIMo is a one-dimensional thermodynamic model employed for freshwater studies and is capable of simulating freeze-up and break-up dates, ice thickness and ice cover composition (black or snow ice). CLIMo has been modified from the 1-D sea ice model of Flato and Brown (1996) and calculates surface energy budget in order to derive the net flux at the ice, snow or open water surface. The model is based on the one-dimensional unsteady heat conduction equation, with penetrating solar radiation.

$$\rho Cp \frac{\partial T}{\partial t} = \frac{\partial}{\partial z} k \frac{\partial T}{\partial z} + F_{sw} I_0(1-\alpha) K e^{-Kz}$$

where ρ (kg m^{-3}) is the density, C_p (J kg^{-1} K^{-1}) is the specific heat capacity, T (K) is the temperature, t (s) is the time, k (Wm^{-1} K^{-1}) is the thermal conductivity, z (m) is the vertical coordinate, positive downward, F_{sw} (Wm^{-2}) is the downwelling shortwave radiative energy flux, I_o (Wm^{-2}) is the fraction of shortwave radiation flux that penetrates the surface, α is the surface albedo, and K is the bulk extinction coefficient for penetrating shortwave radiation (m^{-1}).

From this, calculation of the surface energy budget can be performed.

$$F_0 = F_{lw} - \varepsilon\sigma T^4 (0,t) + (1-\alpha)(1-I_0)F_{sw} + F_{lat} + F_{sens}$$

where F_0 (Wm^{-2}) is the net downward heat flux absorbed at the surface, F_{lw} (Wm^{-2}) is the downwelling longwave radiative energy flux, ε is the surface emissivity, σ is the Stefan-Boltzman constant (5.67 x 10^{-8} Wm^{-2} K^{-4}), F_{lat} (Wm^{-2}) is the downward latent heat flux, and F_{sens} (Wm^{-2}) is the downward sensible heat flux (both positive downward) (Ménard et al., 2002; Jeffries et al., 2005).

CLIMo includes a fixed-depth mixed layer in order to represent an annual cycle. The mixed layer is fixed at the freezing point when ice is present. When ice is absent, the surface energy budget is used to calculate the temperature of the mixed layer thus representing the heat storage in the lake. The water column of shallow lakes is well mixed and isothermal from top

to bottom during the open-water season, allowing a good approximation of the effect of lake depth leading to fall freeze-up based on the mixed layer depth (Duguay et al., 2003).

Growth and melt at the underside of ice are calculated from the difference between the conductive heat flux into the ice and the heat flux released at the upper surface of the mixed layer, thus

$$\frac{\partial hi}{\partial t}\Big/_{z=h} = \left(k\frac{\partial T}{\partial z}\Big/_{z=h} - \int_{h}^{\infty} F_{sw} I_0 (1-\alpha) K e^{-Kz} dz\right)\frac{1}{Lfi}$$

where h_i is the ice thickness and dz is the depth of the vertical coordinate. The last term of the equation is the shortwave radiation that penetrates through the bottom of the ice slab, and is presumed to be absorbed in the mixed layer and returned to the ice underside in order to maintain the temperature of the mixed layer at the freezing point. Melt at the upper surface is calculated from the difference between the conductive heat flux and the net surface flux; any snow on the ice surface is melted first and the remaining heat is further used to melt ice.

The parameterization of albedo in the model is based mainly on surface type (water, ice or snow), surface temperatures and ice thickness, ice composition being considered uniform. In order to represent an annual cycle, CLIMo considers a fixed-depth mixed layer. Duguay et al. (2003) provide a more detailed description of CLIMo.

For the purpose of this research, CLIMo was forced with climate data from the Barrow meteorological station (1950-2011). Two snow depth scenarios were used – one that assumed 0% snow and one that assumed a 53% snow cover depth of that present on land. The 53% snow depth was calculated based on existing field measurements of snow depth measured over land. A fixed snow density of 335 kg m^{-3} was assumed and was based on available *in situ* measurements for the Barrow region from 1991 to 2006. The mean lake depth used in the model was 3 m. Model outputs used in this research include ice thickness, and freeze-up and break-up dates.

2.3.6 ERA-Interim Reanalysis Data

The ERA-Interim is the largest global atmospheric reanalysis product of the European Centre for Medium-Range Weather Forecasts (ECMWF). The full-resolution (~0.75° x 0.75°) gridded product is derived from data assimilation from a variety of sources: radiances from the Special Sensor Microwave Imager (SSM/I), radiosonde temperature, scatterometer ocean surface wind data, including recalibrated data from the European Remote Sensing (ERS-1/2) satellites, and until 2009 from QuickSCAT (Dee et al., 2011) and provides global coverage since 1979. For the purpose of this study, the 2-m near-surface temperature computed with a sequential data assimilation scheme, advancing forward in time using 12-hourly analysis cycles, was utilized. In this study, the ERA-Interim data was used to supplement the limited temperature records from meteorological stations in the Canadian High Arctic.

Chapter 3

Response of ice cover on shallow lakes of the North Slope of Alaska to contemporary climate conditions (1950-2011): radar remote sensing and numerical modeling data analysis

3.1 Introduction

Lake ice cover has been shown to be a robust indicator of climate variability and change. Previous studies have identified lakes as a highly sensitive cryospheric component to climate conditions (Schindler et al., 1990; Robertson et al., 1992; Heron and Woo, 1994; Vavrus et al., 1996; Walsh et al., 1998; Magnuson et al., 2000; Hodgkins et al., 2002; Assel et al., 2003, Bonsal et al., 2006; Duguay et al., 2006). Climate-driven changes have significantly impacted high latitude environments over recent decades, changes that are predicted to continue or even accelerate in the near future as projected by global climate models (Overland et al., 2011; Dufresne et al., 2013; Koenigk et al., 2013). With projected amplified warming of polar regions, the ice cover of shallow Arctic lakes is expected to continue reducing in both thickness and duration. Although the response of lakes may be heterogeneous depending on latitude, lake depth and size, water composition and water dynamics, the majority of lakes demonstrate an overall strong response to surface air temperatures (Palecki and Barry, 1986). Persistent warmer air temperatures (Serreze et al., 2000; Trenberth et al., 2007) and increased snowfall observed in the Arctic over the last decades (Jones et al., 2011; Arp et al., 2012), associated with amplified reduction of sea ice concentrations, thickness and extent (Serreze et al., 2007; Comiso et al., 2008; Walsh et al., 2011), have accelerated during recent years (Walsh et al., 2011). These changes in the Arctic climate system have likely had an impact on ice phenology of lakes in coastal regions adjacent to the Arctic Ocean.

Changes in lake ice-cover could in turn have an important feedback effect on energy exchanges between the lake surface and the atmosphere, and on water levels and therefore on lake water balance, water properties and quality. As a result, water resources, food supply, aquatic habitat, and underlying permafrost conditions undergo changes at various spatial and temporal scales. Through their heat and water budgets, lakes play an important role in the local and regional climate of high-latitude regions. Longer open-water seasons lead to increased exposure to solar radiation that, through evaporation, results in extended latent heat release from lakes to the atmosphere, the amount of latent heat being twice of that released by the adjacent tundra (Mendez et al., 1998). In permafrost areas such as the North Slope of Alaska, changes in lake water balance, dynamics or temperature can also disturb the underlying permafrost layer, resulting in thaw (Romanovsky et al., 2010) with consequent talik formation and lateral lake water drainage, and also in carbon dioxide and methane release to the atmosphere (Walter et al., 2006). The presence of liquid water underneath ice extends fresh water availability for residential and industrial use throughout the winter. The changing ice cover of high-latitude lakes not only alters the physical and thermal properties of lakes but also affects the chemical properties and the dependent biota; warming lake water temperatures may lead to extinction, blooming or migration of various biological species. However, the magnitude to which changes within the Arctic lakes affect the dependent ecosystem is complex and poorly understood, and remains to be further investigated.

In response to warmer climatic conditions and to changes in snow cover in recent decades, break-up dates in particular, have been occurring earlier in many parts of the northern hemisphere (Magnuson et al., 2000; Duguay et al., 2006). The presence of trends in lake ice duration may be occasionally masked by the seasonal, annual or decadal variability that is influenced by the intensity and duration of a climatic episode. Under warmer climate conditions, shallow tundra lakes, many of which are less than 3-m deep, are expected to develop thinner ice covers, likely resulting in a smaller fraction of lakes that freeze to their bed in winter, earlier ice-off dates, and overall shorter ice seasons. Shallow lakes of the

Alaskan Arctic Coastal Plain (ACP), and other similar regions of the Arctic (e.g., Arctic Siberia (Grosswald et al., 1999; Smith et al., 2005; Sobiech and Dierking, 2012)), the Hudson Bay Lowlands (Duguay et al., 1999; Duguay and Lafleur, 2003; Duguay et al., 2003; Brown and Duguay, 2011a), have likely been experiencing changes in seasonal ice thickness and phenology (e.g., freeze-up, break-up, and ice cover duration) over the last decades, but few studies have documented these changes.

Past changes in lake ice-cover have mostly been identified only through non-spatially representative point *in situ* measurements, which have been almost unavailable over the last two decades following the decline of the global terrestrial monitoring network for fresh-water ice (Lenormand et al., 2002; Prowse et al., 2011). Recent studies have demonstrated that satellite remote sensing provides a viable alternative to detecting and monitoring changes of the ice cover on high-latitude lakes (Latifovic and Pouliot, 2007; Arp et al., 2012; Duguay et al., 2012). Previous remote sensing investigations indicate that optical sensors are not the ideal tool for comprehensive monitoring of lakes since they are limited by the presence of cloud cover and extended polar darkness (Hinkel et al., 2012), and in most cases, by moderate spatial resolution (i.e., 100-1000 m). Instead, with fewer restrictions (i.e., allowing imaging under cloudy and darkness conditions), spaceborne SAR has been shown to be the most efficient tool for detecting changes in Arctic lake ice (Jeffries et al., 1994; Morris et al., 1995; Duguay et al., 2002; Jeffries et al., 2005; Cook and Bradley, 2010; Arp et al., 2012; Jones et al., 2013). Recent attempts to identify the responses of shallow lakes of the NSA to contemporary climate conditions exist and changes in the grounded ice fraction has been noticed. However, the short period covered by these studies using satellite observations, 2003-2011 (Arp et al., 2012) and 2008-2011 (Engram et al., 2013) precludes identification of a trend.

The climate trajectory in the Barrow region has taken an abrupt turn during the first decade of the 21st century, with mean air temperatures increasing by 1.7 °C (Wendler et al., 2013), a change that has been shown to alter the lake ice regimes in this coastal region. Consequent to

warmer air temperatures and increased precipitation (Callahan et al., 2011) during recent decades (Figure 3.1), the ice regimes of these shallow lakes are expected to develop thinner ice covers, earlier melt, and shorter ice seasons. Transition toward higher floating ice fractions, with more lakes maintaining liquid water underneath the ice cover and fewer lakes freezing to the bottom by the end of winter is also likely to occur.

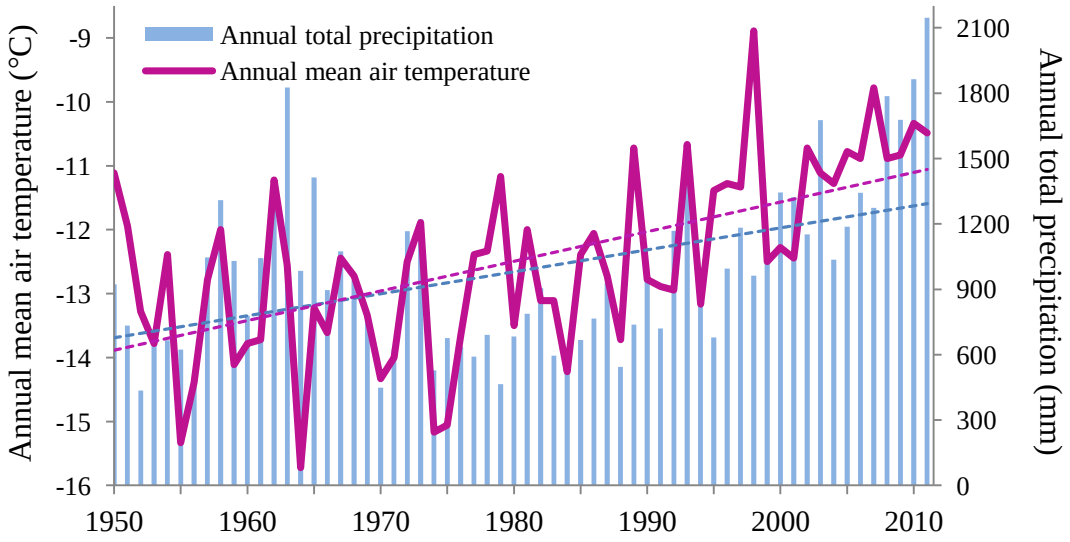

Figure 3.1: 1950-2011 annual mean air temperature and total precipitation (rain and snowfall) as recorded at the National Weather Service station, Barrow, AK. The dashed lines indicate the trend for annual mean air temperature (2.9 °C increase in 62 years, $\alpha = 0.001$) and for annual total precipitation (639 mm increase in 62 years, $\alpha = 0.001$).

The objectives of this study are to identify changes in the maximum ice thickness of Arctic shallow lakes as derived from both SAR satellite observations and numerical modeling scenarios during recent decades, to report observed and simulated changes in the ice phenology of these lakes from 1950 to 2011, and to determine potential ice regime trends during recent decades. To achieve these goals, this study (1) analyzes and reports monthly

changes in the fraction of lakes that froze to the bed in winter between 1991 and 2011, (2) evaluates the rate of change of late winter maximum ice thickness during the past two decades, (3) presents the identified changes in lake ice thickness and duration as derived from a numerical lake ice model (1950-2011), and (4) correlates SAR-detected changes within the lake ice cover with model-simulation results (1991-2011).

3.2 Background

Airborne X-band and C-band SAR images acquired over shallow lake regions have been shown to be useful for determining the presence of floating or grounded ice (Weeks et al., 1978; Mellor, 1982) and timing of lakes that freeze to their bed in winter (Elachi et al., 1976). The first analysis of ERS-1 SAR data over lakes on the North Slope of Alaska was performed by Jeffries et al. (1994) during the ice season of 1991/1992. The study shows that monitoring the evolution of radar return, also referred to as radar backscatter intensity (σ°), is an efficient tool in detecting ice onset and melt, as well as floating or grounded ice. The low temporal resolution of the ERS sensors, a repeat cycle of 35 days would not be suitable for the determination of freeze-up and break-up dates. However, considering that this study focuses on the determination of grounded and floating ice during the ice growth season, this is not a significant issue since high temporal resolution is not necessary (i.e., ERS observations still allow for the monitoring monthly changes in the fraction of floating and grounded ice, and appropriate comparison between years). In order to complement these observations and be able to simulate freeze-up and break-up dates with a daily temporal resolution, CLIMo was employed.

Similar work by Jeffries et al. (1996) used SAR coupled with a numerical lake ice model to determine the timing of maximum ice thickness and the number of lakes on the North Slope of Alaska that freeze to their bottom, and estimate the depth of these lakes. These results are summarized below. Likewise, Duguay et al. (1999) and Duguay and Lafleur (2003)

evaluated the presence of floating and grounded lake ice, and the timing of maximum ice thickness, with ERS-1 SAR observations of the Hudson Bay Lowlands, near Churchill, Manitoba. Methods developed in these earlier investigations have more recently been applied to map fish overwintering habitat in channels of the Sagavanirktok River, Alaska (Brown et al., 2010), to estimate methane sources (Walter et al., 2008) or to determine winter water availability in Alaska (White et al., 2008). Providing that discrimination between floating and grounded ice is facilitated by the high contrast displayed in SAR images, C-band SAR has been shown to be the most useful frequency for distinguishing between the two different ice cover conditions (Engram et al., 2013).

Generally, low radar returns (-17 to -12 dB) in C-band ERS-1/2, VV polarized SAR imagery indicate the presence of a thin, relatively uniform ice cover at the beginning of the ice season, associated with specular reflection off the ice-water interface (Duguay et al., 2002). Low radar backscatter also attests the existence of grounded ice later into the growing season, explained by the low dielectric contrast at the ice-lake bottom interface and the absorption of the radar signal into the substrate (Jeffries et al., 1994). Steady increase in radar backscatter persists during the ice season, from November to April, as ice continues to grow and remains afloat. Maximum returns (-11 to -2 dB) are associated with the presence of floating ice. Higher backscatter from floating ice is a combination of high difference in dielectric properties between the ice and the underlying liquid water (Weeks et al., 1978), and the presence of air inclusions in the ice layer. The higher radar return could also be explained by the presence of smaller tubular bubbles formed during freeze-up or of larger ebullition spherical bubbles, resulting in a double-bounce effect (Mellor et al., 1982). Ice decay at the end of the season is characterized by low radar returns from the melting ice and snow, and/or ponding water that reflect the radar signal in a direction away from the sensor (Duguay et al., 2002).

3.3 Study Area

The study focuses on a region that encompasses 402 lakes, near Barrow (71°31’ N, 156°45’ W) on the NSA (Figure 3.2), an area that is dominated by the ubiquitous presence of shallow thermokarst lakes, lakes being reported to cover up to 40% of the coastal plain (Sellmann et al., 1975; Hinkel et al., 2005).

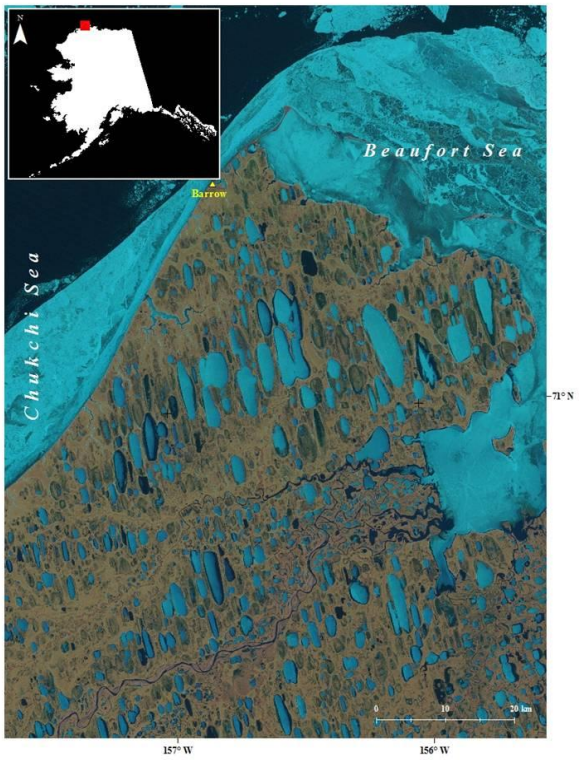

Figure 3.2: Sub-region of the Alaskan Arctic Coastal Plain, near Barrow (71°17’ N, 156 °46’ W). The satellite view of Barrow was provided by NASA, Landsat program 2011, Landsat TM L1T scene (ID: LT50790102011170GLC00). Publisher: USGS. Acquisition date: 9 June 2011.

The area is dominated by a polar marine climate, with cold air temperatures and high-velocity winds. The current mean annual air temperature (1921-2011) recorded at Barrow is -12 °C and the mean annual precipitation fall is 845 mm (106 mm liquid precipitation and 739

mm snowfall). The east, east-northeast prevailing wind has a mean annual speed of 19.1 km h^{-1} (National Climate Data Center, 2012). Summer air temperatures are usually highest in July, with a mean air temperature of 4.4 °C, and lowest in February, with a mean of -26.6 °C.

The area of lakes investigated in this study ranges from 0.1 to 58 km^2. Despite the unknown bathymetry for the majority of these lakes, using a numerical ice-growth modelling approach, Jeffries et al. (1996) determined that 23% of the lakes may be deeper than 2.2 m, 10% with depths ranging from 1.5 m to 2.2 m, 60% between 1.4 m and 1.5 m, and 7% less than 1.4 m.

A considerable number of lakes on the Alaskan ACP freeze to their bed each ice season (Mellor, 1982), and are ice free for only eight to ten weeks per year (Jeffries et al., 1996). Ice formation, mostly a function of lake morphometry and air temperature, commences in mid-September (Jeffries et al., 1994; Liston et al., 2002; Jones et al., 2009) or early October (Hinkel et al., 2003) and attains a maximum growth rate in November (Jones et al., 2009) that is followed by a slower growth rate until early March or later (Jeffries et al., 1996), when many shallow lakes freeze to the bottom. Depending on lake water depth, the timing of maximum ice thickness varies and can occur any time between late April (Jeffries et al., 1996) and May (Jones et al., 2009). Changes in air temperature, snowfall timing and snow depth prior to and during all months of freeze-up (ice-on) and break-up (ice-off) affect the timing of these ice events. However, maximum ice thickness is primarily driven by changes in the April air temperature and it happens earlier by six days following higher air temperatures and is delayed by seven days if lower April air temperatures occur. Changes in snow depth do not affect the timing of maximum ice thickness (Morris et al., 2005).

April air temperature (monthly mean of the 2-m air temperature) was shown to also strongly affect the ice decay of central Alaskan lakes, with a ±1 °C change in air temperature resulting in an advance or delay of break-up dates by ±1.86 days (Jeffries and Morris, 2007). Ice break-up of lakes on the North Slope of Alaska, is driven by changes in air temperatures and the presence of an insulating snow cover, ice break-up that may commence as early as April and last until June (Hinkel et al., 2003) or even July (Hinkel et al., 2012), when lakes become

completely ice free. Field measurements indicate that snow was still present on lakes during the month of April (Jeffries et al., 1994; Sturm and Liston, 2003) hence ice break-up commences after the disappearance of the snow cover on top of lakes in late April or May.

3.4 Data and Methods

3.4.1 SAR-image processing

A time series of a total of 79 SAR images from 1991 to 2011, between December and early May, standard low resolution (100-m pixel size and 240 m spatial resolution) ERS-1/2 (C-band, 5.3 GHz), VV polarized (vertical transmit and vertical receive), ascending and descending passes, was radiometrically calibrated and geocoded with the MapReady software (v2.3.17) provided by the Alaska Satellite Facility (ASF). Following calibration and geocoding, each individual image was segmented in order to derive the ice cover fractions for both floating and grounded (bedfast) ice.

In order to ensure that the images used in the analysis were not affected by possible melt at the end of the ice season, daily air temperatures recorded at the Barrow meteorological station were also taken into consideration in order to confirm that air temperatures values prior to and at the time of SAR acquisitions were below 0° C. Optimum radar images – not affected by possible melt at the end of the ice season – are acquired during April (Mellor, 1982), also coinciding with the approximate timing of maximum ice thickness in this study area. As SAR imagery was not consistently available on the same date during the 20 years of study, assessment of differences in the grounded ice fraction between images acquired a few weeks apart was also performed. April to early May imagery was selected to derive the fraction of lakes frozen to the bed since images acquired later in the season may be affected by the presence of wet snow or ponding water on the ice surface and therefore result in erroneous results (Hall et al., 1994). Evaluation of differences between the ascending and

descending pass acquisitions at a two-day interval showed a difference of 1.5% to 2% in the fraction of grounded ice. The higher fraction of grounded ice was consistently noticed in the descending pass images, acquired two days after the ascending pass. The differences in the grounded ice fraction observed in the overlapping ascending and descending images are attributed to the right-looking ERS geometry. The SAR looking geometry of ERS – from the east in ascending mode and from the west in descending mode – limits the identification of the exact same ground features in overlapping images due to the angle of illumination. Issues such as foreshortening and layover are known to result in possible deformations in area where the topographic slope is greater than 10°. Considering that the study area is a coastal plain, such deformations are likely minimum and the difference in the grounded ice fraction is associated with the illumination differences.

ERS imagery (December to March) was not available on a monthly basis during the 20-year period. However, SAR acquisitions during April were available for each year included in the study, except for 1996, 2002 and 2004 when images acquired on 3 May, 2 May, and 6 May were used to obtain the late-winter grounded ice fractions.

In order to map lake areas frozen to the bed and those with ice afloat in the Barrow region of the ACP, image segmentation was performed for 79 ERS-1/2 acquisitions extending over a 20-year period (Figure 3.3 shows segmentation results of late winter images).

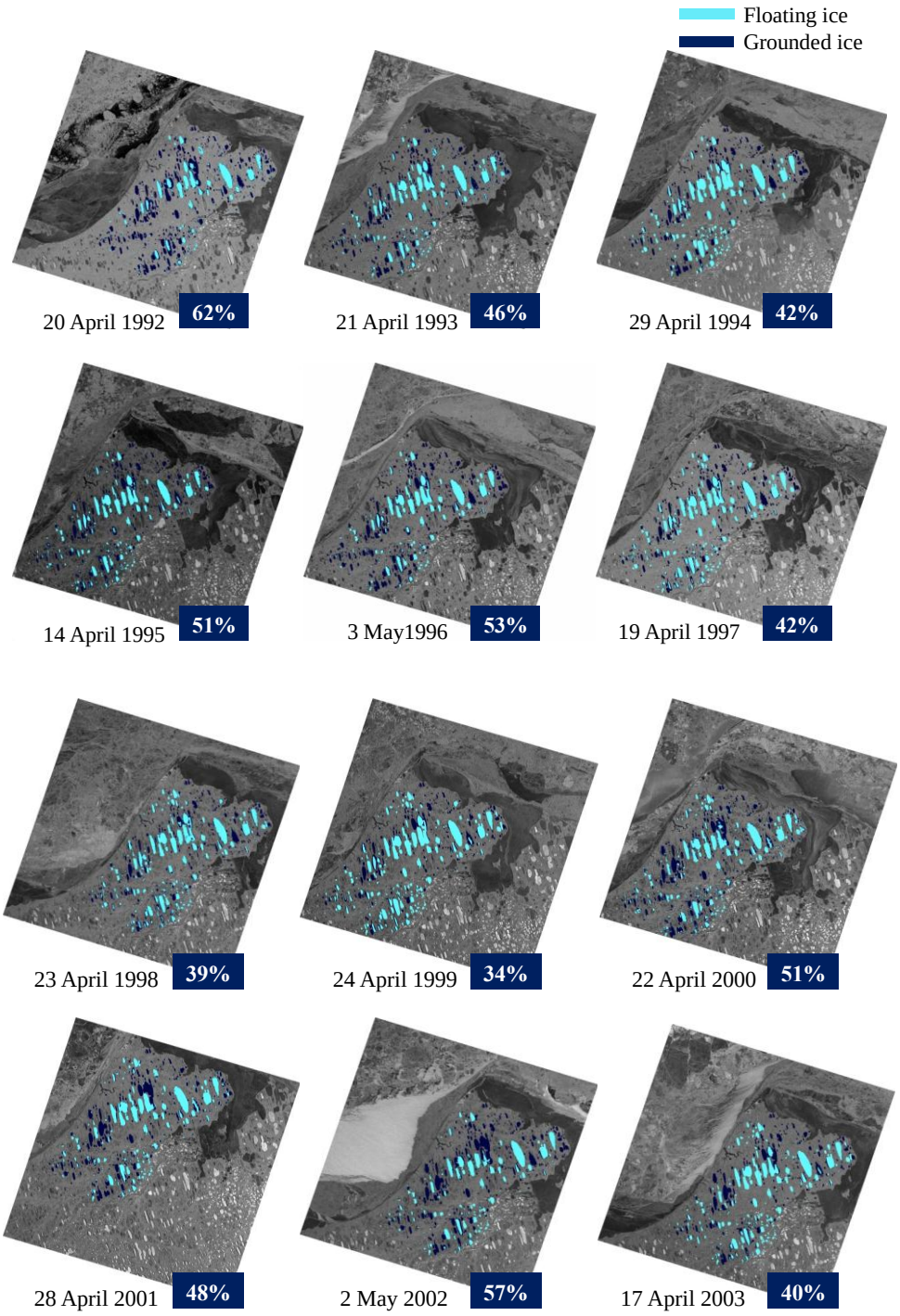
Floating ice
Grounded ice
20 April 1992
62%
21 April 1993
46%
29 April 1994
42%
14 April 1995
51%
3 May1996
53%
19 April 1997
42%
23 April 1998
39%
24 April 1999
34%
22 April 2000
51%
28 April 2001
48%
2 May 2002
57%
17 April 2003
40%

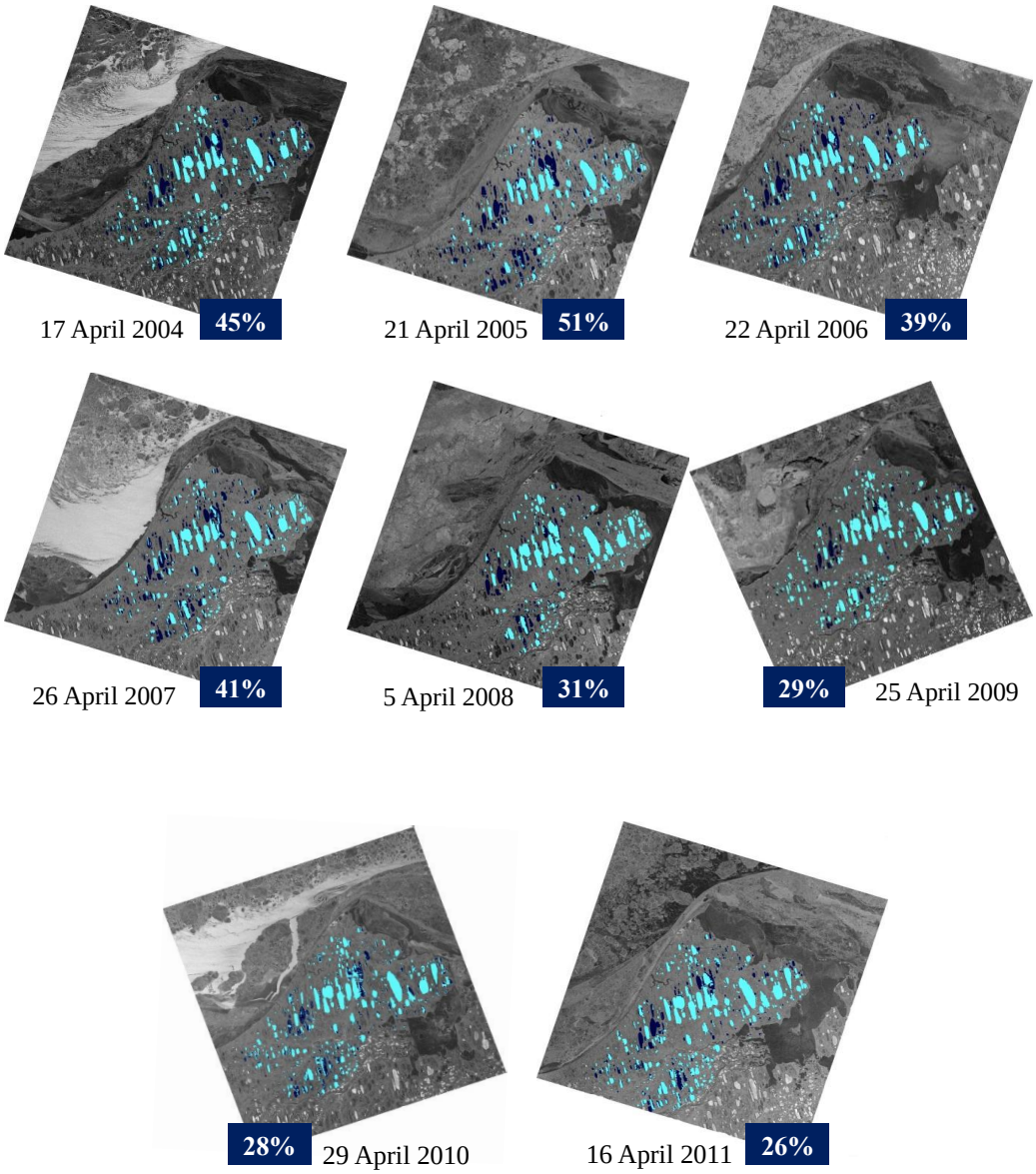

Figure 3.3: Image segmentation results of ERS-1/2 SAR images acquired near the time of maximum ice thickness for lakes near Barrow, from 1992 to 2011. The fraction of grounded ice for each date is also shown. Data source: Alaska Satellite Facility. All SAR images are copyright ESA (1992-2011).

The automated segmentation combines graduated increased edge penalty and region growing techniques, both incorporated in the Iterative Region Growing with Semantics (IRGS) algorithm and implemented in the MAp-Guided Ice Classification System (MAGIC) software (Clausi et al., 2010). The method, proved to be robust, has been fully validated and is being successfully used by Environment Canada's Canadian Ice Service (CIS) for sea ice classification. The statistical and spatial characteristics of pixels in SAR images have been effectively modeled with IRGS and successfully used in a recent study to map and monitor ice cover on large northern lakes (Ochilov et al., 2010). Given that different ice types are present on lakes, a three-cluster segmentation (two floating ice classes and one grounded ice class) was used and in order to further verify the performance of the three-cluster segmentation, a five-cluster segmentation was at times performed. Following the input of each individual SAR image and the corresponding vector file of lakes included in the study area, automated image segmentation is performed with IRGS, and the output is a file that includes fractions for all three classes that were initially selected by the operator. In order to determine the total fraction of grounded and floating ice, visual assessment of each segmentation result against the original SAR image is performed, and all resulting ice classes are merged into two classes (grounded and floating ice) by a human operator. Once merging was completed, a two-class map was generated for each date of SAR imagery included in the analysis. Low-resolution (100-m pixels) images were segmented with IRGS and further classified as floating and grounded ice, respectively. The current study extends the use of IRGS in documenting and analyzing changes in ice cover on shallow lakes.

3.4.2 Lake-ice modeling

The lake ice model CLIMo was used to derive lake ice-thickness, freeze-up and break-up dates. CLIMo was forced using data obtained from the online archives of the National Climate Data Center (mean daily 2-m air temperature, relative humidity, wind speed, cloud

cover fraction, snow depth) from the Barrow meteorological station, for the period 1950-2011. As meteorological data was not available for all years prior to 1950, the model was forced with available data from 1950 onward. In order to capture the typical observed variability in snow depth on Arctic coastal lakes, simulations were performed with two scenarios: one that assumed that no snow was present on the ice surface (0%) and a second one that assumed a 53% snow cover depth, calculated as a fraction from the total snow depth measured over land. The mean lake depth specified in the lake model simulations was 3 m. This model has been extensively tested over various lake regions, including the North Slope of Alaska (Duguay et al., 2003). CLIMo results presented in the study were in good agreement with both ERS-1 SAR observations and *in situ* measurements during the winter of 1991-1992. For example, the simulated ice-on date was 19 September, while satellite observations indicated that freeze-up occurred between 11-20 September 1991 (Jeffries et al., 1994). Similarly, the latest ice-off date simulated with CLIMo in a no-snow scenario was 14 July 1992 and the SAR-derived one was 15 July 1992 (Zhang and Jeffries, 2000), only one day apart. Maximum ice thickness simulations (165-221 cm) in snow depth scenarios ranging from zero to 100% displayed differences of 5-6 cm when compared to field measurements (159-216 cm) during 19-29 April (Jeffries et al., 1994). More recently, the model has been further evaluated for a shallow lake near Churchill, Manitoba (Brown and Duguay, 2011a), and at the pan-Arctic scale for lakes of various depths (Brown and Duguay, 2011b). Analysis of model performance at the pan-Arctic scale showed that the average absolute error for determining ice-on and ice-off dates was less than one week when compared to field observations on 15 lakes in northern Canada. The mean maximum ice thickness difference between simulations and *in situ* measurements for three sites was 12 cm (6.5%).

Wind redistributes snow, resulting in a thinner and denser snow layer over lakes than over land (Sturm and Liston, 2003), with a reported average fraction of 52% between the snow depth measured over lake ice and the snow depth measured over land at the Barrow weather station (Zhang and Jeffries, 2000). Considering the wide fluctuations in snow cover fraction

associated with its redistribution during the winter season and accounting for wide variations observed in snow density (198-390 kg m^{-3}) in this area (Sturm and Liston, 2003), model simulations for the snow scenario were performed with a 53% snow depth fraction and a fixed snow density of 335 kg m^{-3}. The calculated snow depth fraction over lakes and model input for snow density was based on available field measurements in the Barrow region from 1991 to 2006.

3.5 Results

3.5.1 SAR-data analysis

A 20-year time series of ERS-1/2 SAR images (1991-2011) – with acquisition dates between mid-December and late April for all but three years (1996, 2002 and 2004) when April images were not available and early May acquisitions were used instead (Table 3.1) – was analyzed.

The results show not only an expected inter-annual variability but also a gradual transition toward higher floating ice fractions, particularly noticed during recent years. The observed fraction of grounded ice, calculated as a monthly mean, gradually increased during the winter, from a December mean of 15% to a mean of 43% in April, when ice is most likely to grow to its maximum thickness.

Assessment of grounded ice fractions during the winter seasons (1991-2011) with available ERS imagery indicates a gradual trend toward lower fractions of grounded ice in all months of observations in the image time series. The greatest change was observed to occur in April, with maximum deviation values (±15-18%) from the monthly mean of 43% calculated from all years (1992-2011) and a standard deviation of 9.83. The highest positive deviation was observed in 1992 (more grounded ice) and the highest negative value in 2011 (less grounded ice).

Table 3.1: Dates of ERS-1/2 acquisitions used for image segmentation in order to determine the monthly fraction of grounded ice (1991-2011).

	Day and month of SAR acquisition					
Year	December	January	February	March	April	May
1991	30-Dec					
1992	16-Dec	20-Jan	13-Feb	17-Mar	20-Apr	
1993	25-Dec	25-Jan	10-Feb	17-Mar	21-Apr	
1994	10-Dec	21-Jan	17-Feb	16-Mar	29-Apr	
1995	15-Dec	16-Jan	22-Feb	11-Mar	14-Apr	
1996		04-Jan	23-Feb			03-May
1997	20-Dec		08-Feb		19-Apr	
1998	24-Dec	24-Jan	12-Feb	19-Mar	23-Apr	
1999		28-Jan			24-Apr	
2000	28-Dec	13-Jan	17-Feb	23-Mar	08-Apr	
2001	13-Dec			24-Mar	28-Apr	
2002		17-Jan				02-May
2003	18-Dec		06-Feb		17-Apr	
2004	18-Dec	17-Jan	21-Feb	11-Mar		06-May
2005	22-Dec	22-Jan	10-Feb	17-Mar	21-Apr	
2006				16-Mar	22-Apr	
2007	22-Dec			22-Mar	26-Apr	
2008	27-Dec	12-Jan		22-Mar	10-Apr	
2009	31-Dec	15-Jan	19-Feb	26-Mar	09-Apr	
2010		16-Jan	20-Feb	25-Mar	29-Apr	
2011		20-Jan		17-Mar	16-Apr	
				26-Mar		

The transition toward lower fraction of grounded ice during late winter (April) correlates well with the trend toward thinner ice covers as indicated by model simulations during the same period ($r = 0.75$, $p < 0.001$; Figure 3.4).

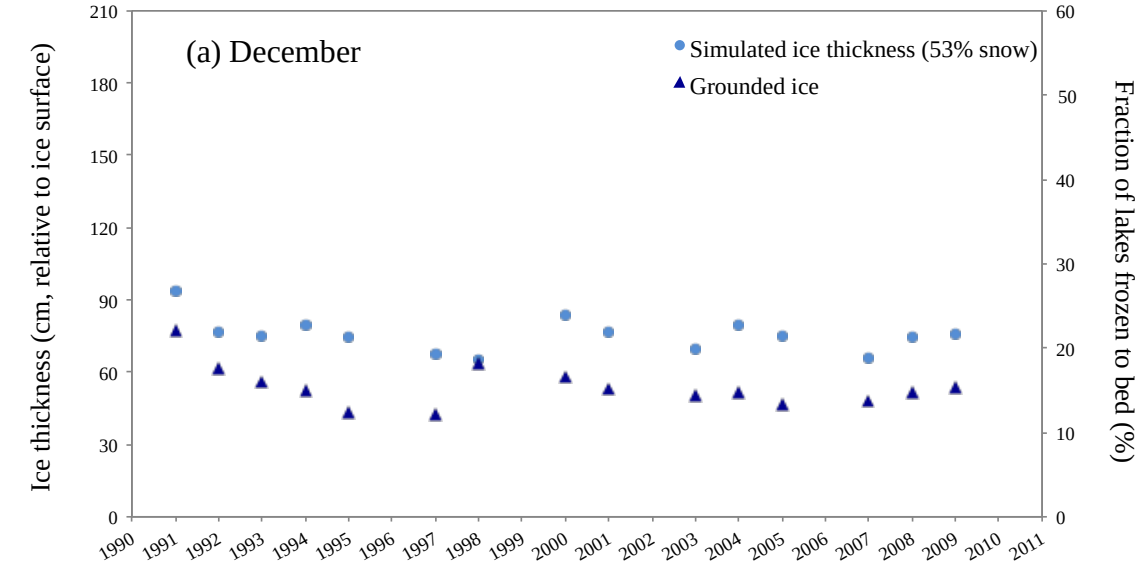
(a) December
Simulated ice thickness (53% snow)
Grounded ice
Ice thickness (cm, relative to ice surface)
Fraction of lakes frozen to bed (%)
210
180
150
120
90
60
30
0
60
50
40
30
20
10
0
1990
1991
1992
1993
1994
1995
1996
1997
1998
1999
2000
2001
2002
2003
2004
2005
2006
2007
2008
2009
2010
2011

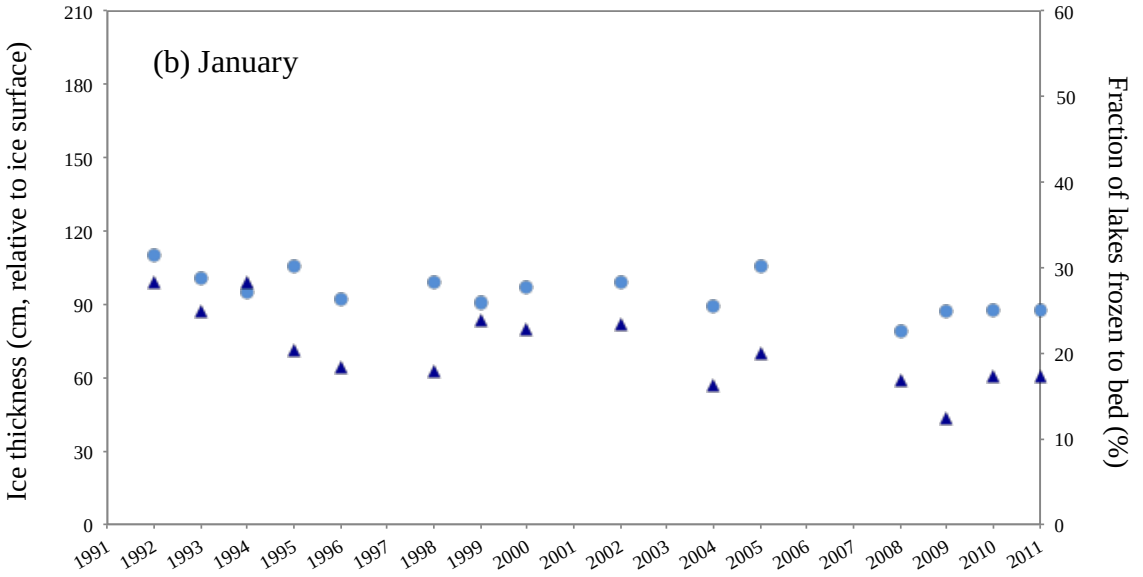
(b) January
Ice thickness (cm, relative to ice surface)
Fraction of lakes frozen to bed (%)
210
180
150
120
90
60
30
0
60
50
40
30
20
10
0
1991
1992
1993
1994
1995
1996
1997
1998
1999
2000
2001
2002
2003
2004
2005
2006
2007
2008
2009
2010
2011

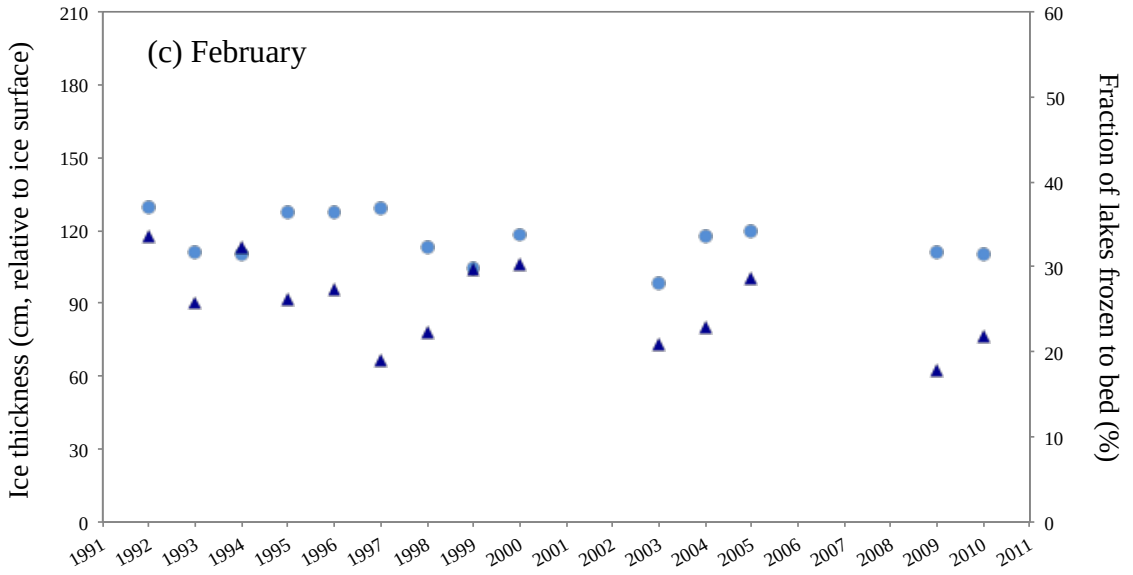
(c) February
Ice thickness (cm, relative to ice surface)
Fraction of lakes frozen to bed (%)
210
180
150
120
90
60
30
0
60
50
40
30
20
10
0
1991
1992
1993
1994
1995
1996
1997
1998
1999
2000
2001
2002
2003
2004
2005
2006
2007
2008
2009
2010
2011

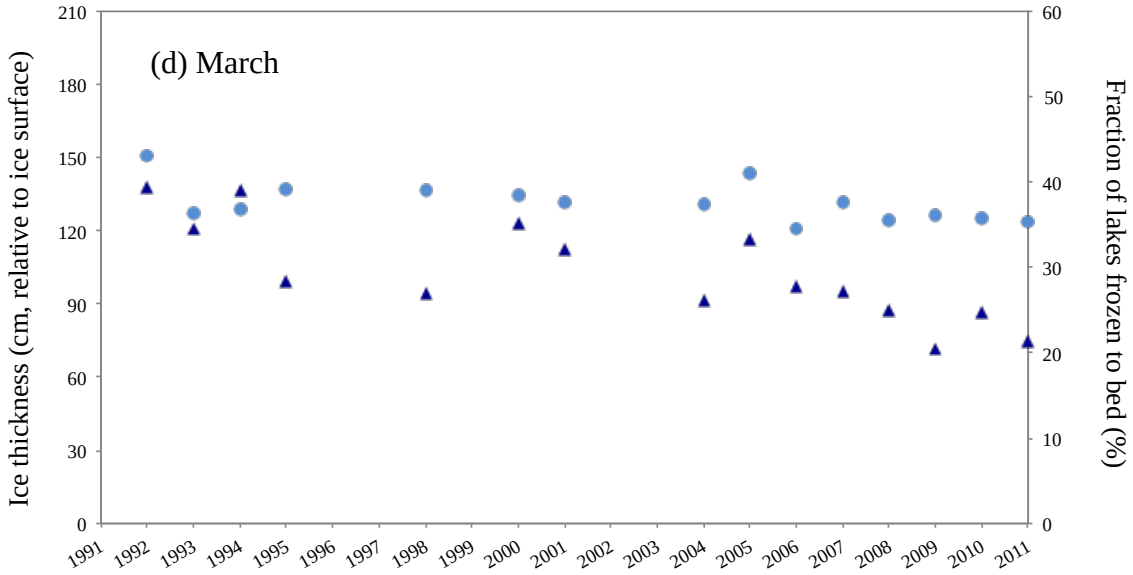
(d) March
Ice thickness (cm, relative to ice surface)
Fraction of lakes frozen to bed (%)
210
180
150
120
90
60
30
0
60
50
40
30
20
10
0
1991
1992
1993
1994
1995
1996
1997
1998
1999
2000
2001
2002
2003
2004
2005
2006
2007
2008
2009
2010
2011

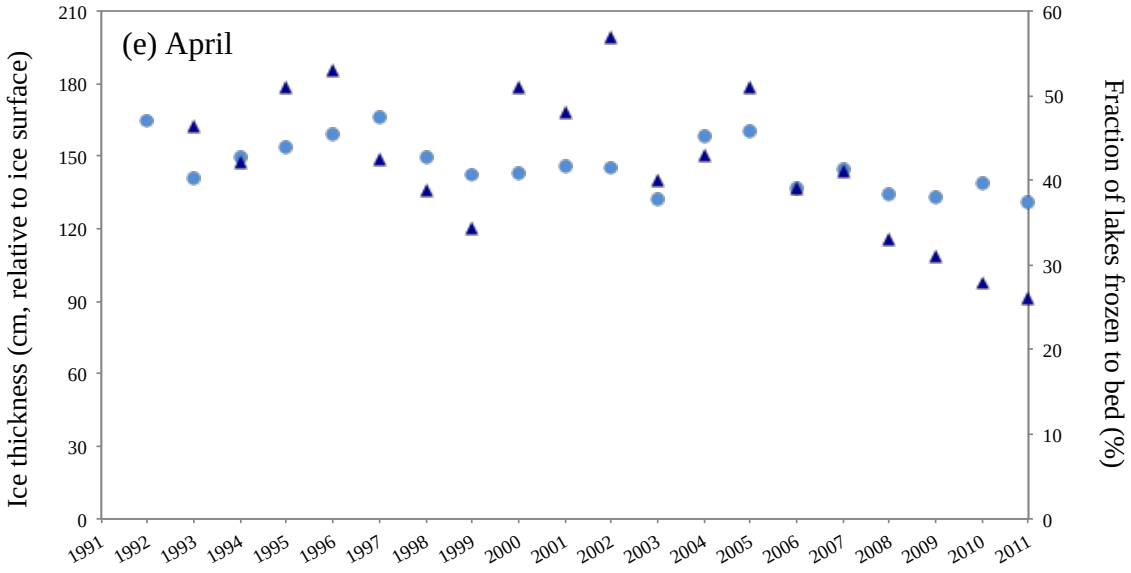

Figure 3.4: Monthly fractions of lakes frozen to the bed as derived from analysis of available ERS images and simulated ice thickness on day of ERS acquisition (1991 to 2011) – (a) December, (b) January, (c) February, (d) March and (e) April.

The trend accentuated from 2006 onward (as observed in Figure 3.5), has also been reported in a similar study from an adjacent region of the NSA (Arp et al., 2012). Trend detection was performed using the Mann-Kendall test, a method often used for detecting the presence of temporal trends in long-term lake ice observations (Futter, 2003, Duguay et al., 2006). Trend magnitude (slope) was estimated with Sen's method (Sen, 1968; Duguay et al., 2006; Noguchi et al, 2011).

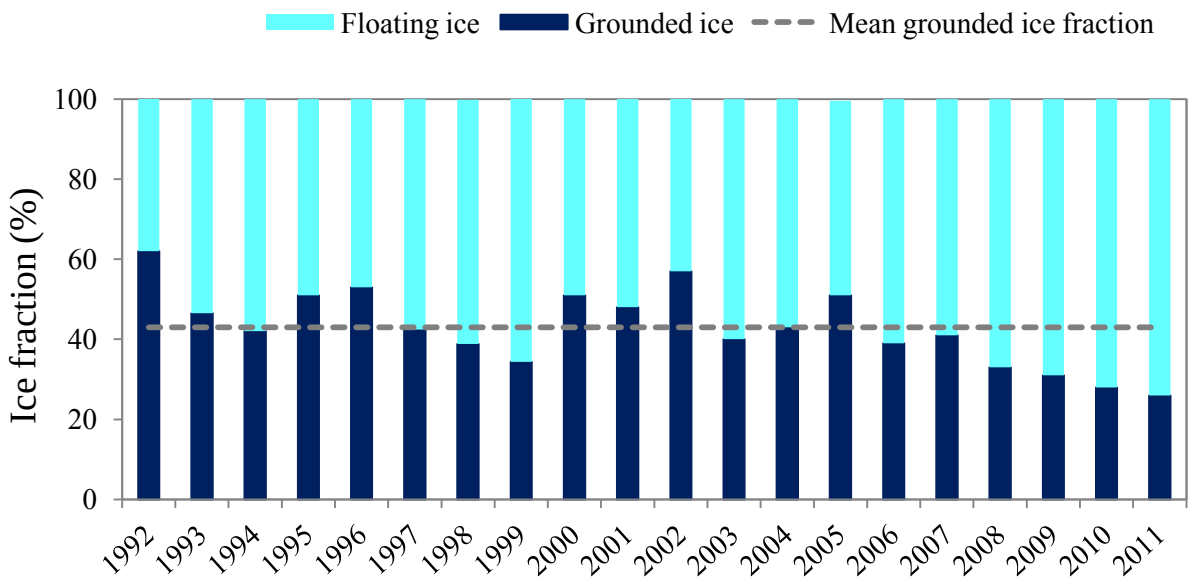

Figure 3.5: Late winter (April/May) floating and grounded ice fractions from 1992 to 2011 resulting from segmentation of ERS-1/2 images.

Statistical analysis of SAR data over the 20-year period, indicates a decrease of 22% in the fraction of lakes that freeze to the bed in April (1.1% year^{-1}, $\alpha = 0.01$). The maximum number of lakes froze to their beds in 1992 when the fraction of grounded ice was 62%, as opposed to 2011 when a minimum fraction of 26% of bedfast ice was noticed. The 2011 lowest April fraction of grounded ice was also observed with Envisat Advanced Synthetic Aperture Radar (ASAR) imagery from 2003 to 2011 (Arp et al., 2012).

3.5.2 Model results

The performance of CLIMo versus field-measured ice-on, ice-off dates, and thickness and against ice-on and ice-off dates from satellite observations was previously shown to agree well (Duguay et al., 2003). To further demonstrate the good agreement of CLIMo with *in situ* measurements, model results were statistically compared to observed mean ice thickness during several years with available field data. Accurate ice thickness simulations are dependent on using representative snow cover depths and densities over lakes for model runs.

Data on ice thickness, snow cover depth, and rarely, snow density over lakes is available for a selection of lakes near Barrow for the 1978/79 (Imikpuk Lake, Ikroavik Lake and West Twin Lake; Mellor, 1982) and 1991/1992 (Ikroavik Lake, Emaiksoun Lake and Emikpuk Lake; Jeffries et al., 1994) ice seasons. The Mean Bias Error (MBE) with both snow scenarios (0% and 53%) compared to *in situ* measurements was +8 cm (4%), indicating that CLIMo generates reliable ice thickness simulations for lakes in the Barrow region.

The longer historical-trend analysis (1950-2011) of maximum ice thickness derived from CLIMo simulations indicates the development of thinner ice covers on the Alaskan shallow lakes. Model runs with two different climate scenarios (0% and 53% snow cover depth), forced with data from the Barrow meteorological station, show a significant decline (α = 0.001) in the maximum ice thickness of a total of 21 cm (no-snow cover) and 38 cm (53% snow cover depth) for the period 1950-2011. Simulated maximum ice thickness with 0% and 53% snow cover depth respectively, ranged from 196 cm and 140 cm in 2011 to 238 cm and 209 cm (α = 0.001) in 1976. The ice thickness simulated with CLIMo using a snow depth of 53% correlates well with the SAR-derived ice cover fractions for lakes frozen to the bed versus lakes with floating ice (r = 0.75, α < 0.001), a thinner ice cover corresponding to a lower fraction of lakes frozen to the bed and thicker ice indicating a higher grounded ice fraction (Figure 3.6). For the overlapping years with the ERS-1/2 SAR images (1991-2011), model simulations with no-snow and 53% snow depth scenarios show a decline in the maximum ice thickness by 18-22 cm (α = 0.01).

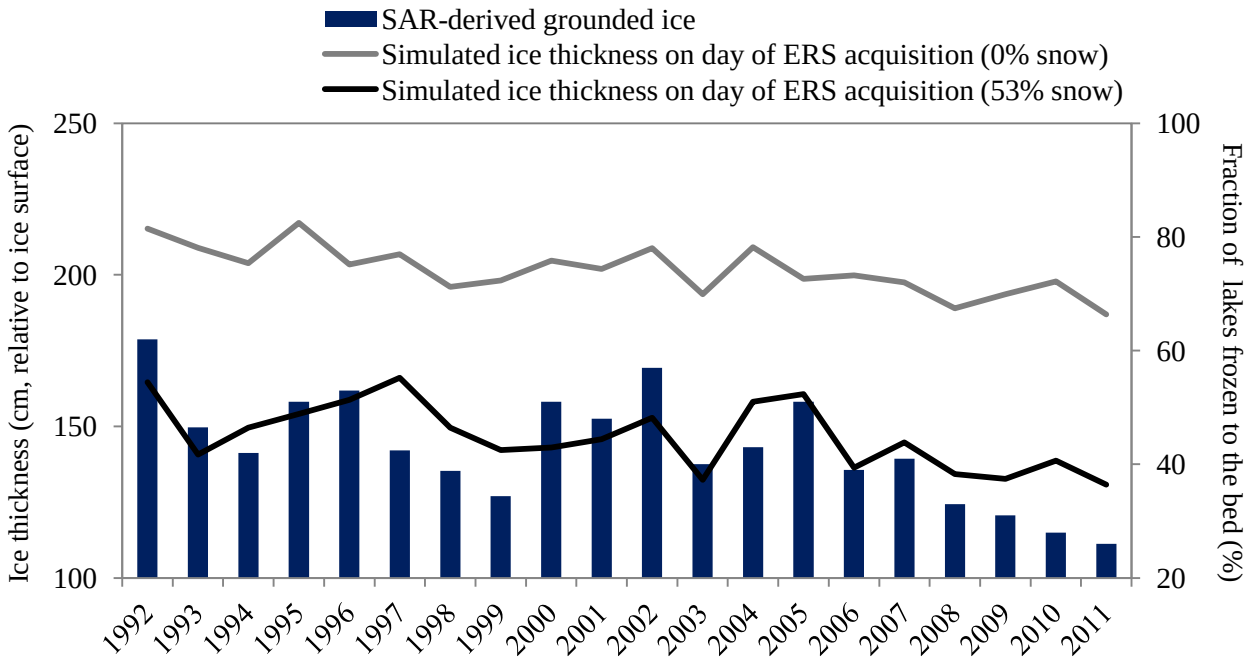

Figure 3.6: SAR-derived fraction of grounded ice and simulated ice thickness from CLIMo on day of ERS acquisitions from 1992 to 2011.

Additionally, CLIMo simulations indicate that, in response to warmer climatic conditions as reflected by the increase in annual mean air temperature and total precipitation during recent decades, the duration of the ice cover has reduced, with later freeze-up dates by 5.9 days and break-up dates occurring earlier in the season by 18.6 days with 0% snow cover and by 17.7 days with the 53% snow cover depth scenario from 1950 to 2011 (Figure 3.7).

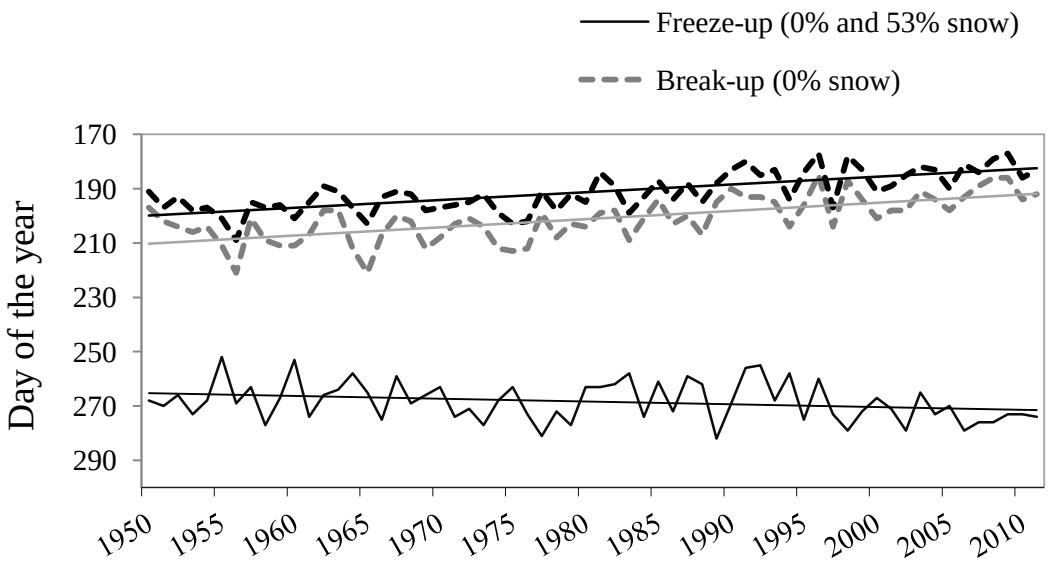

Figure 3.7: CLIMo-simulated freeze-up and break-up dates from 1950 to 2011. Trendlines are also shown.

During the 62-year period, CLIMo indicates a decrease in the duration of the ice seasons by a total of 24.8 days (2.5 days/decade) in the absence of a snow cover and by 23.6 days (2.6 days/decade) with 53% snow cover depth. Statistically, freeze-up and break-up, and the duration of the ice season trends, with both snow cover depth scenarios, are equally significant at the $\alpha = 0.001$ level. For the period of the ERS imagery analysis (1991-2011), model simulations indicate later ice-on dates by 14.5 days ($\alpha = 0.05$), earlier ice-off dates by 5.3 days ($\alpha > 0.1$) with the no-snow scenario and no change in the ice-off dates ($\alpha > 0.1$) with the 53% snow depth scenario.

3.6 Discussion

3.6.1 Ice cover changes: 1950-2011

Analysis of ice-thickness trends from CLIMo simulations during the 1950-2011 period indicates a trend toward thinner ice covers for the Alaskan lakes under study, a trend that is more evident with 53% snow cover depth conditions and that indicates a decrease of a total of 38 cm in ice thickness, at a rate of 0.6 cm $year^{-1}$.

Albeit inter-decadal and inter-annual variability is noted, trend analysis of ice phenology from 1950 to 2011 indicates a slight change in freeze-up dates, ice onset occurring later in the season by 5.9 days and a significant advancement of ice melt by 17.7 to 18.6 days (0% and 53% snow depth scenarios). These results are supported by similar findings that show a significant trend toward later ice-on and earlier ice-off dates, and overall shorter ice seasons of lakes across the northern hemisphere, a trend accentuated during recent decades (Magnuson et al., 2000; Duguay et al., 2006; Benson et al., 2011). Shorter ice seasons have been mainly attributed to the advance of break-up days earlier in the spring (Bonsal et al., 2006), earlier ice-off being associated with higher spring air temperatures and earlier snow melt onset (Duguay et al., 2006). CLIMo simulations for the 1950-2011 period suggest that the length of the ice season has declined by 23.6-24.8 days (53% and 0% snow cover depth scenarios). In a 53% snow cover depth scenario, the shortest ice seasons were identified to have occurred in recent years, with 1998 being the year when lakes were ice free for a total of 101 days, followed by 2006 (ice free for 98 days) and 2009 (ice free for 97 days). Using the same climate scenario (53% snow depth), model simulations show that 1955, 1960 and 1965 (51, 52, and 59 days respectively) were the years when lakes had the most extended ice coverage. To support the strong correlation previously shown to exist between ice-off dates and ice-cover duration (Duguay et al., 2006), shorter ice seasons occurred in all years of early ice-off dates in both snow cover depth scenarios but not all years with reduced ice duration had later ice-on dates.

3.6.2 Ice cover changes: 1991-2011

3.6.2.1 SAR-observed changes

During the 20-year period of SAR analysis, a specific temporal pattern in the evolution of the grounded ice fraction for individual lakes on a yearly basis was not observed. Considering that the fraction of grounded ice is strongly dependent on climate conditions, the inter-annual variability of air temperatures and that of the snow cover impacts is being reflected by the variations in the yearly bedfast ice fraction. For example, the climatic conditions of a cold winter (1991/1992) and a warm winter (2010/2011) season, differed largely. The ice-growing season (October to April) of 1991/1992 was characterized by lower mean air temperatures (-22 °C) and reduced total snowfall (561 mm) as opposed to the higher winter mean air temperatures (-17.7 °C) and greater amount of total snowfall (1199 mm) of 2010/2011. The observed fraction of lakes frozen to the bed was greater during the colder ice season, with values ranging from a minimum of 18% in December to a maximum of 62% in April. Noteworthy is also the fact that the fraction of grounded ice observed in April 1992 (62%) was the highest among all years of available SAR data. In addition to inter-annual variability of the grounded ice fraction, inter-lake differences were observed during the 20 years of available SAR data. For instance, the shallower West Twin Lake (71°16’ N, 156°29’ W, 1.2 m maximum depth), located close to the Beaufort Sea, developed bedfast ice during all years of observations, whereas the deeper Ikroavik Lake (71°13’ N, 156°37’ W, 2.1 m maximum depth), further from the Arctic coast, maintained a floating ice cover throughout all winter seasons.

Ice regimes of shallow coastal lakes on the NSA correlate with the distance from the coast, with lakes closer to the coast in this study area preserving their ice cover later into the season (Hinkel et al., 2012). The discrepancies in ice regimes of these lakes may therefore be attributed to temperature gradients or snow-cover redistribution within the area and that are associated with the distance from the coast. Ice regimes are also related to lake depth, with

deeper lakes maintaining liquid water underneath the ice (Jeffries et al., 1996) in the deeper areas of the lakes while shallower water near the coast could freeze to bed.

3.6.2.2 Simulated changes

Ice growth and downward thickening is strongly influenced by snow cover over lake ice (Vavrus et al., 1996; Ménard et al., 2002; Gao and Stefan, 2004), which influences the vertical conductive heat flow from the ice to the atmosphere through heat loss at the air-snow interface (Jeffries et al., 1999). A thinner and denser snowpack provides less insulation and allows higher rates of heat flow to the atmosphere (Sturm and Liston, 2003). Thus, the accentuated reduction of ice thickness and number of lakes that freeze to the bottom from 2006 onwards may be associated with deeper snow resulting from increased winter precipitation (Callahan et al., 2011), a consequence of higher air temperatures (Schindler and Smol, 2006; Kaufman et al., 2009, Walsh et al., 2011). From 1991 to 2011, simulated ice thickness declined by 18-22 cm (no-snow and 53% snow depth scenarios). Consequently, thinner ice covers are linked to the noticeable trend toward fewer lakes freezing to the bed during the past 20 years, as observed from the analysis of SAR data (Fig. 6). Since ice cover conditions are better captured assuming a 53% snow depth atop lakes versus no-snow cover when compared to available field measurements, analysis of overlapping CLIMo and SAR results indicate a closer agreement between the ice thickness and the fraction of grounded ice during the former scenario, with slight discrepancies in 1994, 1997, 2001 and 2010. The disagreement between model simulations and SAR observations is possibly associated with the timing of snow accumulation during the winter season, greater snow depth at the time of ice formation leading to thinner ice.

From 2006 onwards, model simulations indicate smaller changes in ice thickness whereas satellite observations indicate a significant reduction of the grounded ice fraction. One hypothesis to consider when explaining the considerable SAR-derived changes in grounded ice and the small changes in simulated ice thickness from 2006 onwards is the yearly

variation in ice thickness. Minimum changes in ice thickness should occur, once a threshold is reached, thinner ice covers are reflected by the higher fractions of floating ice. Increasing lake water levels at the time of freeze-up or greater lake depths are aspects to also consider in explaining the differences between the changes in grounded ice and those in ice thickness. Since calculated P – E values do not indicate higher water levels from 2006 to 2011 changes in lake depth may explain the minor ice thickness changes. However, considering the lack of data on lake bathymetry, this hypothesis needs to be further investigated.

3.6.3 Teleconnections and lake-ice regimes

Air temperature changes at high latitudes are often related to the decreasing extent of sea ice, which allows more radiation to be absorbed by the Arctic ocean, heat that is later released to the atmosphere. Additionally, changes in the air temperature are also associated with large-scale atmospheric and oceanic circulations. Previous analysis of teleconnection patterns that affect the northern hemisphere climate and weather reveals that lake ice conditions are partly driven by these large-scale circulations and exhibit stronger correlations with spring (January-April) climatic indices (Bonsal et al., 2006). For western Canada, the strongest correlation between teleconnections and ice phenology was associated with the Pacific North American (PNA), a positive phase of the PNA being highly correlated with earlier break-up dates ($r = -0.74$) and vice versa (Bonsal et. al., 2006). To articulate this relationship, one third of the variability in northern hemisphere winter temperatures variability of previous decades can be explained by the positive phase of the North Atlantic Oscillation (NAO; Hurell, 1996). Likewise, a shift of the Pacific Decadal Oscillation (PDO) in 1976 toward a positive phase contributed to increased northward advection of warm air (Morris et al., 2005), which is highly noticeable in Alaska, being well reflected by the recent increased warming of the area (Hartmann and Wendler, 2005). The PDO shift is also reflected in the CLIMo simulations that indicate a transition toward thinner ice covers from 1976 onward. Given that El Niño years have been associated with up to ten days shorter ice seasons for lakes in western Canada (Bonsal et al., 2006), the fact that the longest open-water season occurred

during an extreme El Niño year (1998) is associated with considerable warmer air temperatures recorded that year at the Barrow meteorological station.

3.6.4 Water levels and lake-ice regimes

In response to warmer climate conditions during recent decades, the spatial distribution and the surface area of Arctic lakes has been noted to change. In ice-rich permafrost areas such as the NSA, changes in air temperature alter the frozen ground layer that, by thawing, may result in the appearance of new water bodies or increasing surface areas of the existing lakes as a result of thermally induced lateral expansion (Jones et al., 2011). Alternatively, as many lakes in this area have low water volumes, lake water levels will rapidly respond to changes in the water budget, expressed as total precipitation (P) minus evaporation (E), P-E. Calculated water balance during the ice-free season also includes spring snow-water equivalent (SWE). Thus, a negative water balance (P<E) results in reduced lake levels and/or intermittent lake disappearance (Smol and Douglas, 2007) with lakes disappearing during dry seasons and refilling during wetter seasons. Hinkel at al. (2007) showed that from 1975 to 2000, over 25% of lakes on the western ACP experienced shoreline retreat through lateral drainage, the lake area change not being strongly supported by climate conditions during the period of analysis. This may be seen in the case of Sikulik Lake (71°18’ N, 156°40’ W) that appears to have experienced fluctuating water levels during the 20-year period as indicated by the differences in radar returns from this lake in late winter (Figure 3.8).

As radar returns for this lake were similar to those of the adjacent land, the assumption made was that the lake drained in most years and that it may have filled in 2000 and 2002, both years with a positive water balance. Lake water levels are greatly controlled by precipitation and evaporation rates during the summer season when lakes are exposed to energy exchanges with the atmosphere and variations in the lake water balance can be explained by fluctuations in the P-E (Bowling et al., 2003). In the case of Arctic lakes, the overall lake water balance is

generally negative, as the high evaporation during summer is not compensated by higher amounts of precipitation (Rovansek et al., 1996).

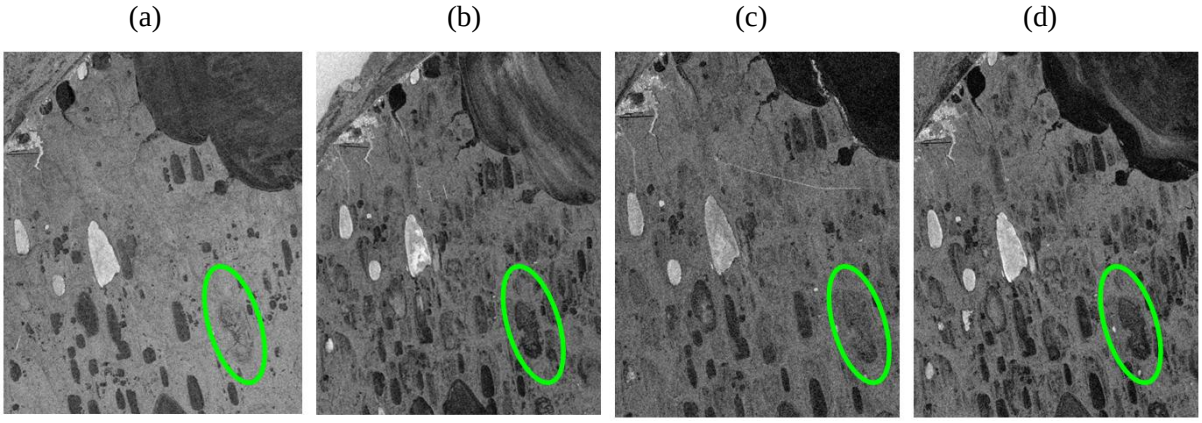

Figure 3.8: Late winter (April/May) differences in radar returns from Sikulik Lake – (a) 1992, (b) 2000, (c) 2001 and (d) 2002.

Positive values of the P-E index are associated with lower annual mean air temperatures and wetter conditions during the ice-free season while lower water levels are recorded during warm and dry years (Labrecque et al., 2009). Extreme P-E values (i.e., 1993, 2010, 2011 - warm years, and 1995, 2005 - cold years) correlate well with the grounded ice fraction, lower grounded ice fraction being strongly related to the positive P-E values, and higher grounded ice values matching well those of negative P-E. During the years of extreme P-E values, grounded ice fractions also correlate with mean air temperatures ($r = 0.68$, $p < 0.0010$). Additional periodic recharge through ground water, spring snowmelt and river inflows, or lateral drainage and ice melt within the underlying permafrost (Young and Woo, 2000) can occur and consequently affect lake water balance, and thus explaining the discrepancies between lake water levels and ice conditions. These are tentative explanations and the relationship between water balance and grounded ice fraction needs to be further investigated.

3.7 Summary and Conclusions

This study aimed to detect changes in ice thickness, the fraction of lakes/lake areas freezing to the bed versus those developing a floating ice cover and phenology (freeze-up and break-up dates, and ice cover duration) of Arctic shallow lakes near Barrow, in a sub-region of the North Slope of Alaska. The methods employed were image segmentation of ERS-SAR images acquired over the region from 1991 to 2011 and simulations with two different snow depth scenarios (0% and 53%) of a numerical lake model forced with climate data from the Barrow meteorological station between 1950-2011.

A trend toward an increasing number of lakes that maintain liquid water underneath the floating ice atop in all months of available SAR imagery (December to early May), and thinner ice covers during the winter months was identified from ERS analysis and CLIMo simulations. Statistical analysis showed that in the case of thermokarst lakes near Barrow, the fraction of bedfast ice as extracted from the analysis of ERS-1/2 SAR data (1991-2011) correlates well with the thickness of the ice layer simulated with CLIMo. The most significant decrease in grounded ice was noticed to occur in late winter, grounded ice that considerably declined since 2006 and reached its lowest in 2011. Model outputs indicate thinner ice covers by 18 to 22 cm (1991-2011) and by 21 to 38 cm (1950-2011), and extended duration of the ice season – a function of later ice-on and earlier ice-off dates – by a total of 23.6 days (1950-2011) with a 53% snow depth scenario.

SAR data provides the opportunity to effectively monitor Arctic lakes and assess the degree of changes in winter lake ice growth in response to climate conditions. Low-resolution ERS imagery allows an adequate detection of the rate at which lakes freeze to their bed for the duration of the ice season and of the grounded ice fraction at the end of winter, thus providing a valuable data set. The use of satellite sensors that provide higher temporal coverage, such as ASAR Wide Swath (2002-2012), would further improve the investigation of ice regimes of high-latitude lakes. Future satellite missions of the European Space Agency

(Sentinel-1a/b), the National Aeronautics and Space Administration (Surface Water and Ocean Topography – SWOT) and the Canadian Space Agency (the RADARSAT constellation) are planned for launch in 2013, 2019 and 2018, respectively. These missions will not only continue the C-band SAR operational applications (Sentinel-1a/b and the RADARSAT constellation) and enable accurate monitoring of water levels (SWOT) but also provide increased temporal resolution, thus ensuring frequent, long-term SAR acquisitions for the Arctic regions.

3.8 Acknowledgements

This research was supported by European Space Agency (ESA-ESRIN) Contract No. 4000101296/10/I-LG (Support to Science Element, North Hydrology Project) and a Discovery Grant from the Natural Sciences and Engineering Research Council of Canada (NSERC) to C. Duguay. The ERS-1/2 SAR images are copyright ESA 1991-2011 and were provided by the Alaska Satellite Facility (ASF).

Chapter 4

Ice freeze-up and break-up detection of shallow lakes in Northern Alaska with spaceborne SAR

4.1 Introduction

Freshwater lakes are a ubiquitous feature of the Arctic landscape. In the lake-rich coastal Northern Alaskan tundra, shallow thermokarst lakes cover up to 40% of the land area (Sellman et al., 1975; Li et al., 2000). During recent decades (1991-2011), these lakes have experienced a shift from a grounded-ice to a floating-ice regime – with 22% less lakes freezing to the lakebed, thinner ice covers by 21-38 cm, and shorter ice seasons as a result of later ice-on dates by 14.5 days and earlier ice-off dates by 5.3 days (Surdu et al., 2014). In an Arctic climate that experiences increasing surface air temperatures (Screen and Simmonds, 2010; IPCC, 2013), higher amounts of snowfall from October to May (1936-2009) in most regions (AMAP, 2012), reduced snow-cover duration (by 3.9 days per decade (1972-2008); AMAP, 2012) and decreased spring snow-cover extent (by 14% in May and 46% in June, from 1967 to 2008; Brown et. al., 2010), thaw lakes are undergoing noticeable changes (Arp et al., 2011; Surdu et al., 2014).

Changes in the ice cover of these Arctic lacustrine ecosystems affect the underlying permafrost by promoting thaw of formerly perennially frozen sediment and leading to talik development, as a result of a regime shift from grounded to floating ice (Ling and Zhang, 2003). Thinner ice covers, earlier timing of lake ice-off dates, and longer open-water seasons influence summer water temperature, lake-water balance, aquatic biota, and water availability for residential and industrial use. The overall shorter ice seasons of lakes on the Alaskan North Slope (Surdu et al., 2014) may also impact ice-road transportation in the region during winter. If the recently investigated changes continue, it is anticipated that Alaska will lose 29% of its ice roads by 2050 (Stephenson et al., 2011).

The ice cover of Arctic lakes has been identified to be very responsive to near-surface air temperatures, particularly during the break-up season (Hinkel et al., 2012). Given the bathymetry-related reduced heat capacity of smaller and shallower lakes, the response of these lakes to changes in air temperatures is rapid. Lakes on the coastal North Slope of Alaska (NSA) strongly reflect this sensitivity (Jeffries et al., 1996).

Previous studies showed that even though both complete-freeze-over and water-clear-of-ice dates are highly synchronous with the 0°C fall and spring isotherm dates, a stronger correlation exists between the timing of water-clear-of-ice dates and surface air temperatures (Duguay et al., 2006); lake ice decay is sensitive to synoptic weather conditions (Palecki and Barry, 1986), including changes in air temperature, snow and/or wind. The effect of air temperature on lake ice is smaller during freeze-up than it is during break-up, as freeze-up is also dependent on lake morphometry (depth, area and volume), wind speed, and non-climatic variables such as elevation or latitude. Recent warming at higher latitudes is likely to result in later ice freeze onset (FO), and earlier water-clear-of-ice (WCI) dates for lakes across the Arctic.

Lake ice phenology has been investigated with both optical and SAR data. Limited by the coarse spatial resolution (e.g., 250-500 m MODIS optical data), low sun elevation and presence of the cloud cover, optical sensors do not allow lake ice monitoring year round at high latitudes. To overcome these limitations, SAR monitoring provides a feasible alternative. With a history of over two decades, SAR systems have demonstrated their ability to monitor ice phenology of Arctic and sub-Arctic lakes through analysis of the backscatter temporal evolution, at C-band (Jeffries et al., 1994, 1996; Morris et al., 1995; Duguay et al., 2002; Duguay and Lafleur, 2003; White et al., 2008; Cook et al., 2010; Geldsetzer et al., 2010; Geldsetzer et al., 2013) and Ku-band frequencies (Howell et al., 2009).

High temporal resolution spaceborne observations are a prerequisite for studying the impact of climate variability and change on Arctic lake ice covers (IGOS, 2007). Previous satellite missions (e.g. ERS-1/2, ENVISAT, RADARSAT-1/2) alone did not provide the required high temporal frequency. This work is the first attempt to combine SAR observations from two different satellite sensors to detect ice phenological events on shallow Arctic lakes. The primary purpose of this study is to explore the potential of high temporal frequency (2-5 days) C-band SAR to detect lake ice events, in light of future Earth Observation satellite missions that will

provide frequent acquisitions at high latitudes. More specifically, the objectives of this study are: 1) to evaluate the ability of combined ENVISAT ASAR and RADARSAT-2 observations for detecting the timing of the initial ice formation (freeze onset), melt onset and end of the ice season (ice-off) of shallow lakes in a sub-region of the Alaskan Arctic Coastal Plain by employing an ice phenology algorithm based on "tracking" of the temporal evolution of backscatter; 2) to analyze the temporal variability in ice phenology from 2005 to 2011 of lakes, with overlapping observations between 2009-2011 prior to the end of the ENVISAT mission in early 2012; and 3) to asses SAR-observed lake ice parameters against results obtained with a numerical lake ice model.

4.2 Study Area

The lakes of interest are located in the vicinity of Barrow, on the North Slope of Alaska (NSA), USA, (71°31' N, 156°45' W), a coastal region bounded by ocean waters to the west (Chukchi Sea), north and east (Beaufort Sea) (Figure 4.1). Thermokarst lakes, mostly shallow (~3 m deep), are the predominant feature of the region and lie atop of a continuous permafrost layer. The ice cover of these lakes, many of which freeze entirely to the lakebed during winter, has been observed to be present for the most part of the year, lakes being ice free for only 6-16 weeks during the warmer summer months (Jeffries et al., 1994, 1996). Between 2005-2011, recorded annual mean air temperature at Barrow was -10°C and mean annual precipitation was 1,545 mm.

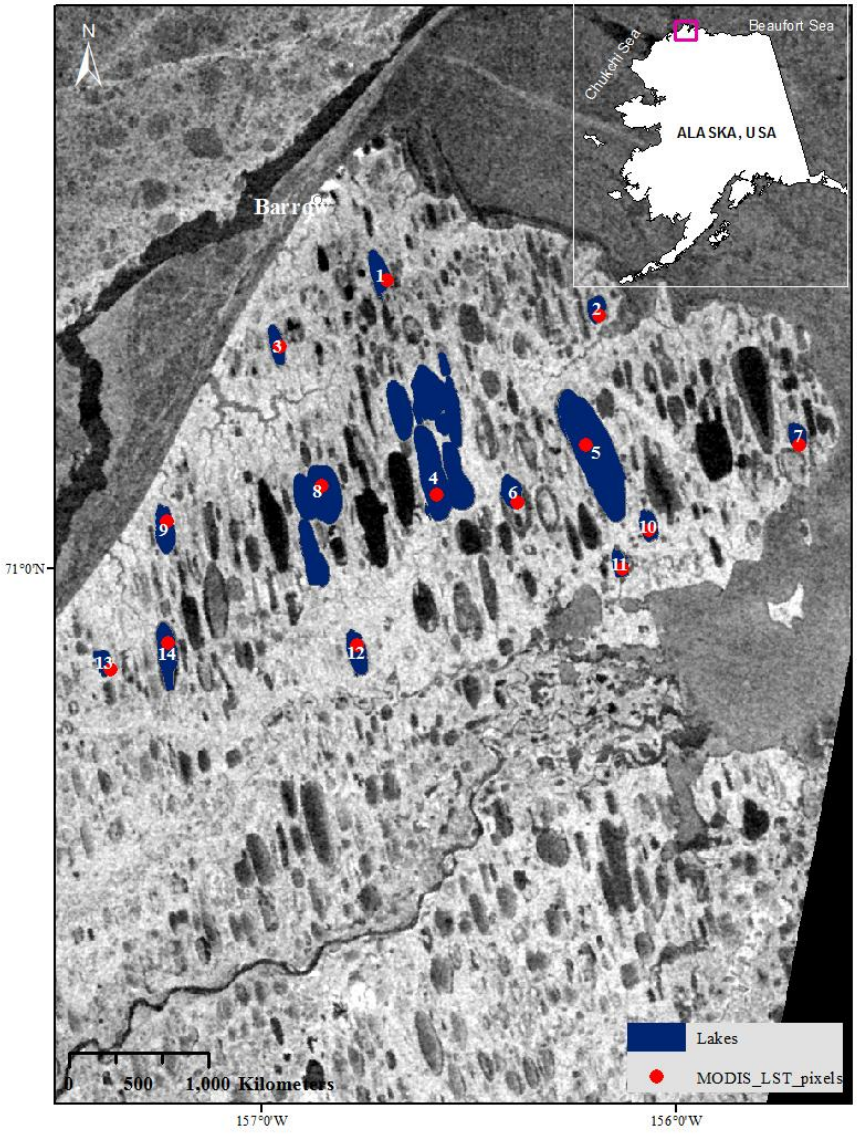

Figure 4.1: Map of the Alaskan North Slope, near Barrow, indicating the location of study lakes (dark blue) and the MODIS pixels used for extraction of lake surface temperature (red). The 5 June 2009 ASAR image is copyright ESA.

4.3 Data and Methods

4.3.1 Synthetic Aperture Radar (SAR)

This study used available C-band time series of ASAR Wide Swath (2005-2011) and RADARSAT-2 ScanSAR Wide A (2009-2011) images. While the RADARSAT-2 mission

continues to deliver data, the ENVISAT mission carrying the C-band ASAR sensor ceased in April 2012. The overlapping ASAR and RADARSAT-2 observation period (2009-2011) provides a higher temporal sampling frequency (2-5 days) than from a single satellite mission, thus enabling a more precise detection of lake-ice events. Ascending and descending, VV- and HH-polarized ASAR acquisitions were used from 2005 to 2011 (536 scenes). In order to maximize the temporal frequency, overlapping HH-polarized RADARSAT-2 observations from 2009-2011 (213 acquisitions) were also included in the analysis.

In order to avoid false detection of ice parameters because of the relatively low signal-to-noise ratio (reduced ice-water contrast) of the HV-RADARSAT-2 imagery (Geldsetzer et al., 2010), backscatter values were solely extracted from HH acquisitions. The two sensors provide observations at a spatial resolution of ~ 150 m for ASAR and 100 m for RADARSAT-2. Pixel spacing is 75 m x 75 m for ASAR and 50 m x 50 m for RADARSAT-2. Following radiometric calibration and geocoding of the images using the Next ESA SAR Toolbox (NEST) software, the inherent speckle present in SAR images was reduced using an adaptive Enhanced Lee filter with a kernel size of 3x3. In order to capture a wide range of lakes with different physical properties and situated in various locations of the NSA – shallow (e.g. West Twin Lake – max depth – 1.2 m)/deep (e.g. Imikpuk Lake – max depth 3.1 m) (Mellor, 1982), small/large (e.g. surface area of 2.7 km^2 for Unknown Lake I, 5.2 km^2 for Ikroavik Lake, 57.7 km^2 for Lake Sungovoak), inland/coastal, central/peripheral, eastern/western, northern/southern, with floating/grounded ice – 14 sample lakes or regions of interest (ROIs) were selected for analysis. The number of pixels within each ROI ranged from 323 to 6131 (Table 4.1). Selection of lakes of different depths was based on previous *in situ* observations for several lakes in this region (Mellor, 1982). Backscatter values (σ^0) of selected ROIs were extracted using the ENVI software, version 5.0. Following σ^0 extraction, the median σ^0 of each ROI was calculated and was used as a unique value for the ice phenological event observed on the date of the SAR acquisition; ranges of dates for important ice events for the 14 lakes were also provided. The terminology used for the purpose of this study applies to the entire area of the investigated lakes.

σ^0 was extracted from the 14 SAR ROIs and used to detect the beginning, the melt onset and the end of the ice season, by analyzing its temporal evolution. Differences in radiometric calibration of the two SAR sensors result in generally lower RADARSAT-2 mean σ^0 values by -3.56 dB,

likely explained by the differences in incidence angle (θ) and orbit between the images. C-band σ^0 between the freeze-up and break-up periods is controlled by ice thickness, snow and/or snow ice, the presence or absence of bubbles (particularly during freeze-up), and by the large difference between the dielectric constant (ε') of ice (3.2) and ε' of water (80) (Hall et al., 1994; Jeffries et al., 1994; Geldsetzer et al., 2013).

Table 4.1: List of the 14 sample lakes (ROIs), number of ASAR and RADARSAT-2 SAR pixels encompassed in each ROI and lake type.

ROI #	Lake Name	Number of ASAR pixels	Number of RADARSAT-2 pixels	Lake type
1	Ikroavik Lake	567	2098	coastal/central
2	Unnamed Lake A	328	1224	coastal/peripheral
3	Unnamed Lake B	390	1442	northern
4	Lake Sungovoak	6131	23148	large
5	Lake Tusikvoak	3833	14416	deep
6	Unnamed Lake C	465	1730	shallow
7	Unnamed Lake D	323	1234	western
8	Sukok Lake	2913	10985	floating ice cover
9	Unnamed Lake E	622	2352	eastern
10	Unnamed Lake F	372	1410	inland/peripheral
11	Unnamed Lake G	299	1103	inland/central
12	Unnamed Lake H	599	2232	southern
13	Unnamed Lake I	290	1094	small
14	Tractor Lake	813	3100	grounded ice cover

At C-band, the start of ice formation over lakes is indicated by the first considerable increase in σ^0 (Morris et al., 1995). FO detection is complicated by the low σ^0 contrast between the open water and the newly formed ice (Cook and Bradley, 2010), by the σ^0 sensitivity to wind speed and direction as well as the ice structure and thickness, roughness of the ice interface, all resulting in higher returns, and snow wetness (Geldsetzer et al., 2013), resulting in lower returns. On shallow lakes, the transition from an ice cover with minimum air inclusions (bubbles) at the beginning of the ice season to an ice layer with increased bubble density as ice growth progresses complicates the σ^0 analysis during freeze-up. As a result, the σ^0 oscillations during ice formation make detection of a continuous ice cover (complete freeze-over) uncertain. Given the limitations associated with deriving an accurate date of complete freeze-over, ice cover duration,

calculated from the date of complete freeze-over to the break-up date, was not computed. The current study considers the first significant σ^0 up-turn as the FO date for the selected ROIs. Once ice has reached its maximum ice thickness, high radar returns have been observed from a floating ice cover while grounded ice, or ice frozen to the lakebed, is indicated by low σ^0 (Jeffries et al., 1994).

Melt onset (MO) is identified by the first significant decrease in σ^0 given by the presence of water from internal melting of ice and/or a melting snow cover, and thus resulting in increased specular (Duguay et al., 2002; Howell et al., 2009). Following initial melt water drains off the ice surface and leaves a rough surface that results in high radar returns. Thaw and re-freeze events of ice and snow during the break-up period result in high fluctuations of σ^0. Low σ^0 is observed at the end of the ice season when water becomes clear of ice. High winds over the lake surface can also result in high σ^0 during the open-water season. The current analysis acknowledges the differences in backscatter as a result of the wide range of beam positions (incidence angles) but in order to increase the precision in detecting the initial ice decay and end of the ice season through more frequent acquisitions, the current analysis includes radar backscatter acquired at all available incidence angles. Incidence angles ranged between 15-42° for ASAR and 20-46° for RADARSAT-2.

In order to avoid false starts, a threshold is applied to the σ^0 values detected during stable ice winter conditions, calculated as the average of each SAR pixel from 1 January (DOY1) to 31 March (DOY90). For FO, an increase of 5.5 dB for ASAR, and an increase of 6.5 dB for RADARSAT-2 change in σ^0 was required to occur for two consecutive dates. This threshold is higher than that selected for MO (4 dB for ASAR and 5 dB for RADARSAT-2) in order to minimize FO detection errors associated with higher σ^0 from wind-roughened cracks, rafting and ridge formation (Howell et al., 2009). For detection of ice-off conditions, the applied σ^0 threshold was a decrease of 7.5 dB for ASAR and a drop of 8.5 dB for RADARSAT-2. A similar approach was employed in detection of ice phenology parameters for Great Bear Lake and Great Slave Lake through analysis of the temporal evolution of Ku-band σ^0 (Howell et al., 2009).

In order to evaluate the SAR observations for the detection of ice-off dates using the threshold method described above, segmentation of available SAR images on the derived mean ice-off date for all lakes was performed. The unsupervised K-means classification algorithm was used to

determine if ice was present on lakes on the date when ice-off was indicated by the σ^0 analysis. This common clustering method provides suitable discrimination between lake ice and water in SAR imagery during the break-up season (Sobiech and Dierking, 2013). Following subsequent iterations of individual image segmentation, each intensity value is assigned to the class with the nearest arithmetic mean. The final segmentation result provides a two-class map (ice and open water), with fractions (%) for each class. The final segmentation result provides a two-class map (ice and open water), with fractions (%) for each class (Figure 4.2).

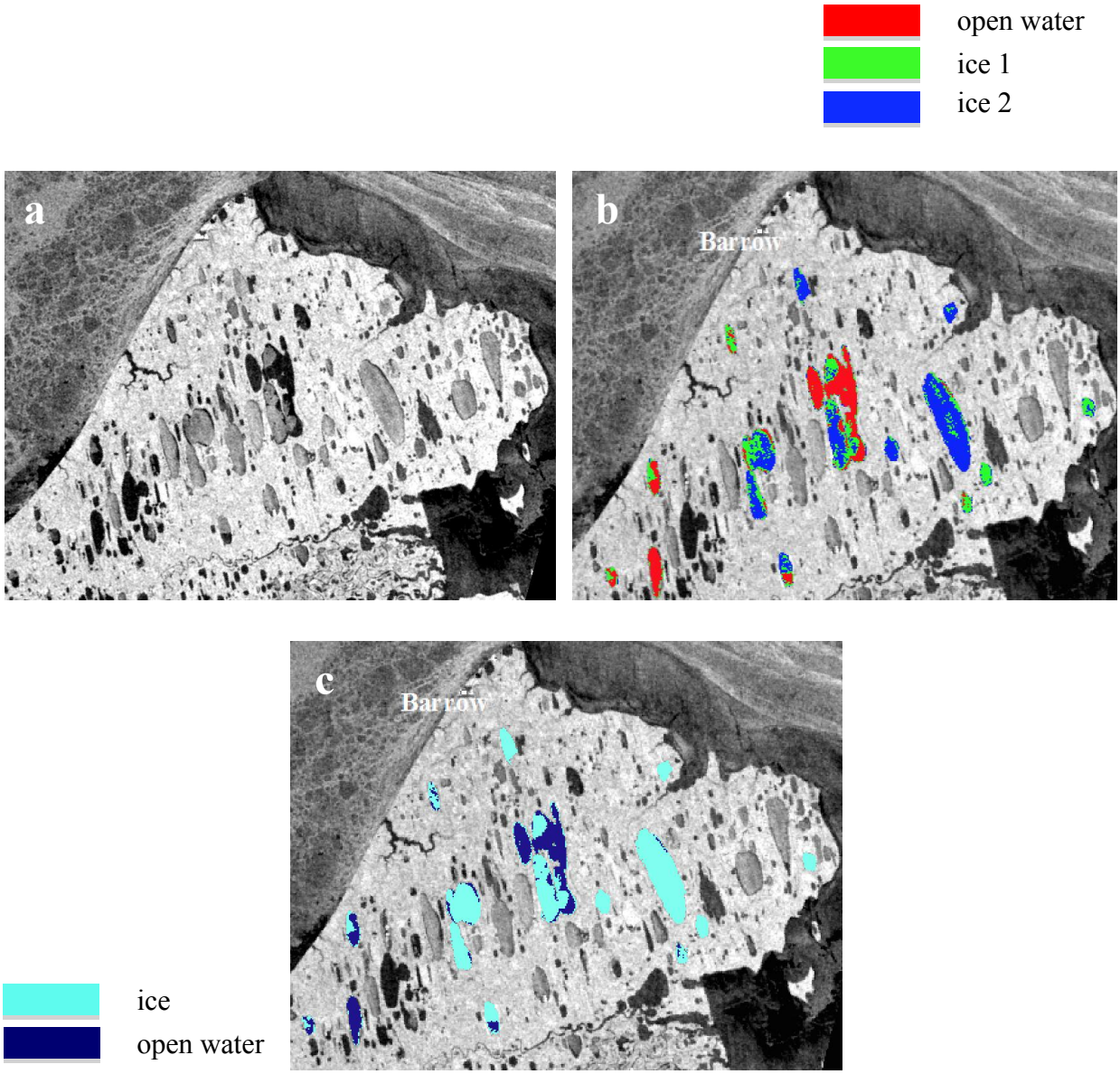

Figure 4.2: K-means image segmentation process of SAR images: (a) original SAR image, (b), K-means segmentation results (one open-water class and two ice classes) and (c) two-class map (ice in light blue and open water in dark blue).

4.3.2 Lake Ice Modeling

The one-dimensional Canadian Lake Ice Model (CLIMo) was used to provide some basis of comparison as to the general ice dates that should be expected from SAR observations. CLIMo was previously tested over freshwater Arctic lakes, including those located in the area of this study (Ménard et al., 2002; Duguay et al., 2003; Jeffries et al., 2005; Brown and Duguay, 2011a; Surdu et al., 2014). Optimal model simulations were obtained for ice phenology of shallow lakes. Previous studies showed that the model performs very well if driven with data representative of the lakes' climate (Duguay et. al., 2003; Brown and Duguay, 2011a). If the model is forced with local climate data, the model provides a first guess of potential values of freeze-up and break-up. The model was driven with climate data acquired from the nearby meteorological station of Barrow. While the spatial variability within a lake or a region is shown by SAR observations, variability values lack for CLIMo, as the one-dimensional model only provides one ice-on and one ice-off date.

Along with energy balance components, on-ice snow depth, and composition of the ice cover (clear ice and snow ice proportions), the model also simulates lake-ice thickness and annual complete-freeze-over (ice-on) and water-clear-of-ice (ice-off) dates. However, in order to better capture the ice conditions over freshwater lakes, parameterization of snow conductivity and surface albedo has been modified in the model (Duguay et al., 2003). Considering the variability of the snow depth over lakes in coastal regions, the model was run with a snow cover depth scenario of 53%. This value represents the ratio (expressed as a percentage) of snow depth measured on lakes to that measured on land in the study area. The ratio was calculated based on *in situ* snow depth measurements available from previous studies (Jeffries et al., 1994; Sturm and Liston, 2003; Surdu et al., 2014). Making reference to existing field measurements, the model was driven with a set dry snow density of 335 kg m^{-3}. Modelled freeze-up and break-up dates were compared to ice-on and ice-off dates as derived from SAR observations.

4.3.3 Meteorological Data

Climate records from the Barrow, AK, meteorological station were obtained from NOAA's National Climatic Data Centre (NCDC), and were used to force CLIMo and to asses the effect of temperature and snow on SAR-detected ice phenology. Mean daily screen-height air

temperature, relative humidity, wind speed, cloud cover fraction, and snow depth, were used to force CLIMo in order to simulate ice-on and ice-off dates for lakes in the region of study.

4.3.4 MODIS Land/Ice Surface Temperature

Moderate Resolution Imaging Spectroradiometer (MODIS) land/lake surface temperature data were acquired from 2006 to 2011. MODIS pixels were identified for each of the 14 ROIs (lakes) shown in Figure 1 and listed in Table 1, and used in the analysis of σ^0 values in relation to lake surface "skin" temperature. Selection of MODIS pixels was carefully performed in order to avoid land contamination and included MODIS pixels closer to the lake areas of interest. The pixels were selected based on two criteria: first – the proximity to the selected SAR ROIs, and second – each 1-km MODIS pixel had to be 95% over lake.

In this study, the MODIS UW-L3 Lake Surface Water Temperature/Lake Ice Surface Temperature (LSWT/LIST) product was used (Kheyrollah Pour et al., 2012, 2014). The product is generated from Aqua and Terra MYD/MOD 11- L2 data, at a spatial resolution of 1 km. A new algorithm was developed to create products at various temporal resolutions from the combination of MODIS data from the Aqua and Terra satellites, which were not available otherwise (see Duguay et al., 2012 and Soliman et al., 2012 for details). The Aqua and Terra satellite platforms follow the same orbit within 3 hours of each other. However, at higher latitudes, it is possible to monitor the same location from both sensors within an hour, considering different viewing angles. In such case, it is feasible to combine observations from both sensors in each pixel during an hour. The MODIS UW-L3 LSWT/LIST product has been evaluated against *in situ* temperature measurements over Finnish lakes (Cheng et al., 2014; Kheyrollah Pour et al., 2014) as well as one-dimensional lake models over two large Canadian lakes (Kheyrollah Pour et al., 2012).

Between 2006-2011, MODIS temperature data highly correlated with that recorded at the Barrow meteorological station ($r = 0.94$-0.99). However, the satellite "skin" temperature within a MODIS pixel over a lake located 9.3 km away from Barrow was generally lower than the 2-m air temperature recorded locally by 1.86 to 2.95°C during all years of analysis. Differences between the two temperatures are expected, as they do not represent the same measurement (2-m

height vs. “skin” temperature). A comparison of near-surface air temperature from the Barrow meteorological station and from MODIS is shown in Figure 4.3.

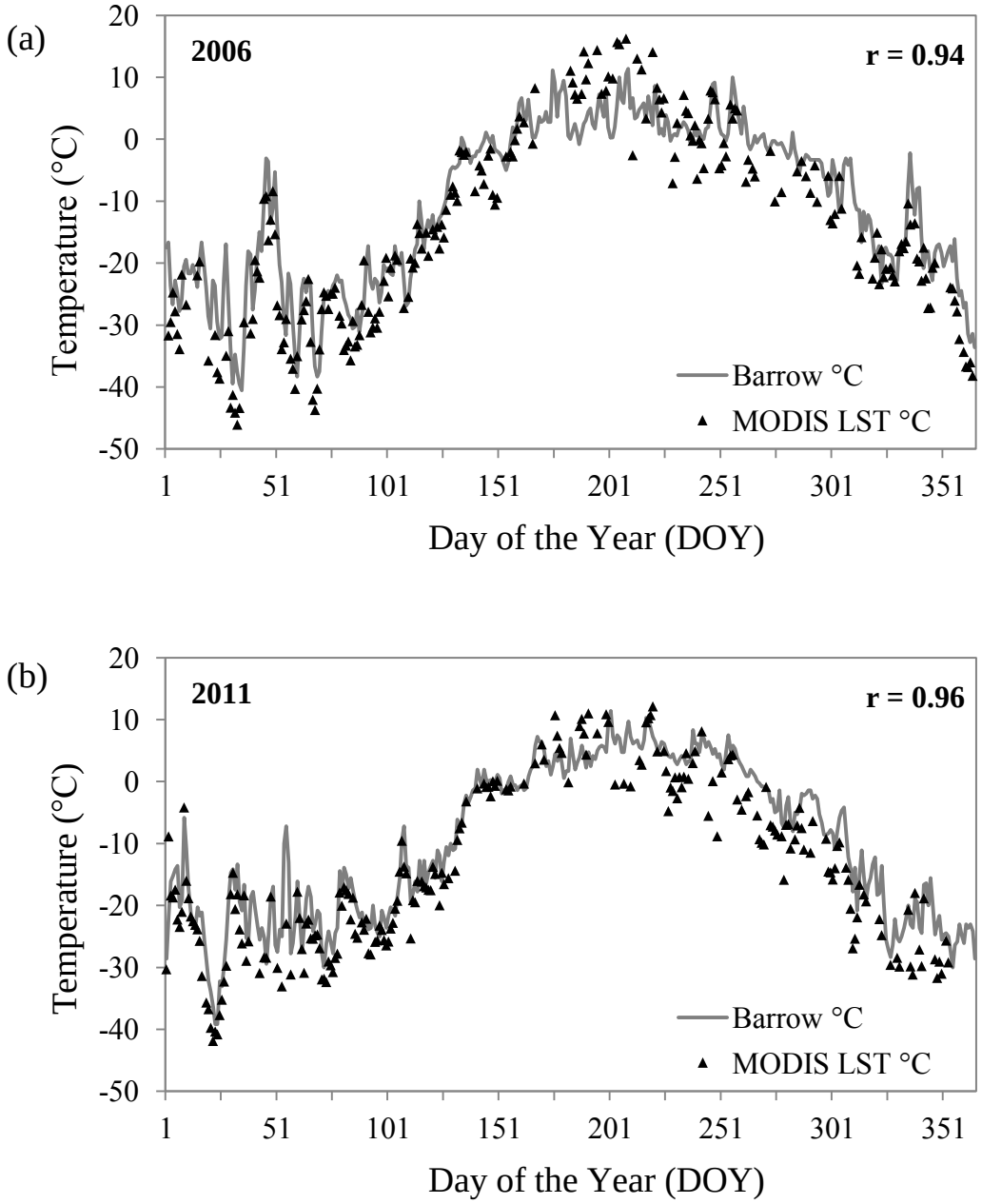

Figure 4.3: MODIS LWST/LIST compared to the surface air temperature registered at Barrow in 2006 (a) and 2011 (b). The Pearson correlation (r) between the observations is also shown.

4.4 Results and Discussion

Timing of initial ice formation (freeze onset), beginning (melt onset) and end of ice break-up (water-clear-of-ice or ice-off) for lakes on the NSA from 2005-2011 was determined for 14 selected ROIs using the SAR σ^0. Temporal evolution of σ^0 was analyzed in relation to MODIS LSWT/LIST and/or weather station temperature (Figure 4.4) and snow depth.

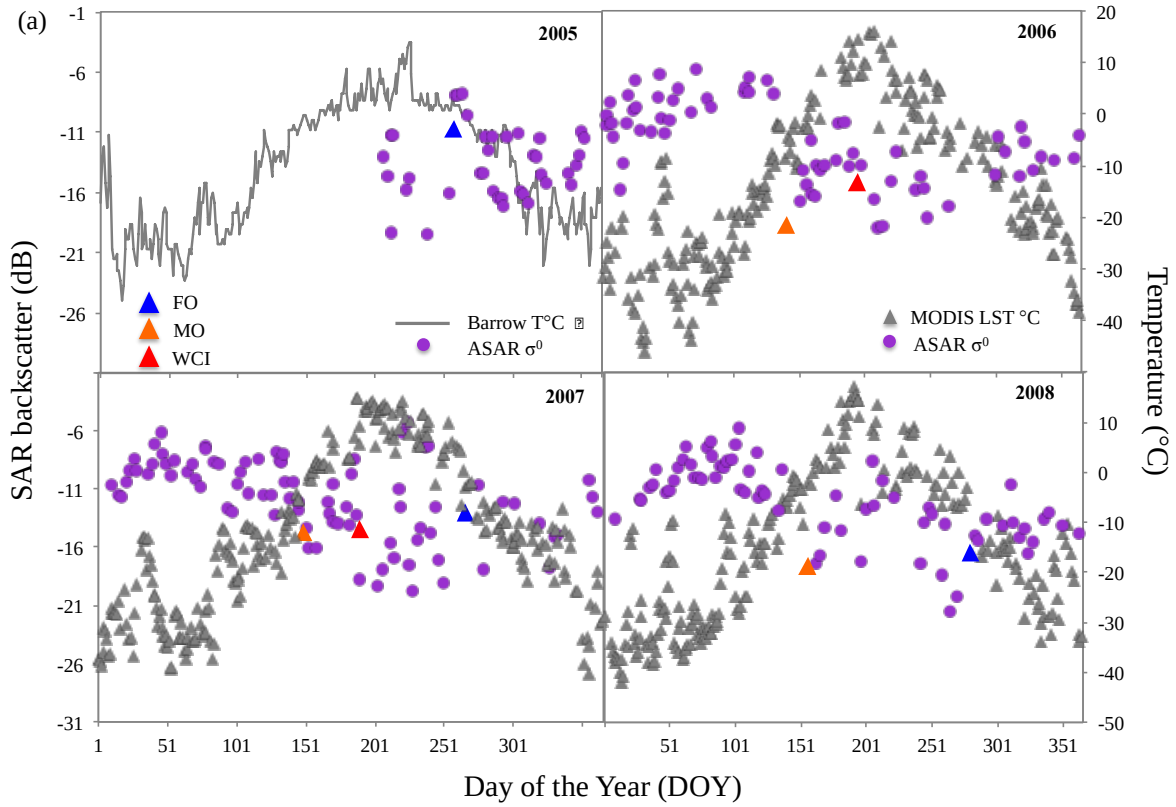

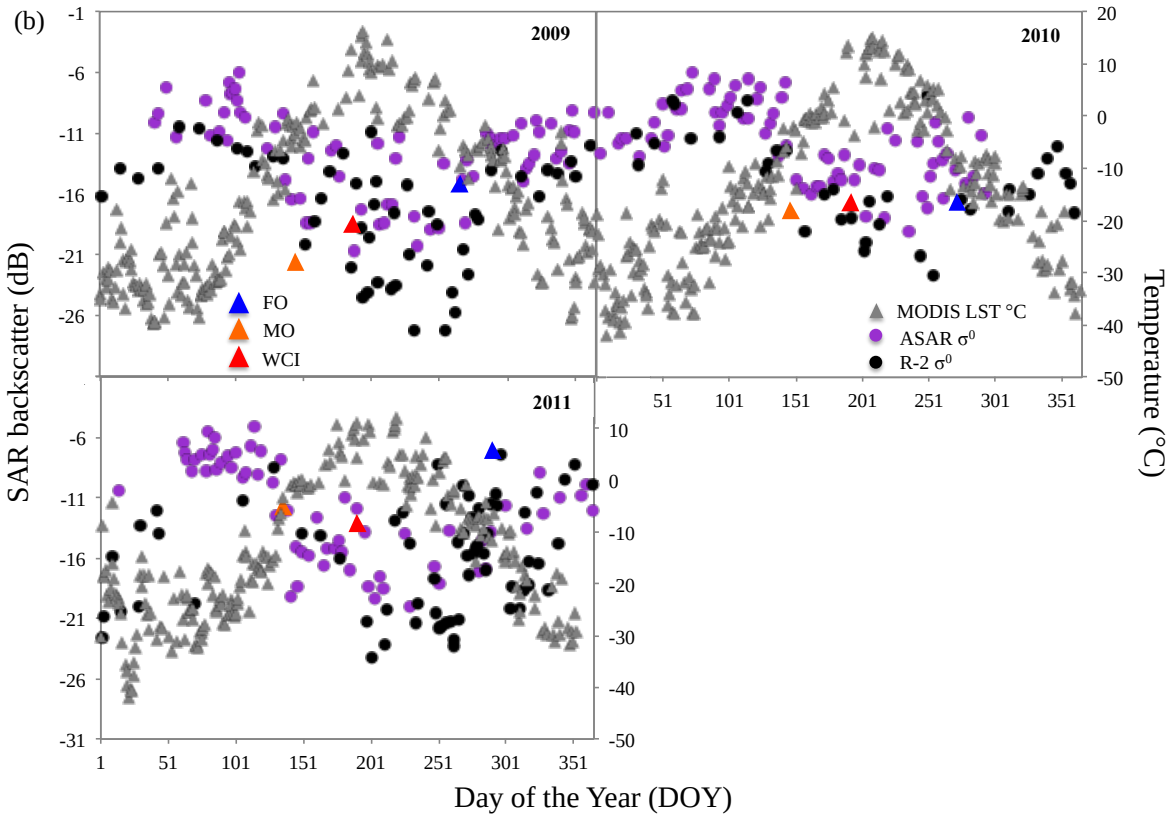

Figure 4.4: Temporal evolution of SAR backscatter over a shallow lake near Barrow, Alaska: a) ASAR (2005-2008) and (b) ASAR and RADARSAT-2 (2009-2011). The solid grey line represents recorded air temperature at the meteorological station and the grey triangles represent the observed MODIS LST. SAR-detected freeze onset (blue triangles), melt onset (orange triangles) and ice-off (red triangles) dates are also shown. No ice-off dates are shown if SAR acquisitions were missing or sparse.

Temporal analysis of radar returns indicates a strong σ^0 relation with temperature, with lower air temperatures generally leading to an increase in σ^0 and higher air temperatures resulting in a decrease of σ^0 values, consequent to snow/ice melt. ASAR and RADARSAT-2 acquisitions were available for a common period (2009-2011). During this period, with more frequent observations, the detection accuracy of ice phenology events increased. However, several limitations have also been identified and they are related to the wide range of incidence angles at which images were acquired, to the different polarization modes of ASAR, and possibly to the alternating ascending and descending orbits for both ASAR and RADARSAT-2.

Snow has been demonstrated to be a significant driver of lake ice growth as variations in snow duration and depth have direct consequences on a lake's thermal regime and winter energy balance (Sturm and Liston, 2003) and impact the timing of WCI. A thinner (about half of the terrestrial snow; Sturm and Liston, 2003) and denser snowpack provides less insulation and allows higher rates of heat flow to the atmosphere in spring (Sturm and Liston, 2003). Knowledge of snow conditions over lakes is useful in predicting timing of ice-off dates, as break-up trends to closely follow those of annual number of snow days (Jensen et al., 2007).

Usually, ice starts forming once air temperatures fall below 0°C. Depending on lake depth and volume, and also on wind events that may occasionally break the thin ice cover, it may take several days from the initial drop in air temperature until a solid ice cover forms. For instance, in 2007 negative air temperatures were registered on 21 September (DOY264) and mean FO date was estimated to be on 23 September (DOY266). Conversely, in 2009 consistent negative air temperatures were recorded after 20 September (DOY263) and mean FO was only detected on 3 October (DOY276). Similarly, in 2011, FO was observed on 3 October, after 12 days of below-freezing air temperatures. On the other hand, MO is associated with positive air temperature values but internal melt of the ice crystals may begin even at air temperatures slightly below 0°C. Air temperatures over 0°C were recorded starting with 6 June (DOY157) in 2006 and 3 June (DOY154) in 2007. In 2008 and 2009, MO occurred 5-6 days after above-freezing temperatures were recorded. In 2008, mean MO was observed on 5 June (DOY 156) and 23 May, (DOY143) respectively while LSWT/LIST above 0°C were recorded starting with 30 May (DOY150) and 18 May (DOY138). In 2010 and 2011, MO preceded above-freezing air temperatures by 4 and 9 days, respectively. Nevertheless, the evolution of σ^0 closely follows that of air temperature and when available that of LSWT/LIST, ice events occurring within 3-16 days prior or subsequent to changes in air temperatures/LSWT/LIST.

4.4.1 Freeze onset

Initial ice formation for shallow Alaskan lakes was monitored from 2005 to 2011 and FO dates were compared to model outputs (Table 4.2). The mean ice onset date for this period as derived from SAR observations is 28 September (DOY271) and it closely aligns with the date indicated by model simulations, 1 October (DOY274). Temporal analysis of σ^0 indicates that the latest freeze onset occurred in 2008 (7 October, DOY280) and the earliest in 2005 (15 September,

DOY258). Results show that with the exception of 2010, ice onset of each year occurred later than the previous year. The σ^0 values at the beginning of ice formation exhibit returns ranging from -15.9 dB to -4.8 dB for ASAR and from -17.4 dB to -11.7 dB for RADARSAT-2.

Table 4.2: Timing of lake ice freeze onset dates between 2005-2011 derived from SAR backscatter and model simulations, shown as day of the year (DOY). The missing value indicates sparse or missing SAR observations. The range of freeze onset dates for the 14 lakes is shown in parentheses.

Year	SAR	CLIMo
2005	258 (255-261)	270
2006	–	279
2007	266 (263-275)	276
2008	280 (279-283)	276
2009	276 (271-280)	273
2010	271 (265-275)	273
2011	276 (274-280)	274
Mean FO 2005-2011	**271 (255-283)**	**274**

As a result of increased sampling frequency (combined ASAR and RADARSAT-2 acquisitions) between 2009-2011, accuracy of FO detection in relation to model simulations increased, fact reflected by the similar mean FO dates observed with SAR, with 1 October (DOY274) as the mean FO date, and those simulated with CLIMo for the same period, with the mean FO date as 2 October (DOY275). Greater differences in timing of mean FO dates were noticed between SAR observations (25 September, DOY268) and model simulations (1 October, DOY274) from 2005-2008, when only ASAR data was available. During years when differences between SAR observations and model outputs are greater (e.g., 2005 and 2006), uncertainties associated with high σ^0 from wind-roughened open water provide a possible explanation for these discrepancies. The differences between observations and simulations can also be explained by the fact that CLIMo was forced with temperature data from the weather station and by the fact that FO dates derived from SAR include ROIs that are located up to 60 km away from Barrow. As a result, the model outputs would indicate later FO (and earlier ice-off) dates. These discrepancies can also be explained by the fact that the model provides only one FO date for all lakes in the Barrow region whereas FO dates observed with SAR apply to each individual lake and display a range (as shown in Table 4.2). The SAR-observed FO dates are then reported as a mean date.

Ice formation is a function of decreasing air temperatures and lake morphometry as lakes store different amounts of heat accumulated in the warmer months prior to the event, depending on depth, area and volume (Brown and Duguay, 2010). Once lake water achieves its maximum density at 3.98°C consequent to heat loss at the air-water interface, deeper warmer waters replace the denser surface ones and additional cooling continues until a solid ice cover develops (Brown and Duguay, 2010). Given that most lakes in the study area are shallow, the effect of heat storage and circulation is reduced (Jeffries and Morris, 2007).

The two extreme FO dates shown by the temporal analysis of σ^0 – late in 2011 (11 October) and early in 2005 (15 September) – could be explained by the differences in air temperatures prior to ice onset (Figure 4.5). Mean September air temperature (2.76°C) possibly contributed to the late FO of 2011. The early ice onset in 2005 was possibly related to the lower mean September air temperature (1.08°C) when compared to the mean air temperature of the same month in 2011.

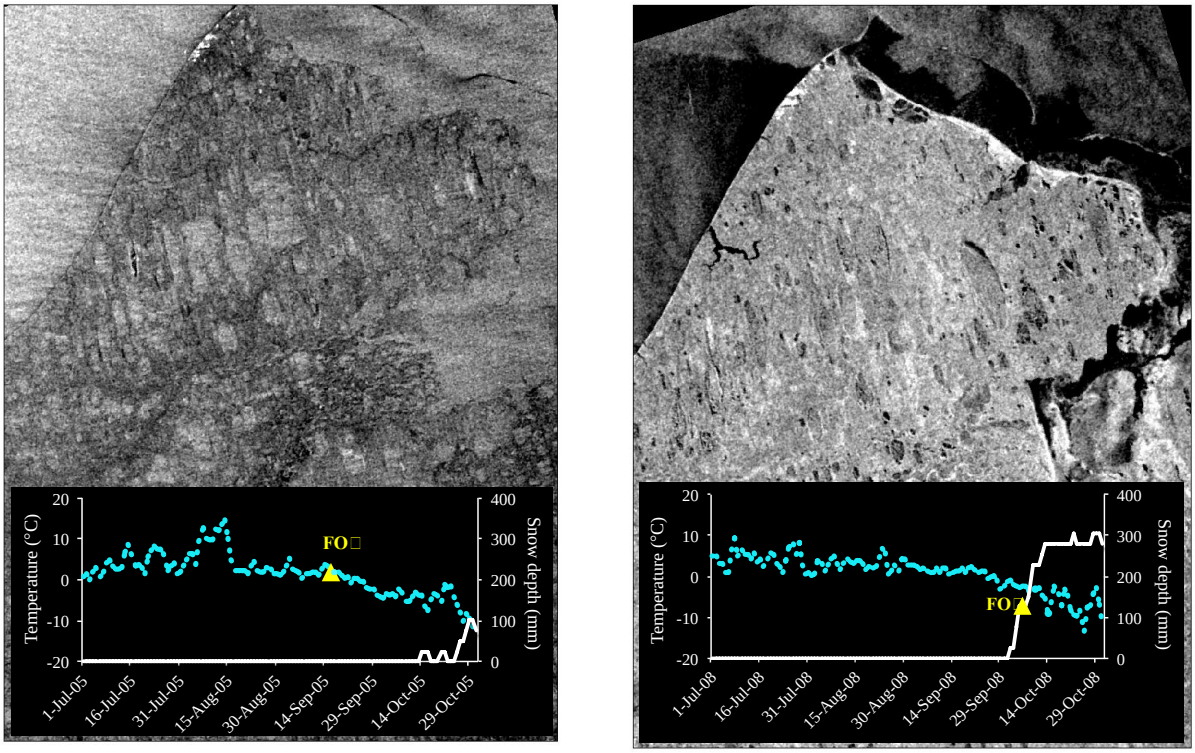

(a) ASAR, 18 September 2005 (b) ASAR, 9 October 2008

Figure 4.5: SAR images acquired at the time of freeze onset – (a) ASAR, 18 September 2005 (b) ASAR, 9 October 2008 – of lakes on the North Slope of Alaska. The bottom graphs show the climate conditions – air temperature (blue dots) and snow depth on ice from CLIMo (white line) prior and at the time of freeze onset. SAR-detected freeze onset dates are also indicated (yellow triangles).

At high wind speeds, radar returns with values close to 0 dB could be distinguished from the newly formed ice. These high σ^0 values were considered to be low-quality pixels were not included in the analysis but were useful as they were indicative of the presence of new ice.

4.4.2 Break-up

Timing of melt onset and ice-off dates for coastal shallow lakes on the NSA is reported from 2006 to 2011. The scarcity of the ASAR acquisitions throughout the 2008 break-up season did not allow accurate detection of ice events and thus these observations were not included in the analysis.

4.4.2.1 Melt onset

Analysis of SAR σ^0 indicates that the mean MO date for shallow lakes on the NSA between 2006-2011 is 23 May (DOY143). SAR observations show a relatively high variability of MO dates during the six years of monitoring, with the latest MO occurring in the spring of 2008, on ~4 June (DOY155) and the earliest in 2011, on ~13 May (DOY133). Results show that SAR-derived mean MO dates are similar to CLIMo simulations (Table 4.3), model outputs indicating 16 May (DOY136) as the mean MO date.

Table 4.3: Timing of lake ice melt onset between 2006-2011, derived from SAR backscatter and model simulations. Dates are shown as DOY. The range of melt onset dates for the 14 lakes is shown in parentheses.

Year	SAR	CLIMo
2006	141 (131-151)	134
2007	141 (136-145)	144
2008	156 (155-158)	138
2009	143 (137-149)	132
2010	147 (144-150)	145
2011	133 (128-145)	139
Mean MO 2006-2011	**143 (128-158)**	**136**

The higher discrepancy between SAR observations and model output in 2008 is explained by the lack of ASAR observations between 15 May (DOY136) and 3 June (DOY155). The differences between SAR-observed and simulated MO dates are partially explained by the gap of 2-5 days (2009-2011) and of 2-19 days (2005-2008) between observations. At the

beginning of the break-up period, σ^0 ranged from -20.44 dB to -15.66 dB for ASAR and from -22.87 dB to -16.11 dB for RADARSAT-2.

At the beginning of the break-up period, snow controls the σ^0, regardless of the ice type, as wet snow prohibits penetration of the radar signal below this layer (Howell et al., 2009) and thus resulting in low radar returns, as a result of the radar signal reflecting off the wet layer (specular reflection). Depending on ice type, the timing and length of ice decay is affected, with snow ice delaying the ice melt. If snow on ice or snow ice is present, its higher albedo delays break-up (Jeffries and Morris, 2007). Once snow has melted, the internal structure of ice crystals is disintegrated by solar radiation and mechanical break-up (Ashton 1986), and the albedo of the lake surface gradually decreases as more water is exposed to radiative warming, and melt accelerates with further heating. This is also the case for melt onset observed throughout the 2006-2011 period. More specifically, in the spring of 2008, climate records from Barrow indicate that following the transition toward above-freezing air temperatures, snow fully melted on 2 June and the melt onset of ice occurred two days later. Similarly, following higher air temperatures in late May 2011, melt onset occurred a few days prior to complete snow melt (Figure 4.6).

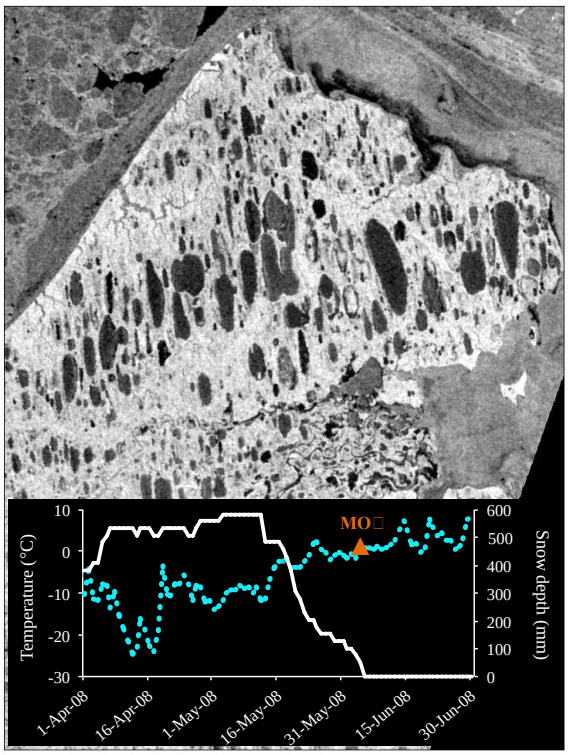

(a) ASAR, 10 June 2008

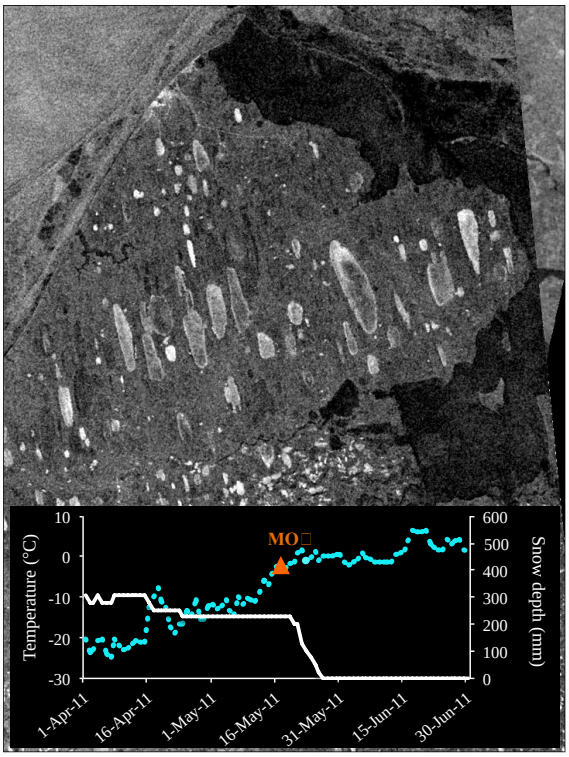

(b) RADARSAT-2, 16 May 2011

Figure 4.6: SAR images acquired at the time of melt onset – (a) ASAR, 10 June 2008 and (b) RADARSAT-2, 16 May 2011 – of lakes on the North Slope of Alaska. The bottom graphs show the climate conditions – air temperature (blue dots) and snow depth on ice from CLIMo (white line) prior and at the time of melt onset. SAR-detected melt onset dates are also indicated (orange triangles). RADARSAT-2 Data and Products © MacDonald, Dettwiler and Associates Ltd., 2011 – All Rights Reserved. RADARSAT is an official trademark of the Canadian Space Agency.

4.4.2.2 Water clear of ice

From 2006 to 2011, the mean WCI (ice-off) date for lakes on the Alaskan North Slope as indicated by SAR observations is 10 July (DOY191). Results are indicative of a relatively small variability (1-8 days) in the ice-off dates during the six-year period, with the latest ice-off date occurring on 14 July 2010 (DOY195) and the earliest on 6 July 2009 (DOY187) (Table 4.4). The sparse SAR acquisitions during the end of the 2008 break-up period did not allow accurate detection of the WCI date. CLIMo mean WCI dates from 2006-2011 are similar with those observed with SAR (10 July, DOY191) during the same period (9 July, DOY190). These results are similar to previous MODIS-Terra observations (with a spatial resolution ranging from 250-1000 m) of ice-out timing of larger lakes on the Arctic Coastal Plain from 2007-2012, identifying 6 July (DOY187) as the mean ice-off date (Arp et al., 2013). More specifically, the same study (Arp et al., 2013) identifies 4 July (DOY185) as the mean WCI date in 2007 and 2008, 2 July (DOY183) in 2009, 13 July (DOY194) in 2010 and 6 July (DOY187) in 2011. The coarser MODIS resolution may explain the generally earlier WCI dates detected by this sensor compared to the WCI dates observed with the higher-resolution SAR.

Table 4.4: Lake ice-off timing between 2006-2011, derived from SAR backscatter and model simulations. Dates are shown as day of the year. The missing value indicates sparse or missing SAR observations. The range of ice-off dates for the 14 lakes is shown in parentheses.

Year	SAR	CLIMo
2006	194 (189-198)	193
2007	190 (189-190)	189
2008	–	186
2009	187 (178-190)	186
2010	195 (192-198)	194
2011	191 (196-201)	192
Mean WCI 2006-2011	**191 (178-201)**	**190**

Radar signals from the ice oscillates during the break-up period. Consequent to warmer air temperatures, the low radar returns at the beginning of spring signal the ice melt onset. Following observations of low σ^0, higher returns are noticed, indicating subsequent re-freeze events, mainly due to ascending (morning) and descending (evening) acquisitions, and/or that water has drained from the ice surface. Excluding the images affected by wind effect indicated by high radar returns, these values gradually decrease closer to the ice-off date, when air temperatures have been consistently positive. The open water season is indicated by consistent significant low σ^0 values (-24.88 dB to -19.62 for ASAR and -28.54 dB to -20.47 for RADARSAT-2).

In 2009, the LSWT/LIST 5 days prior to the WCI date ranged from 4.7-6°C; in 2010, the air temperatures 5 days prior to the 2010 WCI dates were by 2.9-3.3°C lower. Additionally, in 2010 snow melt occurred later by 9 days. Lower air temperatures and later snow melt likely explain the later WCI date of 2010 (Figure 4.7).

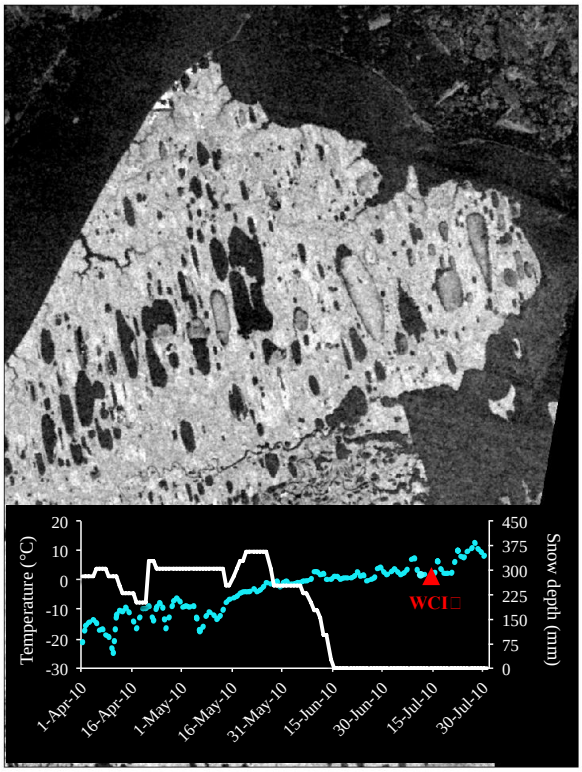

(a) ASAR, 11 July 2010

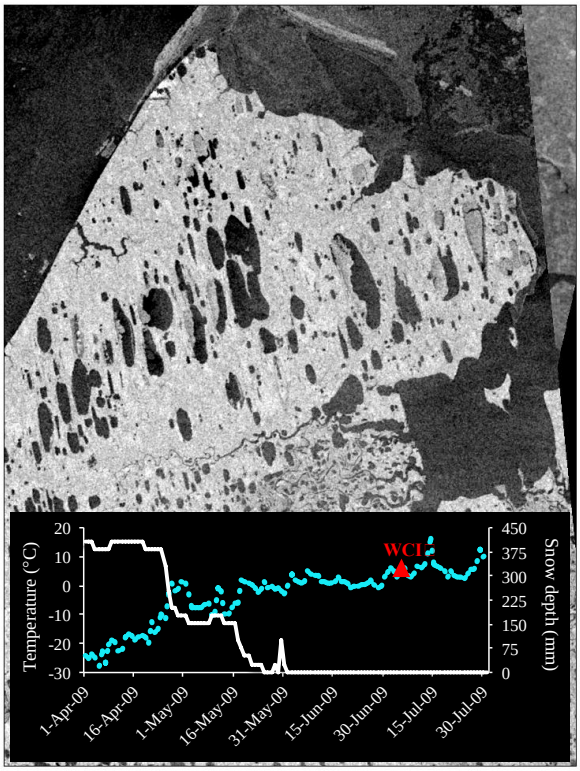

(b) RADARSAT-2, 6 July 2009

Figure 4.7: SAR images acquired at the time of ice-off – (a) ASAR, 11 July 2010 and (b) RADARSAT-2, 6 July 2009 – of lakes on the North Slope of Alaska. The bottom graphs show the climate conditions – air temperature (blue dots) and snow depth on ice from CLIMo (white line) prior and at the time of ice-off. SAR-detected ice-off dates are also indicated (red triangles). RADARSAT-2 Data and Products © MacDonald, Dettwiler and Associates Ltd., 2009 – All Rights Reserved. RADARSAT is an official trademark of the Canadian Space Agency.

In order to compare the results of the σ^0 analysis for ice-off timing, segmentation of available SAR images on/close to the ice-off date was also performed using the K-means algorithm (Figure 4.8). Employing the σ^0 threshold was necessary to detect important ice events throughout the ice season. The K-means classification was solely used for

comparison and could not have been used for FO or MO given the limitations associated with discrimination of ice/open water during these ice events.

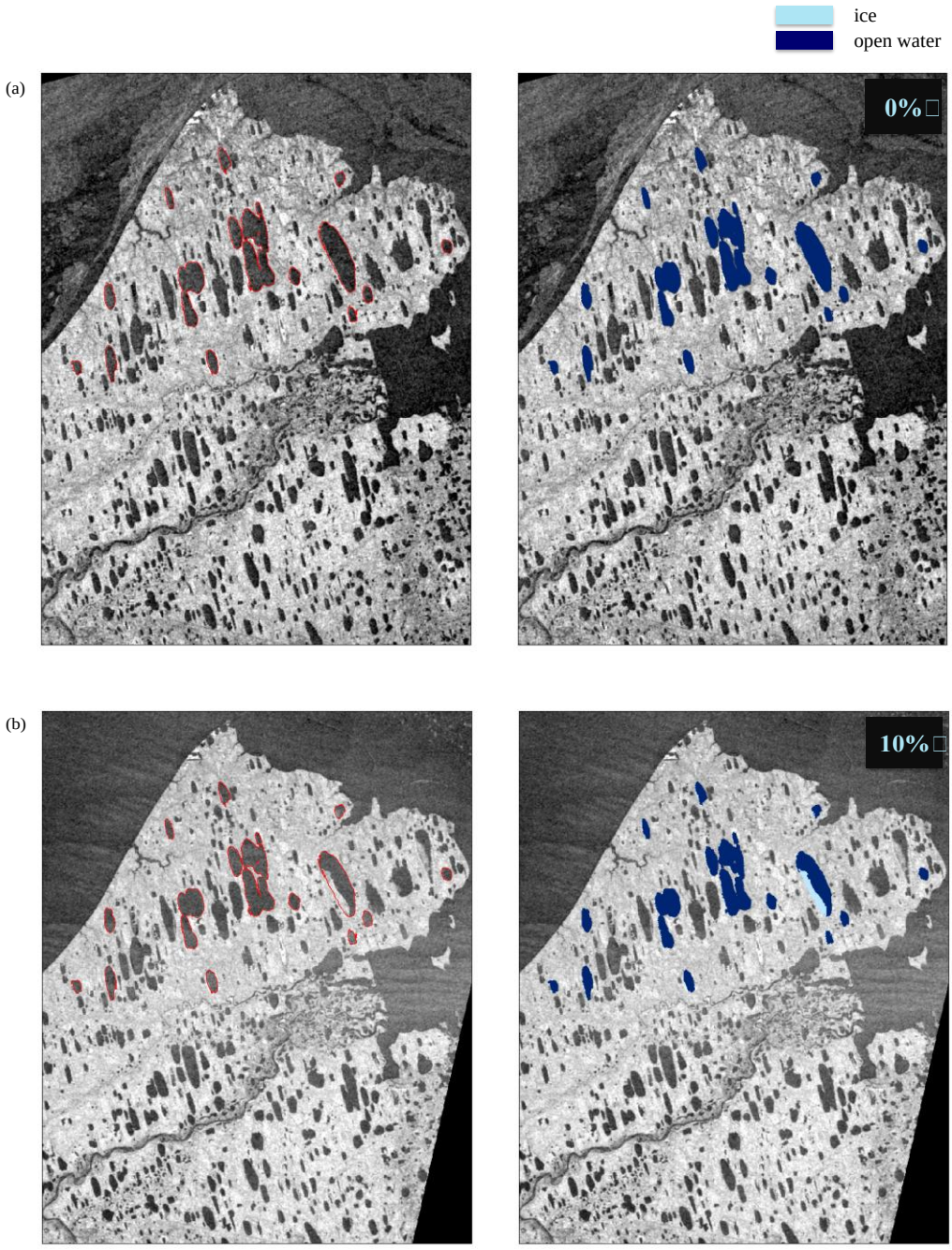

(c)

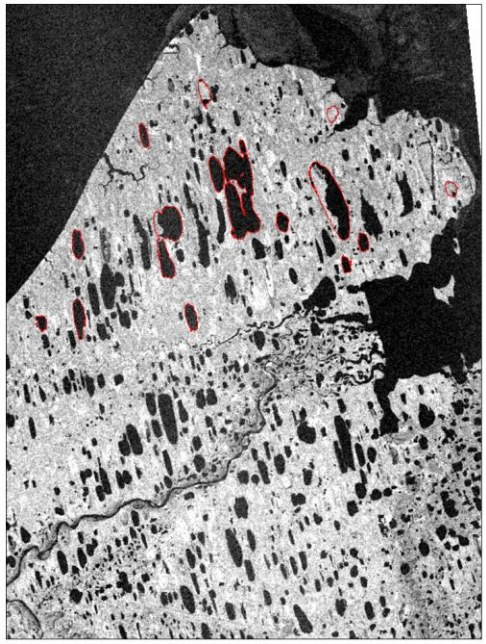

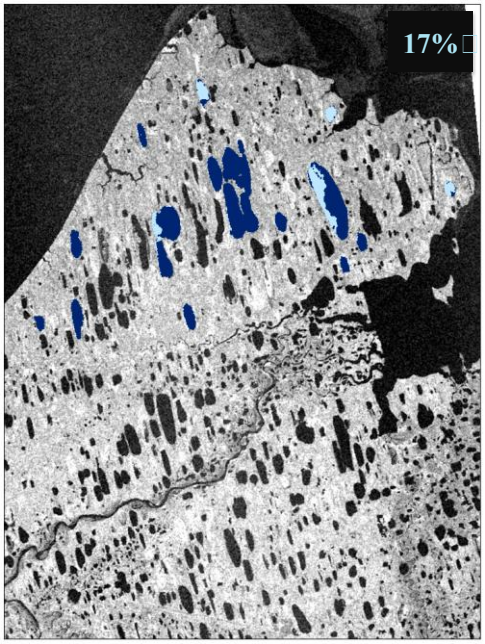

(d)

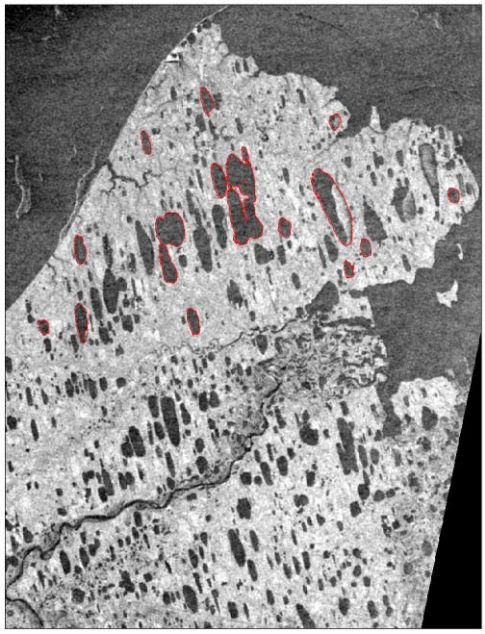

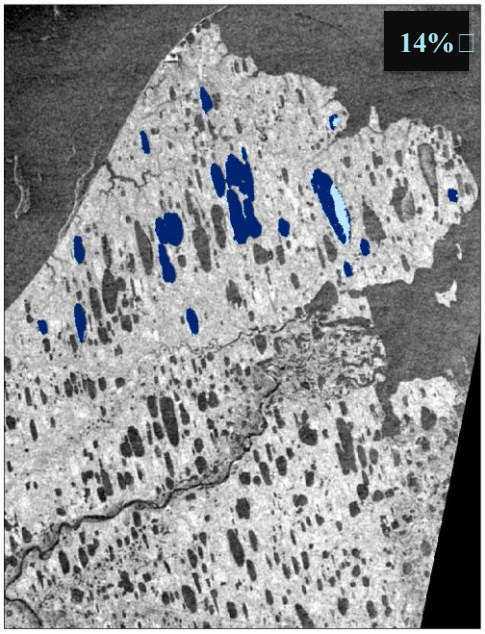

(e)

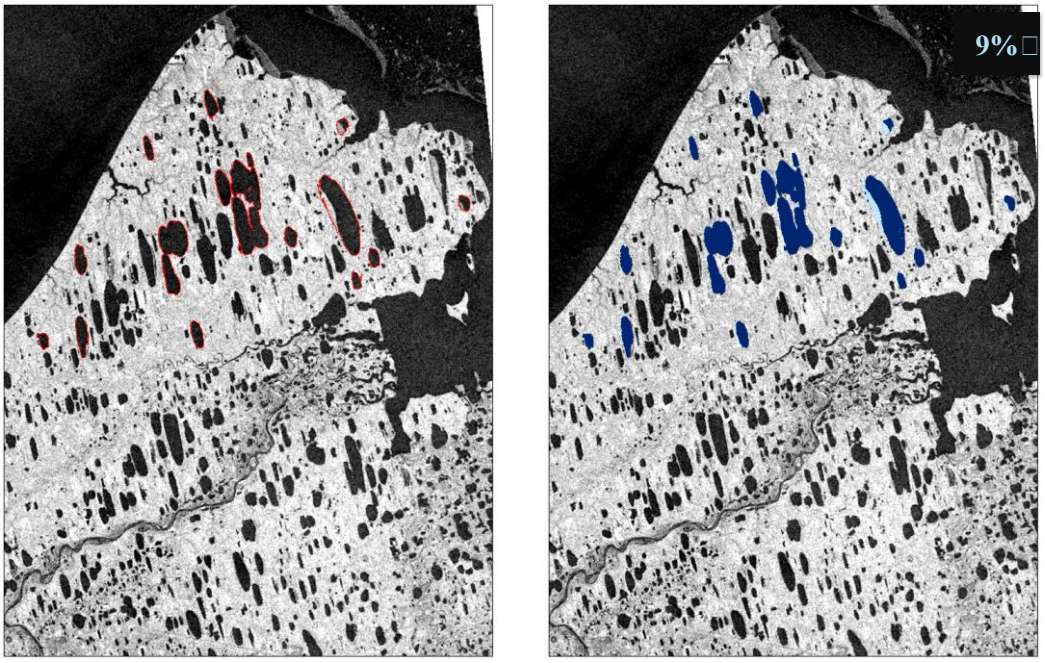

Figure 4.8: Ice fractions (%) for 14 lakes combined near Barrow: (a) 14 July 2006 (DOY195) – ASAR, (b) 9 July 2007 (DOY190) – ASAR, (c) 6 July 2009 (DOY187) – RADARSAT-2, (d) 14 July 2010 (DOY195) – ASAR, (e) 10 July 2011 (DOY191) – RADARSAT-2. Sparse SAR observations did not allow detection of ice-off date in 2008. The red contours in the original images represent the polygons (ROIs) of the 14 lakes. RADARSAT-2 Data and Products © MacDonald, Dettwiler and Associates Ltd., 2009 – All Rights Reserved. RADARSAT is an official trademark of the Canadian Space Agency.

Segmentation results show that no ice was detected on the selected lakes on 14 July 2006, 10% ice 9 July 2007, 17% ice on 6 July 2009, 14% ice on 14 July 2010 and 9% ice on 10 July 2011. These results are satisfactory considering that previous investigations of lake ice break-up using C-band SAR assigned ice-off dates on the dates when the areal fraction of open water first exceeded 90% (Geldsetzer et al., 2010).

Based on the visual analysis of the segmentation results, Lake Tusikvoak (ROI # 5, see Table I and Figure 1) maintains its ice cover later in the summer, being the lake with the latest ice-off date. No other pattern in terms of temporal behavior (i.e. early/late ice-off dates during particular years) from 2006-2011 was observed for the other lakes.

These results show the potential of frequent C-band backscatter for identification of lake ice events, such as freeze and melt onset, and ice-off dates. The potential of C-band backscatter to discriminate between ice and open water, during both freeze-up and break-up, was shown to be a function of incidence angle and wind, and when available, reliable wind data is recommended to be used in analysis (Geldsetzer et al., 2013).

Based on previous findings that suggest that the HV backscatter does not provide the optimum discrimination between ice and water particularly at the beginning of melt onset (Geldsetzer et al., 2010), only HH-polarized RADARSAT-2 images were used in the current study. Yet, wind speed prior to the lakes becoming completely ice-free affects the HH-polarized imagery, resulting in radar returns similar to those from open water in windy conditions. Consequently, the accuracy of ice-off timing could be affected. RADARSAT-2 HH imagery is most useful for ice-off detection at incidence angles ranging from 36.6°-46.9°, with wind speeds between 2.9-7.1 m/s (Geldsetzer et al., 2010). For the purpose of this study, all available HH-polarized SAR images were used. Considering that the frequency of SAR acquisitions ranges from 2-5 days, the accuracy in detecting lake ice events is also dependent on frequency of image acquisition.

4.4.3 Backscatter sensitivity to incidence angle and polarization

SAR microwave backscatter is a function of the dielectric properties of the material, local incidence angle and sensor polarization (Ulaby et al., 1986). Both ASAR Wide Swath and RADARSAT-2 ScanSAR Wide provide imagery acquired at a variety of incidence angles (beam modes) and thus increasing the temporal frequency of image acquisition of a stationary target.

Previous investigations of lake ice during spring melt with C-HH σ^0 measurements report lower σ^0 values (2 to 5 dB) for the same ice cover observed at shallower incidence angles (35-49°) than those at steeper incidence angles (20-35°) (Duguay et al., 2002; Nghiem and Leshkevich, 2007). Similarly, the lake surface σ^0 exhibited a decreasing trend with incidence angle, with a sharper decrease for RADARSAT-2 (Fig. 4.9; Fig. 4.10).

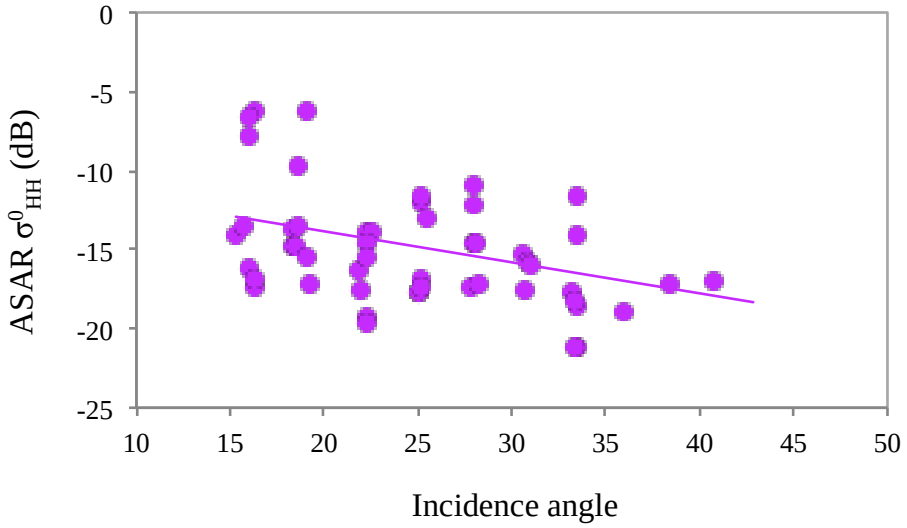

Figure 4.9: Mean ASAR σ^0HH for selected pixels of a lake that freezes to bed in late winter. The solid purple line represents a best fit (linear regression) for the available samples.

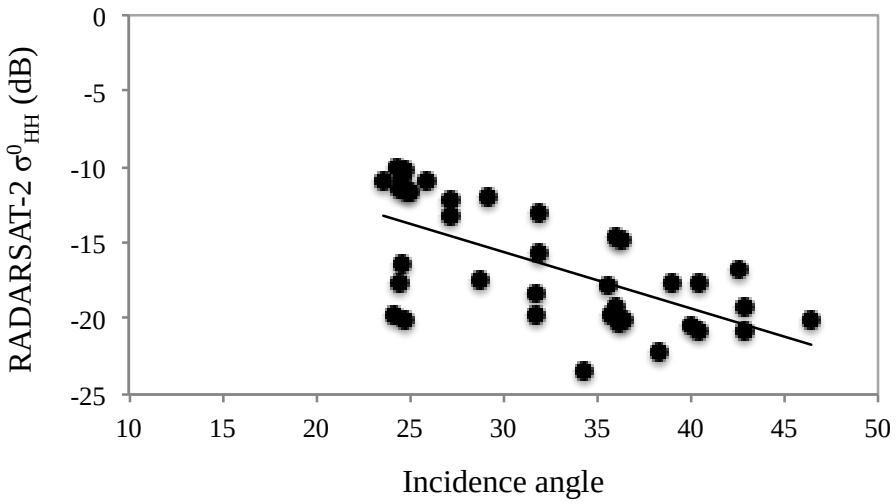

Figure 4.10: Mean RADARSAT-2 σ^0HH for selected pixels of a lake that freezes to bed in late winter. The solid black line represents a best fit (linear regression) for the available samples.

In order to quantify the changes in σ^0, an initial assessment of the incidence angle and polarization effects was performed.

Analysis of ASAR and RADARSAT-2 σ^0 in relation to incidence angles during 2010 shows high oscillations of σ^0 values in images acquired on the same date or one day apart. Results also show that σ^0 differences at similar incidence angle ranges are fairly constant for images acquired on the same date. For example, same-day and –orbit (ascending/descending) ASAR and RADARSAT-2 acquisitions, with differences between incidence angle ranging from 1.17-7.71°, σ^0 fluctuations were small and ranged from 1-3 dB. When differences in the incidence angle of acquisitions from the two sensors are greater than 8°, differences in σ^0 range from 3-9 dB (Table 4.5).

Table 4.5: Same-day ASAR and RADARSAT-2 σ^0, incidence angle and orbit.

Date of acquisition	ASAR θ (°)	ASAR σ0 (dB)	ASAR orbit	R-2 θ (°)	R-2 σ0 (dB)	R-2 orbit
14-Feb-10	21.78	-16.31	DESC	36.18	-20.19	DESC
03-Apr-10	33.52	-18.59	DESC	36.45	-20.17	DESC
08-May-10	35.89	-18.89	DESC	42.88	-20.85	DESC
24-May-10	28.32	-16.82	ASC	36.03	-19.28	ASC
31-May-10	22.52	-13.81	ASC	34.27	-23.5	ASC
21-Jun-10	28.32	-16.85	ASC	27.15	-13.22	ASC

For same-day ASAR and RADARSAT-2 images, in order to correct the differences in incidence angle between the two sensors, a adjustment of 0.9 dB could be applied to RADARSAT-2 images acquired at incidence angles of 20-33° and one of 1.6 dB to images acquired at incidence angles of 33-46°. These values were calculated based on the sum of same-day ASAR and RADARSAT-2 power over the selected ROI, sum that was divided by two and then converted to σ^0. Considering that lake surface conditions (e.g. ice thickness, transition from a floating to a grounded ice cover, transition form open water to an ice cover and vice versa) change in time and that consequently the bulk dielectric properties of the lake surface also change and affect in turn the surface and/or volume scattering, this correction is highly recommended to only be applied to same-/consecutive-day images. Applying the same approach when images are acquired at intervals of 2-12 days is only appropriate when knowledge of ice conditions confirms that ice conditions remain constant and thus the observed change in σ^0 is solely from surface scattering as a result of changing SAR incidence angle. Without additional information, applying an incidence angle correction to ASAR and RADARSAT-2 images that are acquired at intervals greater than two days would have to assume that lake surface conditions remain constant between the observations. However, in order to evaluate the possibility of using this approach, this hypothesis was assumed and differences in incidence angle were corrected by 0.9 dB for

RADARSAT-2 images acquired at incidence angles of 20-30° and by 1.6 dB for RADARSAT-2 images acquired at incidence angles of 30-46° (Fig. 4.11)

(a)

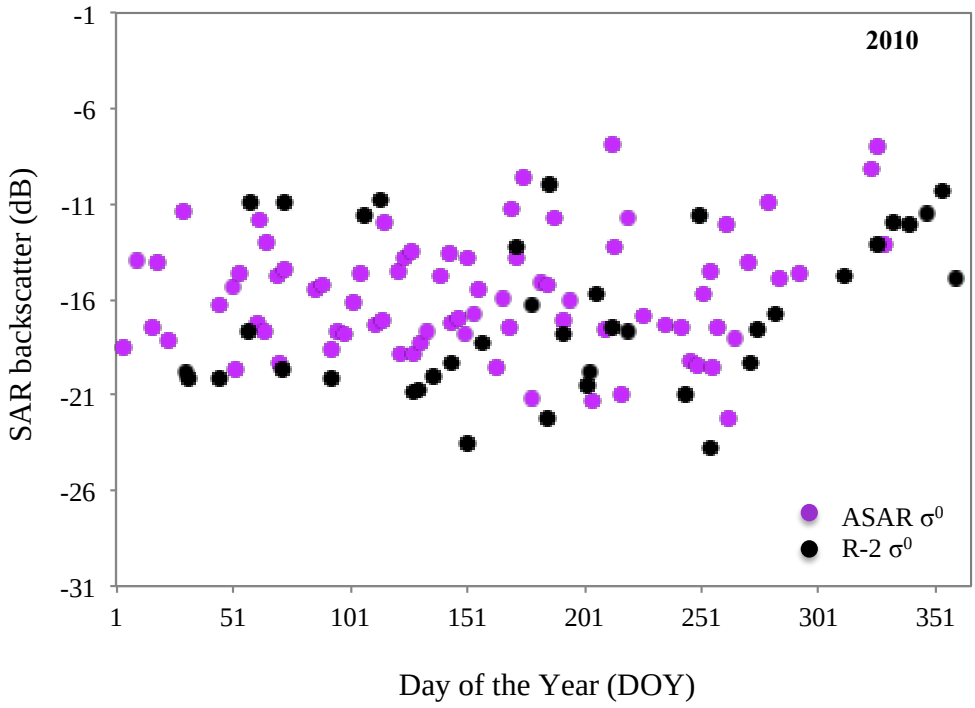

(b)

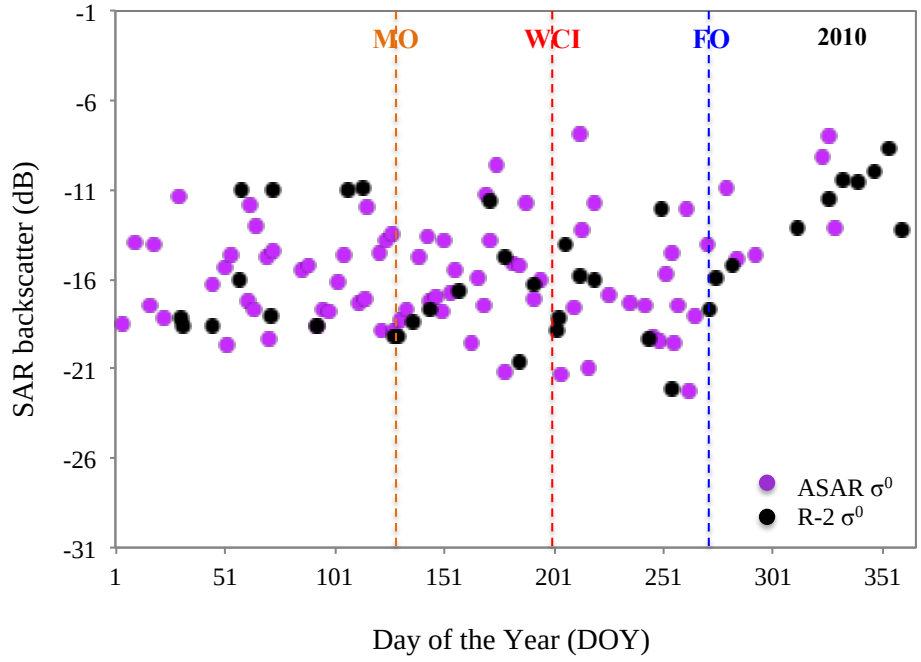

Figure 4.11: (a) Uncorrected temporal evolution of ASAR and RADARSAT-2 backscatter over a lake that freezes to bed, near Barrow, Alaska) in 2010; (b) Incidence-angle corrected temporal evolution of ASAR and RADARSAT-2 backscatter over a lake that freezes to bed, near Barrow, Alaska) in 2010. Freeze onset, melt onset and water-clear-of-ice dates are also shown.

Results show that based on the hypothesis that surface conditions remain constant between the ASAR and RADARSAT-2 observations, applying an incidence angle correction calibrates the two data sets and has the potential to improve detection of important lake ice events. However, if this correction is applied, the thresholds for detection of FO, MO and WCI dates using the RADARSAT-2 data need to be adjusted accordingly.

Evaluation of an ASAR descending-pass image (38.4° incidence angle) and a RADARSAT-2 ascending-pass image (36.03° incidence angle) acquired on 24 May 2010 show a difference in σ^0 of 2.08 dB. If the calculated incidence angle correction of 1.6 dB is applied,

it can be derived that the change in σ^0 is only of 0.48 dB. A more comprehensive analysis of orbit effects on σ^0 was not possible in this study given that these were the only available overlapping ASAR and RADARSAT-2 images acquired at similar incidence angles and at different orbit modes. This suggests that σ^0 differences for the selected ROIs are likely to be related to differences in incidence angle rather than the orbit mode.

These results show that oscillations and magnitude of σ^0 variations is a function of changes in lake surface type (ice versus open water) and differences in incidence angle. Although incidence angle correction improves detection of lake ice events by combing acquisitions from two SAR satellites, the changing ice conditions (e.g. transition from floating to grounded ice) between images acquired at more than 1-2 day differences may justify the differences in σ^0.

However, considering the numerous unknown parameters (e.g. ice cover type, ice thickness, wind conditions, the timing of transition from a grounded ice cover to initiation of melt) and the limited same-day ASAR and RADARSAT-2 acquisitions, calculation of an incidence angle correction for such a diversified data set is difficult and therefore not applied to the full dataset analyzed for the determination of ice dates in this paper. However, this is a topic that warrants further investigation in light of new and upcoming C-band satellite missions.

4.5 Conclusions

The primary objective of this study was to investigate the potential of high temporal frequency C-band backscatter from combined ASAR and RADARSAT-2 observations for detection of ice phenological events, such as melt and freeze onset, and ice-off timing. Results show that C-band SAR is generally suitable for discrimination between ice and open water, however some limitations were also identified.

SAR observations fall within similar ranges with CLIMo simulations, particularly for the FO dates of 2009-2011, when increased satellite observations were available, and for the WCI dates during all years of the time series. Detection of freeze and that of a continuous ice

cover onset is made difficult by the wind effect (speed and direction) on radar backscatter during freeze-up, by the similar backscatter signal from the newly formed ice and that of open water. Moreover, the presence or absence of bubbles, and/or locally drifted snow, resulting in high oscillations of radar returns, complicate freeze onset and complete freeze-over detection on the shallow lakes examined in this study.

Limitations for melt onset are related to the intensity of backscatter signal from the ice cover of the shallow lakes that freeze to the bottom during the winter. Lakes on the North Slope of Alaska are in their majority shallow lakes, with depths ranging from under 1.4 m (7% of the lakes) to 1.4-1.5 m (60% of the lakes) and 1.5-2.2 (10% of the lakes). The remaining 23% represents lakes that may be deeper than 2.2 m (Jeffries et al., 1996). By late winter (end of April), many of these lakes freeze to lakebed (Jeffries et al., 1994). The backscatter signal from lakes frozen to lakebed is already low prior to melt onset. Identifying the differences in backscatter returns from grounded ice poses its challenges. The differences in lake ice cover types (grounded versus floating ice) would eventually result in threshold values close or below the noise floor, or melt onset may be mistaken with water-clear-of-ice conditions for lakes frozen to lakebed. A more fitting approach would be to perform image segmentation of datasets acquired in late winter, determine the lakes with a floating or grounded ice cover, and according to the derived segmentation results, apply a lower threshold on the backscatter from lakes frozen to lakebed in order to detect more accurately melt onset for these lakes.

This was the first study of its kind to evaluate the performance of C-band backscatter from the combination of two different SAR sensors to derive important lake ice dates. Overall, this work showed the potential of high temporal frequency SAR for detection of lake ice events, within an accuracy of 2-5 days. In order to maximize observations, this study used all available data. However, limitations exist and further improvements are needed in order to increase the accuracy of this method. Future work in using the analysis of the backscatter temporal evolution from the existing dual-polarized C-band sensors should investigate in

more detail the effect of incidence angle and that of dual polarization (HH and VV) on the backscatter signal for the ASAR acquisitions. The use of reliable wind data (from weather stations or spaceborne altimeters) is also recommended in interpretation of C-band backscatter for detection of ice events. Moreover, use of polarimetric parameters from RADARSAT-2 observations could improve detection of FO (Geldsetzer and van der Sanden, 2013).

The newly launched Sentinel-1a, and follow-up Sentinel-1b mission, with a spatial resolution of 20 x 40 m in extra-wide swath mode, and the upcoming RADARSAT constellation, will not only continue the records of the ERS-1/2 and ENVISAT (C-band) missions but will also provide more frequent acquisitions that will improve timing estimates of ice phenology parameters. In addition, the multi-spectral Sentinel-2a/b missions, with a spatial resolution of 10-20 m in visible to mid-infrared bands are planned for launch in 2015 and 2016. These missions will deliver optical data that will increase the frequency of acquisitions (every 1-2 days at high latitudes in cloud-free conditions) and be an invaluable complement to SAR observations of lake ice. Combining observations from multiple missions complies with the Integrated Global Observing Strategy (IGOS, 2007) requirements for comprehensive global monitoring and the possible delivery of an operational product, with nearly daily observations.

4.6 Acknowledgements

Financial assistance was provided through a Discovery Grant from the Natural Sciences and Engineering Research Council of Canada (NSERC) to Claude Duguay. Great support was provided by the Grid Processing on Demand (GPOD) team of the European Space Agency (ESA) led by Roberto Cuccu and Giovanni Sabatini through the pre-processing of the ASAR images. The authors would like to thank Luis Veci (Array Systems Computing) and Chris Stewart (ESA) for technical support with processing of the RADARSAT-2 data. The ASAR

scenes were provided by ESA. RADARSAT-2 data and products, © MacDonald, Dettwiler and Associates Ltd., 2009-2011, all rights reserved. RADARSAT is an official mark of the Canadian Space Agency. MODIS-Aqua and -Terra Land Surface Temperature (LST) data to produce the UW LWST/LIST product were provided by the National Aeronautics and Space Administration (NASA) through the Land Processes Distributed Active Archive Center (LP DAAC).

Chapter 5

Evidence of recent changes in the ice regime of High Arctic lakes from satellite observations

5.1 Introduction

In a rapidly changing climate, with each of the last three decades being successively warmer than any preceding decade (IPCC, 2013) and as a result of complex energy exchanges between atmosphere, ocean and land, the Arctic cryosphere is possibly transitioning towards a new state. As a major feature of the Arctic landscape, lakes, through their ice cover phenology (timing of ice formation, melt onset and end of break-up), are a key indicator of climatic changes (Heron and Woo, 1994; Duguay et al., 2006; Williamson et al., 2008) that the high-latitude environment is experiencing. Lake ice phenology is dependent on several factors, including meteorological conditions (e.g., air temperature, lack or presence of snow, snow depth and density, wind speed) and lakes' physical characteristics (e.g., surface area, bathymetry, elevation). However, long-term analysis indicates that lake ice phenology is primarily responsive to air temperature (Palecki and Barry, 1986; Jeffries et al., 1996, Duguay et al., 2006). Increasing air temperatures in the Canadian Arctic in all seasons, with an almost total absence of negative temperature anomalies over the past four decades, have led to later freeze-up and earlier break-up of lakes in this region (Derksen at al., 2012) and appear to have altered the ice regimes of many Arctic lakes.

Changes in the ice phenology of Arctic lakes have major implications for the physical and biogeochemical processes, and the aquatic primary production and fauna, as they are strongly dependent on the presence of ice. Recent studies of Arctic lakes indicate thinner ice covers and less lakes freezing to bed on the North Slope of Alaska during the winter (Surdu et al.,

2014) and reduced summer ice cover, leading to the loss of perennial ice of lakes on Northern Ellesmere Island (Mueller et al., 2009), in the Canadian Arctic Archipelago (CAA).

The CAA is part of the Canadian High Arctic, a region projected to experience the greatest annual temperature increase in the North-American Arctic during the course of the next eight decades (ACIA, 2005). Projected climate conditions (2041-2070) employing two similar Canadian Regional Climate Model (CRCM) scenarios (Brown and Duguay, 2011) show that consequent to loss of perennial ice, lakes on Ellesmere Island will experience maximum ice regime changes. As a result, lakes are projected to break-up earlier by over 30 days, with lakes in the CAA being expected to experience shorter ice seasons by 25 to 40 days.

Monitoring changes in the lake ice cover and the rate at which they occur in the High Arctic is limited by the sparse and inconsistent observations, and the short observational period in these remote regions. Accurate and consistent monitoring of small Arctic lakes requires a complex combination of spaceborne observations, model simulations, and where available, *in situ* measurements. Opportunities exist to monitor small lakes across the Arctic by exploiting the existing observations from heritage C-band synthetic aperture radar (SAR) missions (i.e. ERS-1/2, ENVISAT's Advanced Synthetic Aperture Radar (ASAR), RADARSAT-1/2). These missions, complemented with data from optical sensors (i.e. Landsat) improve detection of ice cover conditions of Arctic lakes.

A limited number of recent studies investigating ice phenology (i.e. the timing of ice break-up of two lakes on Ellesmere Island; Cook and Bradley, 2010) and summer ice minimum on lakes (i.e. the amount of ice present at the end of summer on four lakes in the Canadian High Arctic; Mueller et al., 2009) exist. However, changes that lakes have undergone over the last two decades and the current state of ice conditions for most High Arctic lakes remain unknown.

With the purpose of identifying the changes in the ice regime of 11 lakes in the CAA as derived from existing spaceborne satellite observations (SAR and Landsat) from 1997 to

2011, this study: (1) analyzes and reports annual changes in the timing of ice melt onset, summer ice minimum and end of ice break-up, (2) assesses the rate of change in the timing of start and end of break-up, and of the minimum ice cover at the end of summer and (3) comparatively investigates the changes in the ice regimes of polar desert lakes versus those of polar oasis lakes.

This study aims to reveal recent changes in the ice cover of lakes in the CAA and thus to provide a glimpse into foreseeable changes that these sensitive Arctic lacustrine systems are likely to experience if climate conditions of the last two decades persist. Moreover, this analysis continues observation records of some lakes that have been previously studied and sets the basis of a monitoring record for High Arctic lakes that have not yet been investigated.

5.2 Study Area

The High Arctic is in its majority a polar desert area with mostly barren land surfaces, intense and persistent coldness, and low amounts of precipitation (Woo et al., 2006). Mean annual temperature (1950-2011) at Alert, Nunavut (82°30’ N, 62°20’ W) is -19°C, at Eureka, Nunavut (79°59’ N, 85°56’ W) is -18°C, and at Resolute, Nunavut (74°41’ N, 94°49’ W) is -15°C. For the same period, mean total precipitation fall is 158 mm at Alert, 161 mm at Resolute and 79 mm at Eureka (Environment Canada, 2011).

Positive temperatures are registered only during July and August, and occasionally in June and September, and most precipitation falls between July and October, mostly as snow (Environment Canada, 2011). The summer melt periods are shortest (~ 3 weeks) for the north coast, while they last ~8 weeks near Alert and ~10 weeks at Lake Hazen (Thompson, 1994). Results of this study indicate that melt periods of lakes on Northern Ellesmere Island last ~6

weeks, melt periods of Lake Hazen last ~6.6 weeks while all other lakes have melt periods lasting ~4 weeks.

The current study focuses on 11 lakes located in the CAA, mostly small lakes with surface areas between 4 km^2 and 16 km^2, with the exception of lake L11 on Baffin Island (64 km^2), Stanwell Fletcher Lake (339 km^2) and Lake Hazen (542 km^2) – the largest lake within the Arctic Circle (Figure 5.1).

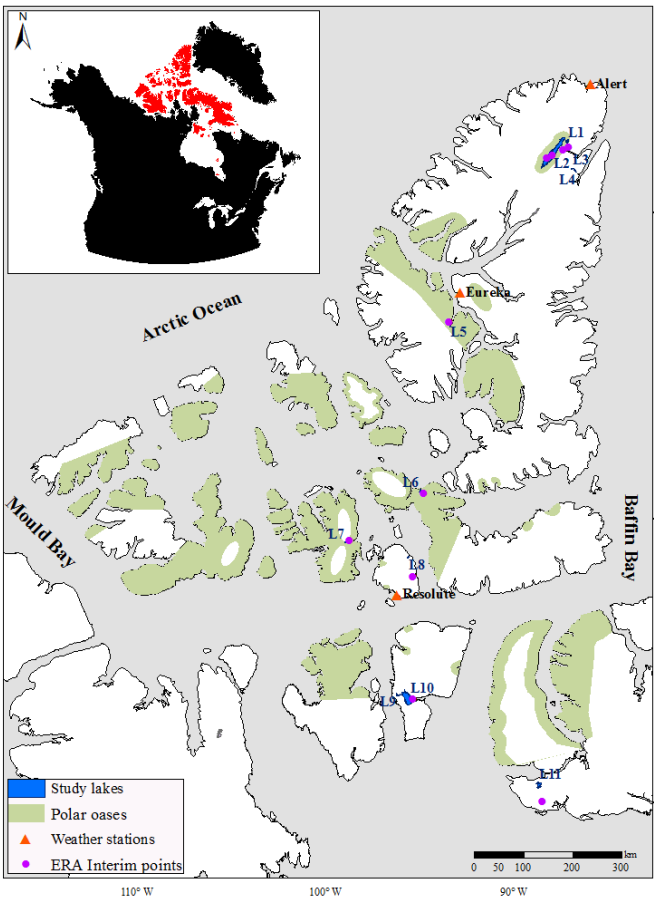

L1. Craig Lake (Ellesmere Island)
L2. Lake Hazen (Ellesmere Island) - polar oasis
L3. Upper Murray Lake (Ellesmere Island)
L4. Lower Murray Lake (Ellesmere Island)
L5. Buchanan Lake (Axel Heiberg Island) - polar oasis
L6. Unnamed Lake (Devon Island) - polar oasis
L7. Unnamed Lake (Bathurst Island) - polar oasis
L8. Eleanor Lake (Cornwallis Island)
L9. Unnamed lake (Somerset Island)
L10. Stanwell Fletcher (Somerset Island)
L11. Unnamed lake (Baffin Island)

Figure 5.1: Location of monitored lakes in the Canadian Arctic Archipelago. Distribution of polar oases is also shown (Woo and Young, 1997, after Bliss, 1977). Inset shows location of the Canadian Arctic Archipelago within the North-American Arctic.

Observed maximum ice thickness of lakes on Northern Ellesmere at the beginning of winter ranges from 1.1 to 2 m (Jeffries and Krouse, 1985; Belzile et al., 2001; Mueller et al., 2009). *In situ* observations on Upper and Lower Murray Lakes at the start of the melt season in early June 2005 indicated an ice thickness of 1.5 to 2.2 m (Cook and Bradley, 2010). Previously recorded early-season snow depth on Northern Ellesmere lakes ranged from 42 to 52 cm (Belzile et al., 2001; Mueller et al., 2009). Recent records of snow depth over these northern lakes do not exist. While the majority of the study lakes are dominated by typical polar desert climate, four lakes are located in so-called polar oasis environments.

Polar or High Arctic oases, are fairly small regions (with surface areas ranging from 10^{-2} to 10^{2} km^{2}) (Woo and Young, 1996) of relatively great biological production and diversity, with warmer soil and longer growing season (Courtin and Labine, 1977), discretely localized from the surrounding arid landscape of polar deserts (Svoboda & Freedman, 1981). Lakes with longer frost-free seasons are associated with higher primary productivity and more rapid nutrient cycling (Perren et al., 2003; Keatley et al., 2007; Callaghan et al., 2012). They are characterized by a milder microclimate (Woo and Young, 1997) that is mainly attributed to higher incoming radiation given by the fact that most frequently they develop in relatively flat coastal lowlands, exception being the thermal oasis surrounding Lake Hazen (France, 1993). Lake Hazen is situated in a trough, and is sheltered from the cold Arctic Ocean air by the Grant Land Mountains (> 2000 m) in the north and a plateau (400-900 m) in the south.

Ellesmere Island contains some of the largest polar oases in the Queen Elisabeth Islands of Arctic Canada, including Eureka, Tanquary Fiord and Lake Hazen (Edlund and Alt, 1989). Other High Arctic oases have been identified on Devon Island *(*Bliss, 1977), Alexandra Fiord (Freedman et al., 1994), Polar Bear Pass (Bathurst Island), at Sherard Bay (Melville Island), and Mould Bay on Prince Patrick Island (Aiken et al., 1999). Given that the current analysis is limited by the low spatial resolution of the SAR sensors (150 m for ASAR, and 200 m for RADARSAT-1/2), Lake Hazen, Buchanan Lake, lake L6 on Devon Island and lake L7 on Bathurst Island were the only investigated lakes located in polar oases environments.

5.3 Data and Methods

5.3.1 Satellite acquisitions

Due to frequent revisits at high northern latitudes and their ability to acquire data during polar darkness and through cloud cover, spaceborne SAR sensors are suitable for monitoring changes in the ice cover of High Arctic lakes. In C-band (~5.3 GHz) SAR imagery, the high contrast between ice and open water, representing the amount of radar signal or backscatter (σ°) returned to the sensor, allows detection of the timing of summer ice minimum and water-clear-of-ice (Morris et al., 1995; Duguay et al., 2002; Geldsetzer et al., 2010). Given the relatively coarse spatial resolution of SAR images used in this study, melt onset detection is limited, particularly for small lakes (Cook and Bradley, 2010). Robust determination of the timing of lake freeze-up using SAR is limited by the low σ° contrast between the open water and the newly formed floating ice (Cook and Bradley, 2010) and also because the C-band co-polarized backscatter from water is not only sensitive to wind speed but also to wind direction (Geldsetzer and Van der Sanden, 2013). Considering the limitations that freeze-up detection pose with SAR, particularly at VV polarizations and to a lesser degree for HH-polarized images, this study focuses on monitoring the break-up period of High Arctic lakes in the CAA.

Given that the current study includes 11 lakes that were monitored for a period of 15 years, the number of satellite observations employed in the analysis was considerable: ~22,148 SAR acquisitions (RADARSAT-1/2 and ASAR) (Table 5.1) and over 2,000 Landsat images; ~1,600 SAR images were segmented to derive ice/open water fractions.

Table 5.1: Total number of satellite images used for monitoring the ice cover of 11 lakes in the Canadian High Arctic during the break-up season from 1997 to 2011.

Year of observations	RADARSAT-1	RADARSAT-2	ASAR
1997	231	-	-
1998	761	-	-
1999	787	-	-
2000	718	-	-
2001	1777	-	-
2002	1476	-	-
2003	1431	-	-
2004	1392	-	-
2005	1282	-	126
2006	1202	-	403
2007	1435	-	316
2008	1100	2740	339
2009	65	1561	539
2010	155	1077	380
2011	-	-	855
Total	**13812**	**5378**	**2958**

The ASAR images were provided by the European Space Agency (ESA) as a Wide Swath Mode Medium Resolution Image (ASA_WSM_1P) product. The ASAR instrument, on board of ESA's ENVISAT, when in wide-swath mode is using the ScanSAR technique (the same as RADARSAT-1/2), provides a spatial resolution adapted for regional monitoring (approx. 150 m, with a pixel spacing of 75 m). The combination of HH- and VV-polarized images was acquired at incidence angles ranging from 17° to 42°. The time lapse between repeat passes (or revisit time) of ENVISAT is 35 days. In order to increase the frequency of observations, data from different tracks, descending and ascending orbits, were used.

RADARSAT-1/2 data, with a spatial resolution of 100 m and a pixel spacing of 50 m, 2x2 block averaged to 100 m (obtained from the Canadian Ice Service), acquired at incidence

angles of 19°-49° (RADARSAT-1) and 20°-46° (RADARSAT-2), is a ScanSAR Wide mode product. The single-polarized (HH) RADARSAT-1, and single- and dual-polarized (HH+HV) RADARSAT-1/2 images were acquired approximately every 2-3 days during the break-up season of each year of study.

In addition to SAR data, archived Landsat 4 Thematic Mapper (TM) and Landsat 7 Enhanced Thematic Mapper Plus (ETM+) imagery, with a spatial resolution of 30 m, was also used. Because of the data gaps in the Landsat imagery from 1997 to 2003 and the limited number of images during spring melt after 2003 for some of the lakes included in this study, the Landsat images were not used for calculating ice/open water fractions. Instead, the Landsat imagery was utilized to complement and evaluate the SAR observations, and thus build a reliable record from the beginning to the end of the ice season during the 15 years of record.

5.3.2 Climate data

Climate records of air temperature, including daily, monthly and seasonal averages from 1997-2011, were collected in support of the analysis of satellite-derived ice phenology parameters. Given that the majority of weather stations in the CAA with longer climate records are situated at a significant distance from most lakes included in the current study, with distances ranging from 60 to 255 km, a combination of weather station and surface air temperature reanalysis data was used to assess the observed changes in lake ice regimes.

5.3.2.1 Weather station records

Meteorological station data from Environment Canada's National Climate Data and Information Archive was used for post analysis of the spaceborne observations. These records include mean temperature and precipitation data from 1 January 1997 to 31 December 2011, for three permanent weather stations: Alert, Eureka and Resolute, Nunavut. Air temperature anomalies from 1997 to 2011 based on the available weather station annual mean temperature records are shown in Figure 5.2.

(a)

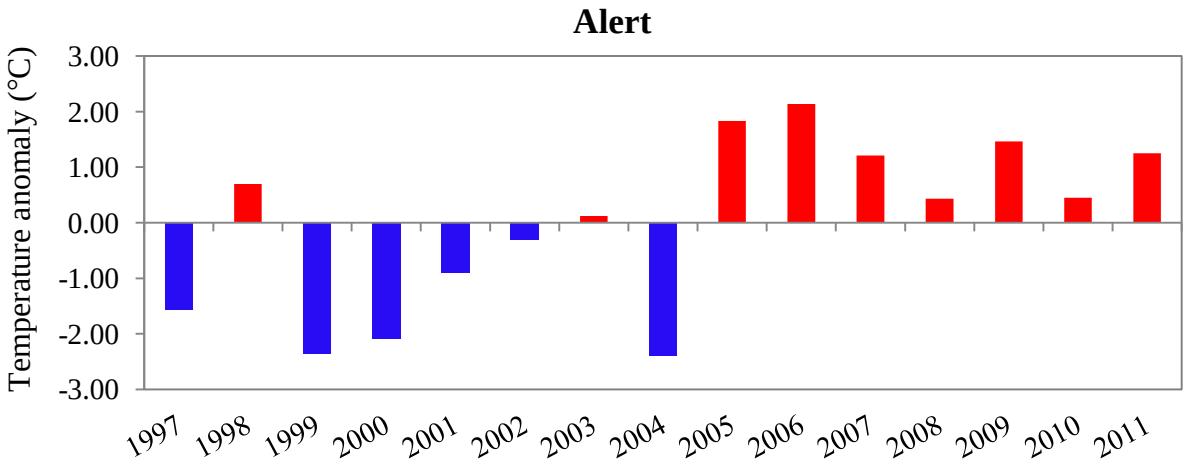
Alert
Temperature anomaly (°C)
3.00
2.00
1.00
0.00
-1.00
-2.00
-3.00
1997
1998
1999
2000
2001
2002
2003
2004
2005
2006
2007
2008
2009
2010
2011

(b)

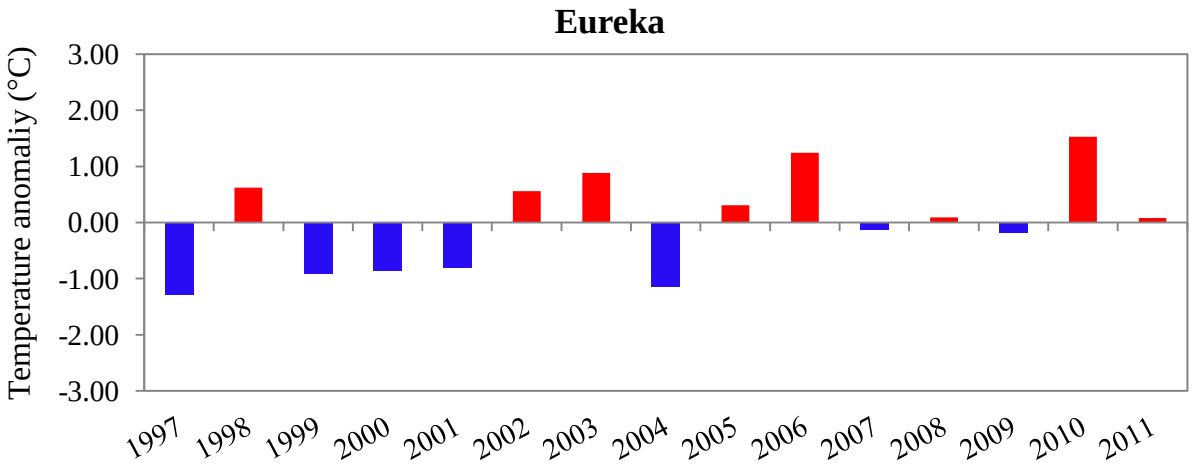
Eureka
Temperature anomaliy (°C)
3.00
2.00
1.00
0.00
-1.00
-2.00
-3.00
1997
1998
1999
2000
2001
2002
2003
2004
2005
2006
2007
2008
2009
2010
2011

(c)

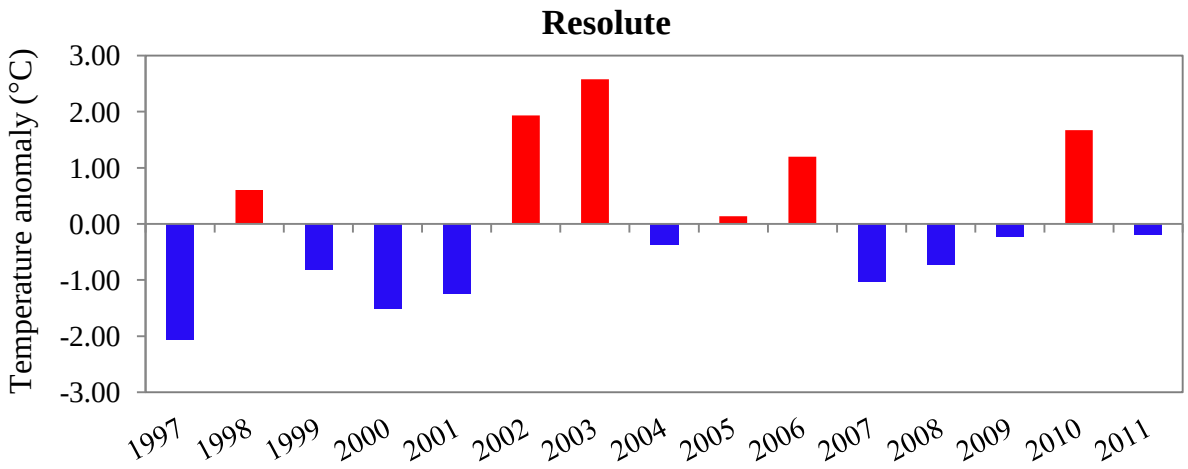

Figure 5.2: Air temperature anomalies for (a) Alert, (b) Eureka and (c) Resolute relative to the 1997-2011 mean annual temperature.

These anomalies are to be used as a reference in interpretation of lake ice events during the same period. The weather station records, complemented by ERA-Interim reanalysis data, were used for assessment of the relation between air temperature and ice phenology of lakes situated within a 0-120 km range from the weather station. Temperature records for lakes located further from the weather stations were based exclusively on ERA-Interim reanalysis data.

5.3.2.2 ERA-Interim reanalysis data

The ERA-Interim is the largest global atmospheric reanalysis product of the European Centre for Medium-Range Weather Forecasts (ECMWF). The full-resolution (~0.75° x 0.75°) gridded product is derived from data assimilation from a variety of sources: radiances from the Special Sensor Microwave Imager (SSM/I), radiosonde temperature, scatterometer ocean surface wind data, including recalibrated data from the European Remote Sensing (ERS-1/2) satellites, and until 2009 from QuickSCAT (Dee et al., 2011) and provides global coverage since 1979. For the purpose of this study, the 2-m near-surface temperature computed with a

sequential data assimilation scheme, advancing forward in time using 12-hourly analysis cycles, was utilized.

5.3.3 Image processing and analysis

A total of ~1600 SAR images acquired from the beginning of the melt season until the water was clear of ice (WCI or break-up end or 100% ice free), or in cases when perennial ice was identified, until the beginning of freeze-up were selected. The selected images were segmented using the most common clustering method, the unsupervised K-means classification algorithm. This algorithm has proved to be a suitable method to discriminate between ice and open water and thus monitor the lake ice break-up using SAR data (Sobiech and Dierking, 2013). Keeping in mind the large number of images analyzed in this study, the K-means algorithm was preferred over a fixed threshold method as it performs better given the changing ice conditions (Sobiech et al., 2013) during the melt season. The unsupervised K-means classification is an iterative process in which image intensity values are divided into 'k' classes or clusters. Throughout the 20 iterations performed for each segmentation, the K-means classification assigned each intensity value to the class with the nearest arithmetic mean (minimum-distance technique).

In order to reduce the inherent speckle present in SAR images, a Lee filter (Lee, 1980) with a kernel size of 3x3 was applied to all geocoded images. After the speckle was removed, regions of interest (ROIs) covering the lake areas were selected. Following ROI designation, image segmentation of each ROI was performed. The classification only included the pixels inside the ROI, all other pixels being excluded from analysis. The segmentation was set to five clusters that were further merged into two classes, one for open water and one for ice, that were next represented on a two-class map generated for each segmented image (Figure 5.3). Text files showing the percentage (%) or fraction of open water and ice were extracted for each ROI of the classified maps to quantify the amount of ice present on lakes from the start of the break-up process until the end of the melt season.

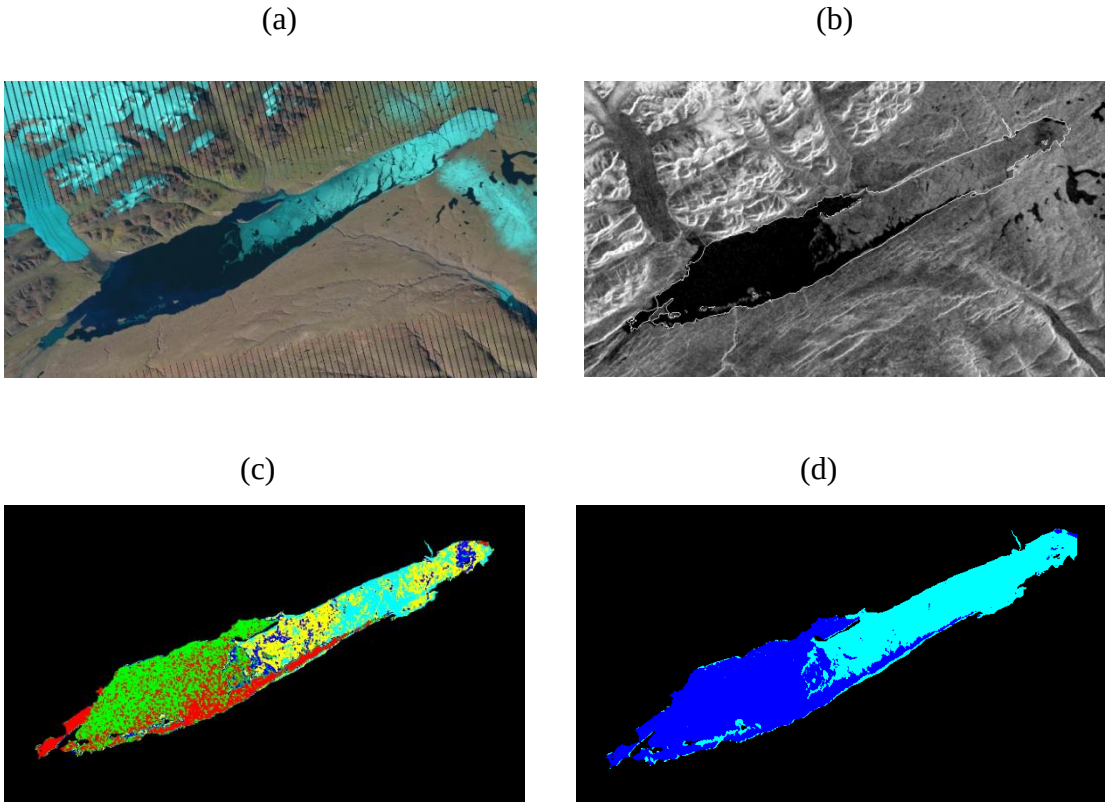

Figure 5.3: SAR-image segmentation processing steps: (a) Landsat image of Lake Hazen, 19 July 2010, (b) original ASAR image of Lake Hazen acquired on 19 July, 2010, (c) K-means classified image (five clusters), (d) two-class map of ice (light blue) and open water (dark blue). The white line in the original SAR image represents the lake polygon that was used for defining the ROIs covering the lake.

In order to estimate the magnitude and significance of changes during the 15-year period, a Mann-Kendall test using Sen's slope (Sen, 1968) was performed. This method has previously been used for detecting the presence of trends in long-term observation of lake ice (Duguay et al., 2006). However, caution should be used in interpretation of the statistical significance values considering that the trend analysis was performed on a relatively short-term time series of 15 years.

5.4 Results and Discussion

Previous knowledge about past ice conditions for small High Arctic lakes is limited to a few lakes located on Northern Ellesmere Island (Belzile et al., 2001; Jeffries et al., 2005; Mueller et al., 2009; Cook and Bradley, 2010) and Colour Lake located on Axel Heiberg Island (Adams et al., 1989; Doran et al., 1996). Latifovic et al. (2007) have provided records of ice conditions for larger High Arctic lakes, results obtained from the Advanced Very High Resolution Radiometer (AVHRR), at 1.1 km spatial resolution. Lakes that have been previously studied and are also analyzed in the current study include Upper and Lower Murray Lakes, previously monitored between 1997-2007 (Cook and Bradley, 2010), Lake Hazen, and Stanwell Fletcher Lake between 1995-2004 (Latifovic et al., 2007). The medium resolution of the SAR data used in this study (1997 to 2011) did not allow continuation of monitoring records for the smaller lakes on Northern Ellesmere Island that were investigated in previous studies.

Satellite observations of the ice cover on 11 lakes in the Canadian High Arctic from 1997 to 2011 reveal great variability in the timing of ice melt onset, summer ice minimum and water-clear-of-ice, with a noticeable direction toward earlier ice-off dates. Compared to the 1997-2011 mean, melt onset started earlier for all lakes, typically in June when positive air temperatures were recorded at these latitudes but cases of melt onset occurring in July were observed. With the occasional perennial ice persisting throughout the short High Arctic summers on Lake Hazen, Upper and Lower Murray Lakes, lake L6 on Devon Island and Stanwell Fletcher Lake, a direction toward earlier ice minimum dates was observed for all lakes during most years of observation. The timing of melt onset was observed to occur earlier in the spring for all other lakes. With the exception of Lower Murray Lake for which delayed summer ice minimum and water-clear-of-ice dates were observed, all lakes experienced earlier ice minimum and water-clear-of-ice dates. Water-clear-of-ice dates ranged from the second week of July to the third week of August. Lakes remained

completely ice free for several weeks prior to starting to refreeze, usually at the beginning of September when below-freezing air temperatures returned.

The analysis focuses on the response of lakes to changes in air temperatures, however, wind speed during spring melt could also contribute to the break-up of the ice cover and play an important role during the break-up process (Liston and Hall, 1995). However, physical break-up by wind is dependent on the lake surface therefore the likeliness of wind to be a contributing factor to ice break-up is mainly limited to the larger lakes, Hazen and Stanwell Fletcher.

5.4.1 Melt onset

Melt onset (start of break-up) was considered as the first date when surface melt or patches of open water were noticed in satellite observations through image segmentation for the SAR acquisitions and visual assessment of the Landsat images.

At the start of the break-up season, pooling water was observed atop the ice cover of lakes on Ellesmere Island (Cook and Bradley, 2010). Considering the similar backscatter characteristics of pooling water on the ice surface and open water (Hall, 1998) at the beginning of lake ice break-up, discriminating between ice and open water in SAR images poses certain challenges. In order to improve the accuracy of melt onset detection, the Landsat imagery provided a valuable complement to the SAR observations.

The Landsat data was also used to detect melt onset as identifying the small areas of open water in the SAR images was more difficult and thus area calculations of open water with image segmentation was not possible for those images acquired at the very beginning of the break-up period. Spaceborne observations were available for most lakes during melt onset from 1997 to 2011 (Table 5.2).

Table 5.2: Melt onset dates shown as day of the year (DOY) for the 11 lakes included in the analysis from 1997-2011. Missing values (n/a) indicate the lack of available satellite imagery. The statistical significance is indicated by the α values.

Year of observations	L1	L2	L3	L4	L5	L6	L7	L8	L9	L10	L11
1997	n/a	205	194	194	209	232	200	208	183	169	182
1998	168	168	184	184	193	184	171	193	170	165	169
1999	184	177	176	176	189	217	171	194	183	180	178
2000	165	171	165	164	172	191	192	198	186	177	185
2001	167	167	167	169	188	200	177	200	184	178	185
2002	167	173	n/a	n/a	195	196	175	203	184	179	197
2003	n/a	n/a	171	173	192	191	180	191	186	181	194
2004	166	162	171	164	199	233	186	200	186	188	210
2005	170	171	182	182	191	210	174	200	181	175	189
2006	183	197	168	168	186	213	173	199	179	181	192
2007	162	168	166	165	185	183	167	185	178	172	179
2008	166	160	166	164	185	184	167	186	179	167	180
2009	165	179	166	162	191	194	170	194	184	179	187
2010	163	159	172	174	180	175	169	175	178	171	179
2011	172	174	n/a	n/a	172	172	164	173	173	168	174
1997-2011 mean	169	175	173	172	188	198	176	193	181	175	185
1997-2011 total days	**-3.3**	**-14**	**-13**	**-19.5**	**-15**	**-39**	**-19.5**	**-22.5**	**-6.7**	**-2.7**	**-2.7**
α	0.1	0.1	0.1	0.05	0.05	0.05	0.01	0.05	0.1	0.1	0.1

During the 15-year period with available satellite acquisitions, advanced melt onset was observed for all 11 lakes, with earlier melt onset by a total of 39 days for lake L6 on Devon Island ($\alpha = 0.05$) and by 2.7 days for Stanwell Fletcher Lake, and lake L11 on Baffin Island ($\alpha = 0.1$). Mean melt onset dates for lakes on Northern Ellesmere Island (i.e. Craig Lake, Upper and Lower Murray Lakes, and Lake Hazen) ranges between 18 June (DOY169) and 24 June (DOY175). Melt onset for lake L6 on Devon Island, Eleanor Lake and Buchanan Lake, was observed to start between 7 July (DOY188) and 17 July (DOY198). Overall, the greatest changes in timing of melt onset dates were observed for lakes located in polar oasis environments (Figure 5.4).

In order to analyze the melt onset-air temperature relation, based on the approach described in Bonsal and Prowse (2003), 0°C spring isotherm dates were calculated. The 0°C spring isotherm date is considered as the date when mean daily air temperature rises above 0°C. Taking into consideration the large variability in daily air temperature, a 31-day running mean filter is used for the mean daily air temperatures.

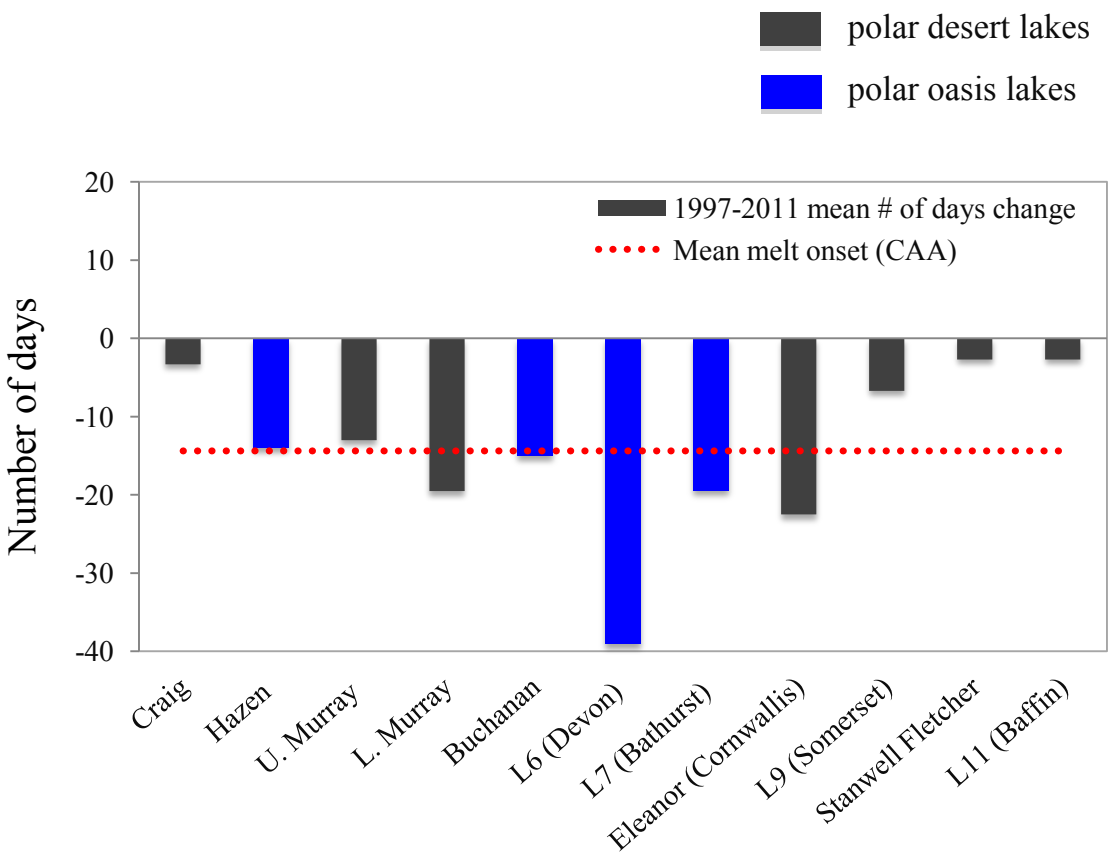

Figure 5.4: Changes – shown as number of days – in the mean melt onset date of lakes in the Canadian Arctic Archipelago (1997-2011). Lakes in polar desert environments are shown as grey bars and lakes in polar oasis environments are shown as blue bars. The red line indicates the 1997-2011 mean number of days change for melt onset.

The date when the running mean rises above 0°C marks the 0°C spring isotherm date. While interannual variability in the melt onset dates existed from 1997 to 2011, lakes generally experienced earlier melt onset during the years with positive anomalies of the 0°C spring isotherm date and later melt onset during the years with negative anomalies of the 0°C spring isotherm date. The 0°C spring isotherm date anomalies from 1997 to 2011 based on the available weather station temperature records are shown in Figure 5.5.

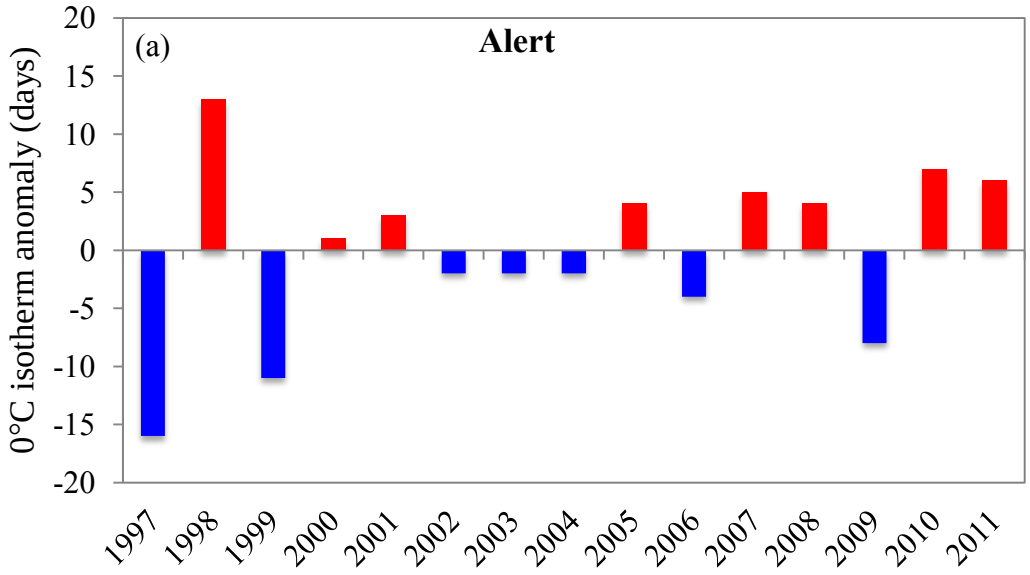
(a)
Alert
0°C isotherm anomaly (days)
20
15
10
5
0
-5
-10
-15
-20
1997
1998
1999
2000
2001
2002
2003
2004
2005
2006
2007
2008
2009
2010
2011

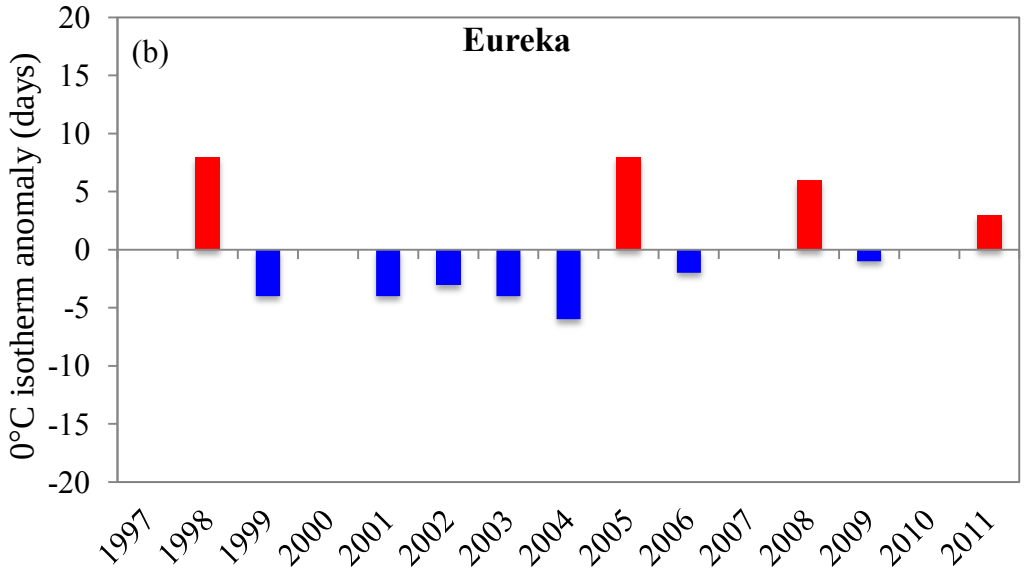
(b)
Eureka
0°C isotherm anomaly (days)
20
15
10
5
0
-5
-10
-15
-20
1997
1998
1999
2000
2001
2002
2003
2004
2005
2006
2007
2008
2009
2010
2011

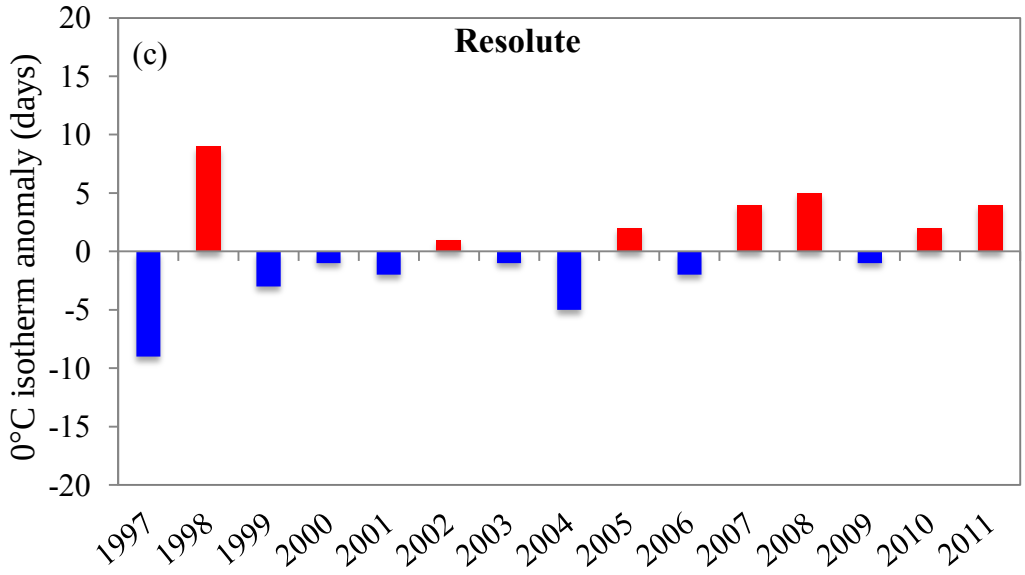

Figure 5.5: The 0°C spring isotherm anomalies (shown as number of days) relative to the 1997-2011 mean 0°C isotherm for (a) Alert, (b) Eureka and (c) Resolute.

For instance, in 1997, a year with negative 0°C isotherm date anomaly (16 days late) at Alert, NU, melt onset for Lake Hazen was observed on 24 July (DOY205). Melt onset for the same lake occurred by 49 days earlier (6 June, DOY157) in 2010, when the 0°C isotherm date anomaly at Alert, NU was positive (7 days earlier). The large positive 0°C isotherm date anomaly (e.g., 1998, 2007, 2010, and 2011) is at Alert a consequence of higher spring air temperatures during these years. Positive temperature anomalies have been associated with episodes of advection of moist, warmer air (Overland et al., 2004) from the anomalous higher sea surface waters of the northwest Atlantic (Sharp et al., 2011). These episodes of warmer air advection in spring/early summer result in large positive anomalies in the near surface temperature that initiate snowmelt (Tisler et al., 2008) and consequently contribute to lake ice melt onset.

The break-up period (1997-2011) for most lakes covered the months of June, July and August (JJA). The relation between the timing of melt onset dates and 0° isotherm date was

determined with Spearman's rank correlation coefficient (R). Analysis shows an overall correlation of R = 0.67 between timing of melt onset and the spring 0° isotherm date.

However, observed earlier/later melt onset is not correlated on a consistent basis with positive/negative 0°C isotherm date anomalies for the study lakes. These discrepancies could be explained by several other factors, including but not limited to the ability of ERA-Interim data to not always accurately express the local meteorological conditions on/around the lakes, the presence or lack of snow over lakes at time of melt onset, the duration of sunlight, wind intensity and the effect of warmer inflows into the lakes.

The presence of the Greenland Ice Cap (Alert, Northern Ellesmere Island), glaciers (Northern Ellesmere Island, Devon Island) and high topographic features (mountains > 2,200 m around Lake Hazen and near Eureka) could lead to discrepancies between the weather station and reanalysis data. Hence, the gridded ERA-Interim data for the Northern Ellesmere Island tends to underestimate the surface air temperature and is not always able to precisely reflect the microclimates, or warmer/colder climatic episodes that develop in some of the High Arctic regions (Brown, 2014, unpublished work).

Given the high albedo of snow, melt onset (the first appearance of open water) could be delayed if a layer of snow or snow ice formed during freeze-up is present on lakes at the beginning of the break-up season. Previous field observations revealed that the ice cover of Murray Lakes at the beginning of the 2005 break-up season entirely consisted of black ice thus lacking the snow-ice layer (Cook and Bradley, 2010). Additionally, most of the high-latitude regions generally experience low amounts of snowfall (< 158 mm/year). These facts could suggest that the presence of snow ice and/or snow on High Arctic lakes is not a significant driver of the break-up process. However, the sparse *in situ* snow accumulation, thickness and ice type measurements limit the evaluation of the importance of snow in the timing of melt onset for the lakes in the CAA.

Another factor to be taken into consideration when discussing the timing of melt onset for lakes is water inflow into the lakes. Nine out of the 11 lakes included in this study have streams flowing into the lake. The origin of the warmer streams flowing into the lakes could be from melting glaciers (i.e. Murray Lakes and Lake Hazen on Northern Ellesmere Island, Buchanan Lake on Axel Heiberg Island) and/or runoff from snowmelt (e.g., lake L6 on Devon Island). The ice break-up of the northern Craig Lake seems to be initiated by a runoff stream outflowing from Lake Hazen (Figure 5.6).

(a) (b) (c)

(d)

Figure 5.6: Landsat images acquired at the start of ice break-up showing melt and/or open water adjacent to water inflows: (a) Upper and Lower Murray Lakes (17 June 2007), (b) Buchanan Lake (8 July 1999), (c) Lake L6, (10 July 2003) (d) Lake Hazen and Craig Lake (16 June 2001).

5.4.2 Summer ice minimum

The last date with a floating ice cover on the lake surface was considered the ice minimum date. During years when lakes maintained a perennial ice cover, the summer ice minimum date was usually observed in late August to mid-September when melt does not occur any longer, and most lakes start refreezing. The mean ice minimum date ranges from 12 July (DOY193, Craig Lake) to 25 August (DOY237, Stanwell Fletcher Lake). From 1997 to 2011, most lakes lost their ice cover during all years of investigation (Table 5.3).

Generally, lakes were observed to lose their ice covers earlier in the season during the years with positive JJA air surface temperature anomalies and retain it later into the summer during the years with negative JJA air temperature anomalies. Similarly, perennial ice lasted from one year to the other during the years with negative JJA air temperature anomalies. With the exception of the polar desert Upper and Lower Murray Lakes that maintained relatively consistent ice conditions or extended the ice cover duration into the summer by 12.4 days (α = 0.1, Lower Murray Lake) during the 15-year observation period, all other lakes experienced earlier minimum ice during the summer and thus earlier ice-off dates. Lakes located in polar oasis environments experienced the earliest summer ice minimum dates, with lake L6 on Devon Island (30 days earlier, $\alpha = 0.1$) and Buchanan Lake (22.5 days earlier, α = 0.05), experiencing the greatest change.

Table 5.3: Dates, shown as DOY, when minimum ice cover was observed for the 11 lakes included in the analysis from 1997-2011. Missing values (n/a) indicate the lack of available imagery. The statistical significance is indicated by the α values.

Year of observations	L1	L2	L3	L4	L5	L6	L7	L8	L9	L10	L11
1997	205	232	231	232	233	246	224	229	215	213	215
1998	182	209	220	220	214	217	186	213	199	217	203
1999	193	249	243	243	208	267	205	221	215	252	215
2000	182	255	212	212	200	214	209	217	211	237	214
2001	188	213	220	229	197	245	203	224	214	253	208
2002	194	238	n/a	241	203	230	206	227	224	257	218
2003	198	n/a	n/a	n/a	197	241	200	212	217	258	218
2004	210	246	213	213	218	244	238	245	244	258	233
2005	187	209	222	223	203	231	206	219	223	232	223
2006	192	234	243	257	202	254	211	222	213	235	215
2007	191	220	234	234	200	214	196	208	202	219	208
2008	191	223	213	226	193	227	191	208	208	238	209
2009	205	250	262	262	205	226	207	218	210	232	213
2010	189	206	210	212	196	216	199	206	212	236	215
2011	186	223	222	249	184	202	195	195	202	217	198
1997-2011 mean	193	229	227	232	204	232	205	218	214	237	214
1997-2011 total days	**-2.1**	**-9**	**0**	**12.4**	**-22.5**	**-30**	**-15**	**-18.8**	**-5**	**-1.5**	**-1.7**
α	0.1	0.1	0.1	0.1	0.05	0.1	0.1	0.05	0.1	0.1	0.1

Eleanor Lake was the only polar desert lake with considerably earlier summer ice minimum dates (18.8 days earlier, $\alpha = 0.05$). All other polar desert lakes experienced minimum negative change (1.5 to 5 days earlier) in the timing of the summer ice minimum date (Figure 5.7).

Perennial ice was observed on occasional years for Lake Hazen (2004 and 2009), Upper Murray Lake (1999), Lower Murray Lake (1999, 2002 and 2006), lake L6 on Devon Island (1997, 2001, 2003, 2004 and 2006) and Stanwell Fletcher Lake (2001 and 2002). Lakes formerly observed to maintain perennial ice covers, such as Lake Hazen in the 1950s (Hattersley-Smith, 1974) and Stanwell Fletcher Lake in the early 1960s (Coakley and Rust, 1968) have preserved a partial ice cover into the following season only during two years out of the 15-year time series of the current investigation. The loss of the perennial ice cover for most lakes is mainly a consequence of the warmer air temperatures recorded in the High Arctic during recent decades.

Conversely, in the case of lakes that did not fully melt during the summer on occasional years, there are other factors that are likely contributing to preserving the ice cover of lakes into early autumn when it starts refreezing. These factors could be related to colder air temperatures during those years, the presence of glaciers (Lake Hazen, Upper and Lower Murray Lakes) that stabilizes the lake ice cover (Doran et al., 1996) through generally persistent low air temperatures, the vicinity of a partially frozen Arctic Ocean and reduced wind action over lakes with smaller surfaces (lake L6 on Devon Island and Lower Murray Lake).

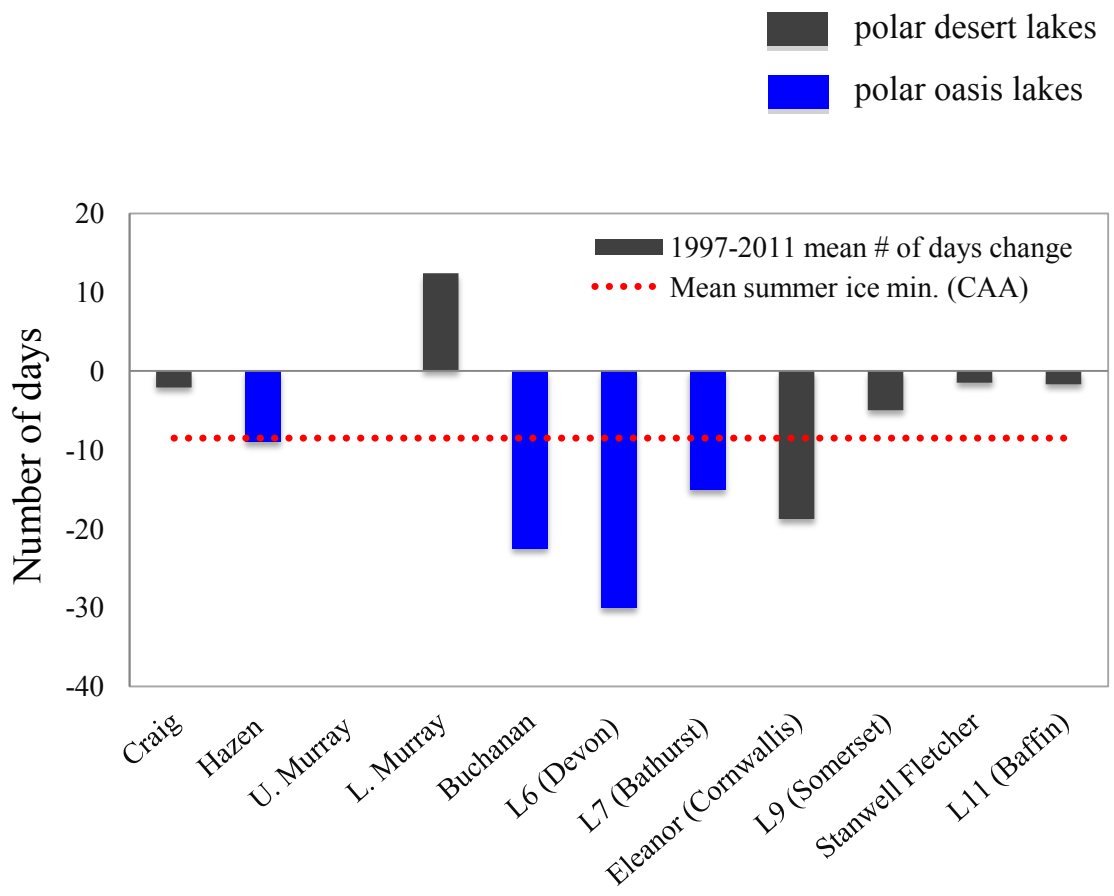

Figure 5.7: Changes – shown as number of days – in the mean summer ice minimum date of lakes in the Canadian Arctic Archipelago (1997-2011). Lakes in polar desert environments are shown as grey bars and lakes in polar oasis environments are shown as blue bars.

5.4.3 Water clear of ice

The end of break-up was indicated by the absence of an ice cover over lakes (0% ice) also known as water clear of ice (WCI). For years with sparse satellite imagery at the end of break-up, the date when the lake became ice free was estimated by interpolating between the date of the last satellite image (either SAR or Landsat) that indicated the presence of ice on

lake surface and the date of the next available satellite observation that showed 100% open water, based on the observed rate of ice decay from previous images.

While most lakes lost their ice cover every summer, observations indicate that a few lakes did not completely melt during the summer months (Table 5.4) of years with greater negative JJA air temperature anomalies (e.g., 1997, 1999, 2004). Analysis indicates that the ice-off date was generally earliest for polar oasis lakes: Lake Buchanan (by 23.6 days, $\alpha = 0.01$), lake L7 on Bathurst Island (by 15 days, $\alpha = 0.1$), Lake Hazen (by 9 days, $\alpha = 0.1$) and lake L6 on Devon Island (by 8.4 days, $\alpha = 0.1$). WCI for the polar desert Eleanor Lake occurred earlier by 20 days ($\alpha = 0.05$). The polar desert Lower Murray Lake experienced later WCI dates by 12.5 days ($\alpha = 0.1$).

Table 5.4: Water-clear-of-ice dates shown as DOY for 11 High Arctic from 1997-2011. Missing values (n/a) indicate the lack of available imagery. Dash indicates that complete melt did not occur. The statistical significance is indicated by the α values.

Year of observations	L1	L2	L3	L4	L5	L6	L7	L8	L9	L10	L11
1997	208	233	232	n/a	234	–	225	232	216	230	216
1998	191	213	221	221	215	220	187	217	204	219	207
1999	201	250	–	–	209	–	207	226	216	255	220
2000	195	–	219	219	201	217	210	218	215	239	219
2001	196	219	220	230	208	–	204	225	215	–	210
2002	195	241	237	–	204	233	209	230	227	–	222
2003	199	n/a	n/a	n/a	198	–	202	214	219	–	220
2004	210	–	n/a	n/a	219	–	244	248	–	–	234
2005	188	210	223	230	204	233	207	220	224	237	224
2006	194	235	249	–	203	–	212	225	215	236	217
2007	200	221	237	241	201	217	197	210	203	222	209
2008	195	224	219	228	194	228	195	214	209	246	210
2009	209	–	–	–	206	227	208	219	212	234	215
2010	192	210	211	217	197	217	200	207	213	237	219
2011	192	225	224	251	185	204	197	196	203	223	199
1997-2011 mean	198	226	227	230	205	222	207	220	214	234	216
1997-2011 total days	**-4.1**	**-9**	**-1.6**	**12.5**	**-23.6**	**-8.4**	**-15**	**-20**	**-4.7**	**-4.4**	**-5**
α	0.1	0.1	0.1	0.1	0.01	0.1	0.1	0.05	0.1	0.1	0.1

Comparative changes in the timing of the water-clear-of-ice date between lakes located in polar desert environments and those in polar oasis environments are shown in Figure 5.8.

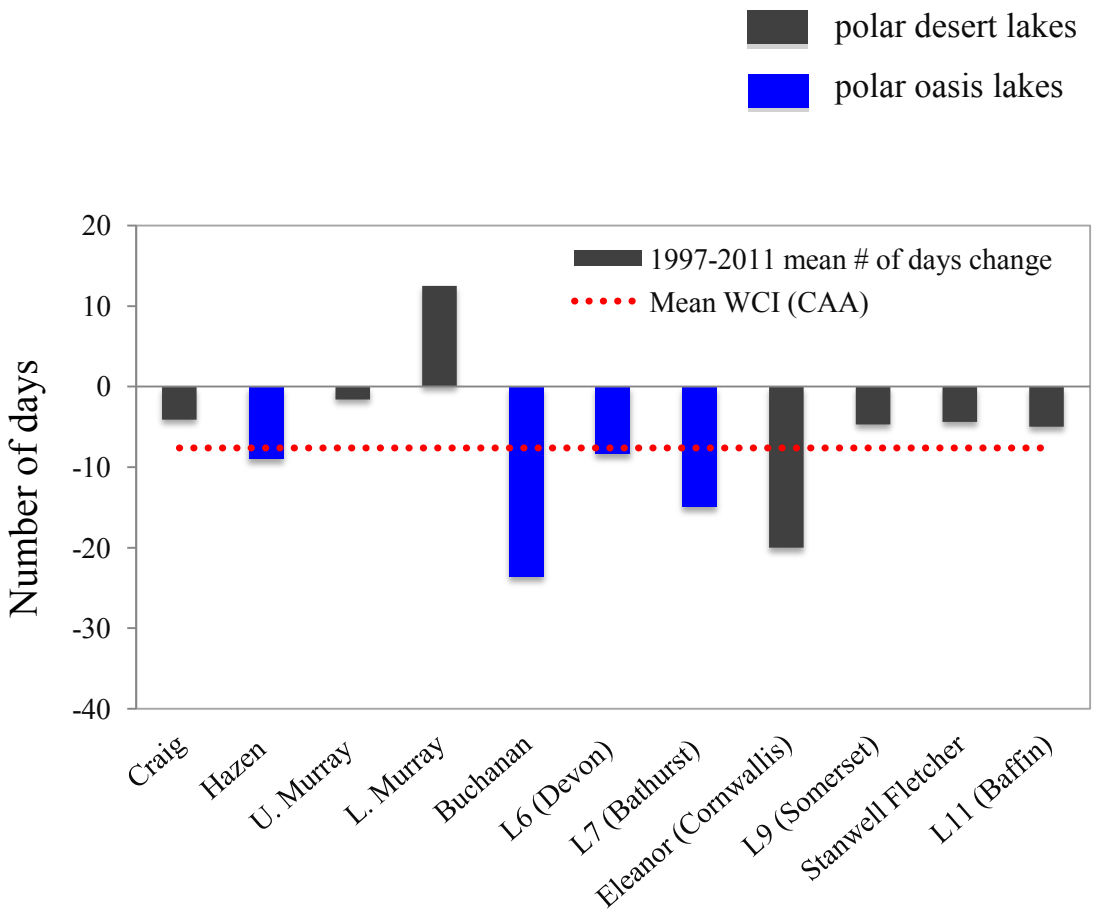

Figure 5.8: Changes – shown as number of days – in the mean water-clear-of-ice date of lakes in the Canadian Arctic Archipelago (1997-2011). Lakes in polar desert environments are shown as grey bars and lakes in polar oasis environments are shown as blue bars.

Analysis of break-up dates in relation to the JA mean air temperature for four lakes – two located in polar oases environments (lake L6 and Buchanan Lake) and two situated in areas

dominated by typical polar deserts climate (Lower Murray Lake and Eleanor Lake) – shows moderate to high correlation between the timing of ice-off dates and the JA air temperature. The highest correlation between ice-off dates and the JA air temperature (weather stations for the nearby lakes and ERA-Interim for lakes located further from the weather station) was observed for Eleanor Lake (R = - 0.70), a lake located closer to a weather station (Resolute). The lower correlation for the other lakes emphasizes the limited ability of the gridded data to accurately represent local climate conditions for the lakes located further from permanent weather stations. These lakes are likely influenced by local microclimates due to the effect of the nearby glaciers and high mountains.

The range of mean WCI dates for the observed lakes from 1997 to 2007 falls between 17 July (DOY198, Lake Craig) and 22 August (DOY234, Stanwell Fletcher Lake). The mean WCI date for Upper Murray and Lower Murray Lake is 15 August (DOY227) and 18 August (DOY230), respectively. The mean duration of the break-up season for Upper Murray Lake is 52 days and for Lower Murray Lake is 55 days. Previous findings of ice regimes for Murray Lakes between 1997-2007 indicate 16 August (DOY228) as a mean ice-off date for Upper Murray Lake and 24 August (DOY236) for Lower Murray Lake, and an average duration of the melt period of 74 and 81 days, respectively (Cook and Bradley, 2010). The earlier timing of WCI dates and shorter break-up seasons for Murray Lakes shown by the current study, are indicative of positive air temperature anomalies at Alert during all years from 2007-2011. Earlier positive air temperatures at the beginning of summer and consecutive days with temperatures higher by 2°-4°C than temperatures recorded during previous break-up seasons of 2007-2011 are likely the main drivers of the earlier ice-off dates and shorter break-up periods for Murray Lakes shown in this study.

AVHRR observations of WCI dates for Lake Hazen and Stanwell Fletcher Lake from 1995-2004 reveal earlier break-up by < 10 days for the former and by 4-6 days for the latter (Latifovic and Pouliot, 2007). The current analysis shows that during the 1997-2011 period, break-up occurred earlier by a total of 12 days for Lake Hazen and by 6 days for Stanwell

Fletcher Lake. Considering that break-up is highly correlated with air temperatures (Duguay et al., 2006), the increase in the number of days revealing even earlier WCI dates for Lake Hazen and Stanwell Fletcher Lake is reflective of higher mean air temperatures during 1997-2011 shown by the gridded ERA-Interim data.

Using all available RADARSAT-1/2, ASAR and Landsat images from the beginning to the end of the break-up period between 1997-2011, WCI timing was determined with an accuracy of 1-3 days, three days being the longest period with no available satellite imagery from any sensor at the end of break-up. A time series of multiple-sensor acquisitions for Lake Hazen during the 2010 break-up season (Figure 5.9) shows the ice cover changes from the beginning to the end of break-up.

Landsat, 8 June 2010

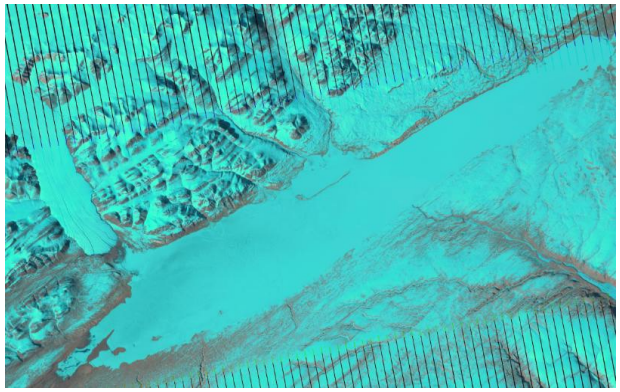

ASAR 9 June 2010

Landsat, 18 June 2010

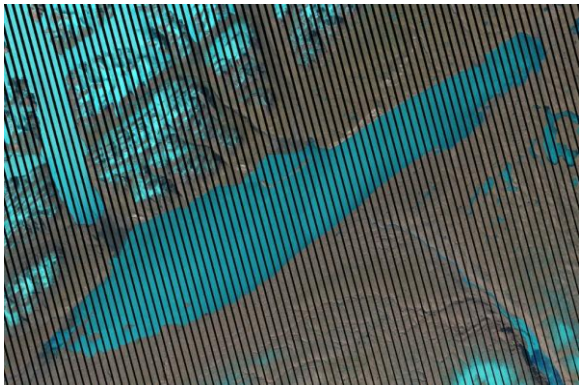

Landsat, 24 June 2010

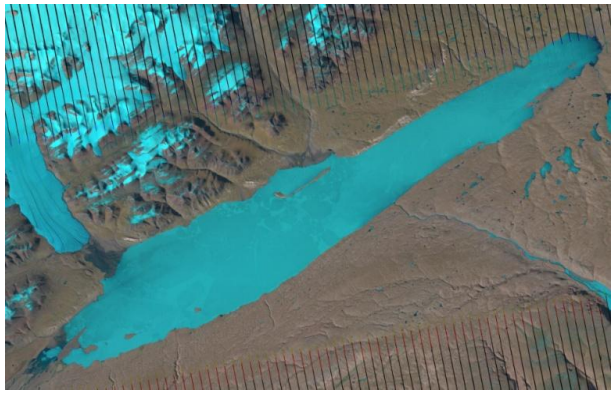

Landsat, 26 June 2010

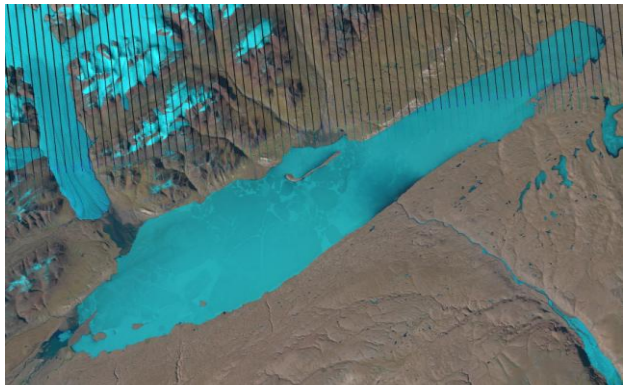

Landsat, 29 June 2010

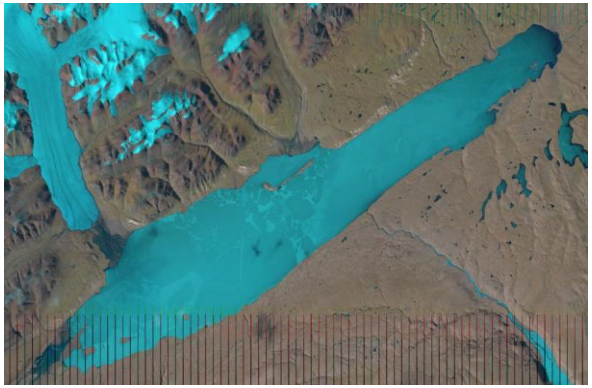

ASAR, 30 June 2010

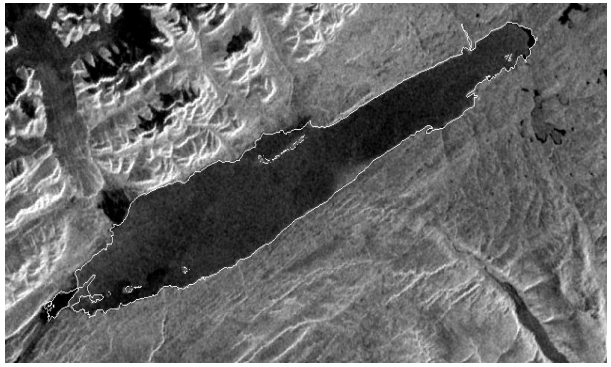

Landsat, 2 July 2010

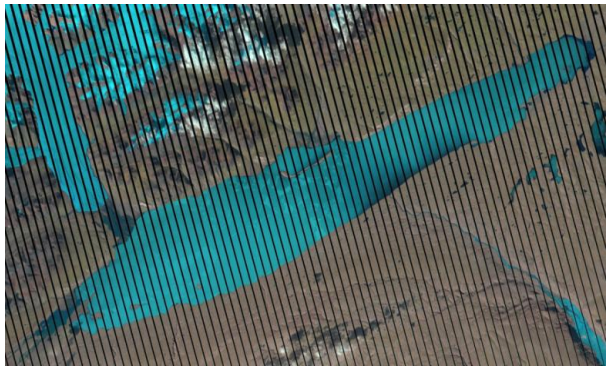

Landsat, 5 July 2010

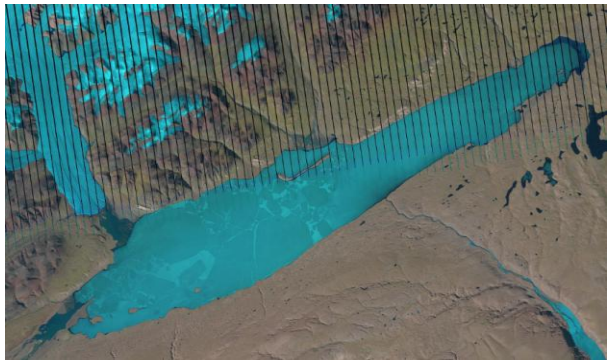

Ice 98%

ASAR, 7 July 2010

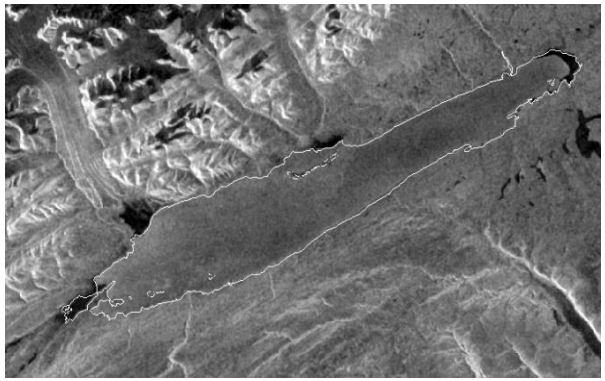

ASAR, 11 July 2010

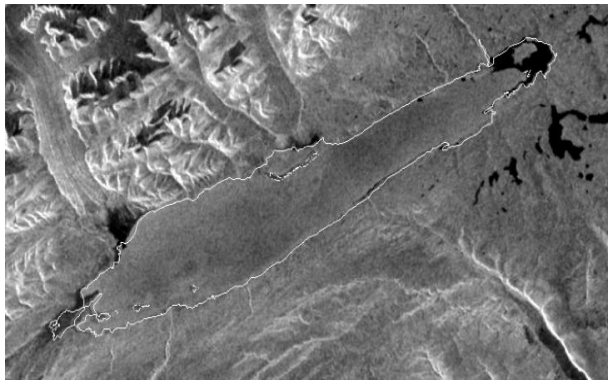

Landsat, 13 July 2010

Ice 97%

Ice 96%

ASAR, 14 July 2010

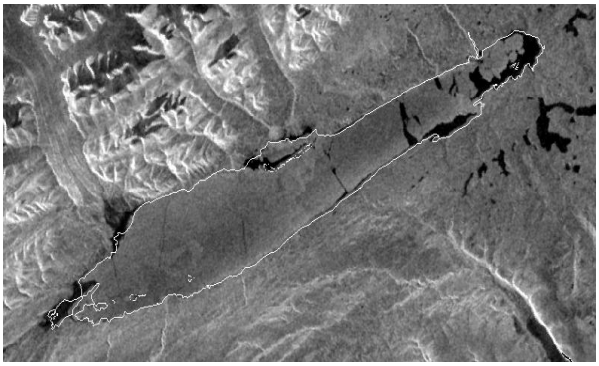

Ice 93%

ASAR, 17 July 2010

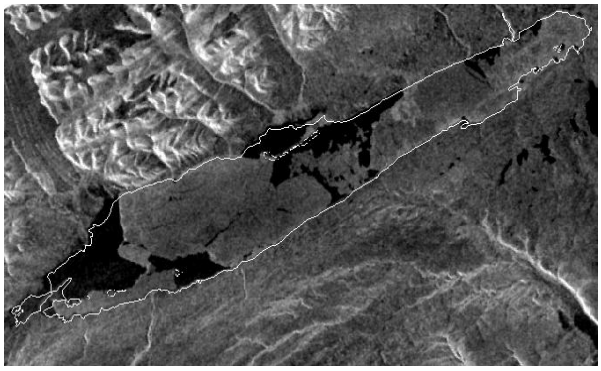

Ice 76%

ASAR, 19 July 2010

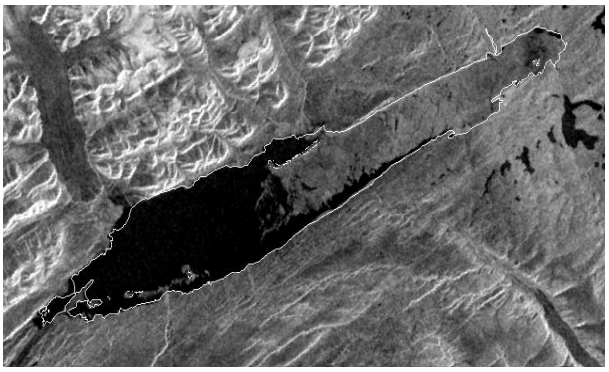

Ice 44%

ASAR, 22 July 2010

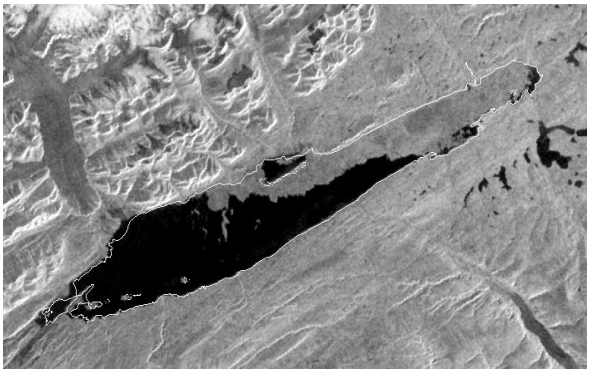

Ice 33%

RADARSAT-2, 25 July 2010

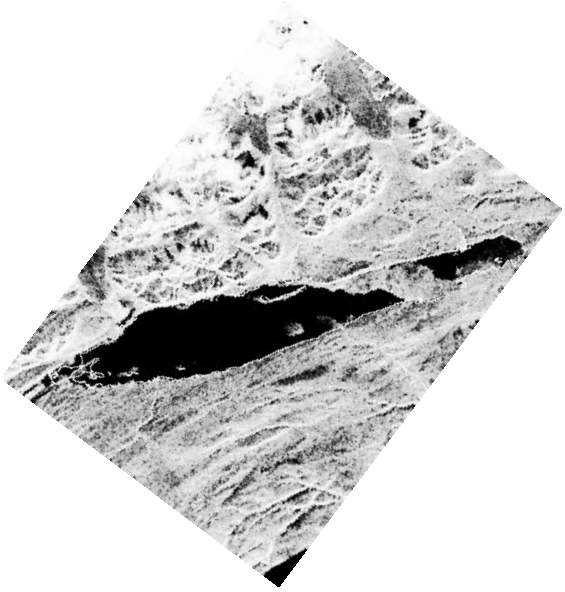

Landsat, 27 July 2010

Ice 18%

ASAR, 29 July 2010

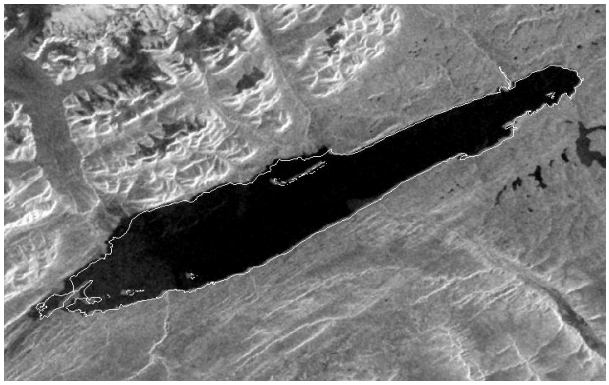

Ice 4%

RADARSAT-2, 31 July 2010

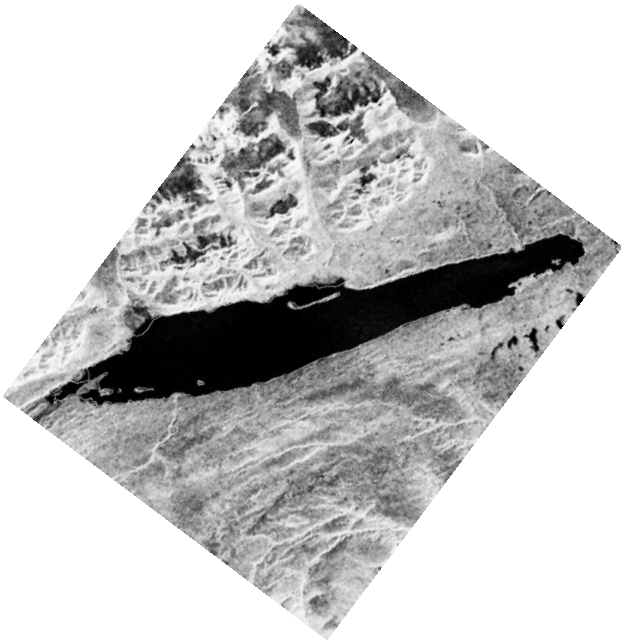

Ice 0%

Figure 5.9: Time series of combined satellite observations (Landsat, ASAR and RADARSAT-2) for Lake Hazen during the break-up period of 2010. RADARSAT-2 Data and Products © MacDonald, Dettwiler and Associates Ltd., 2010 – All Rights Reserved. RADARSAT is an official trademark of the Canadian Space Agency. Ice fractions for available SAR images are also shown. No ice fractions are shown for Landsat observations as image segmentation was only performed on SAR imagery.

Changes in the ice cover of Lake Hazen during the 2010 break-up season reflect the lake ice/temperature relation, the decrease in the ice cover fraction being correlated (R = -0.88) with the number of cumulative thawing degree days (CTDD) calculated based on the ERA-Interim daily mean air temperatures (Figure 5.10). CTDD are a running total of days with mean air temperatures above 0°C.

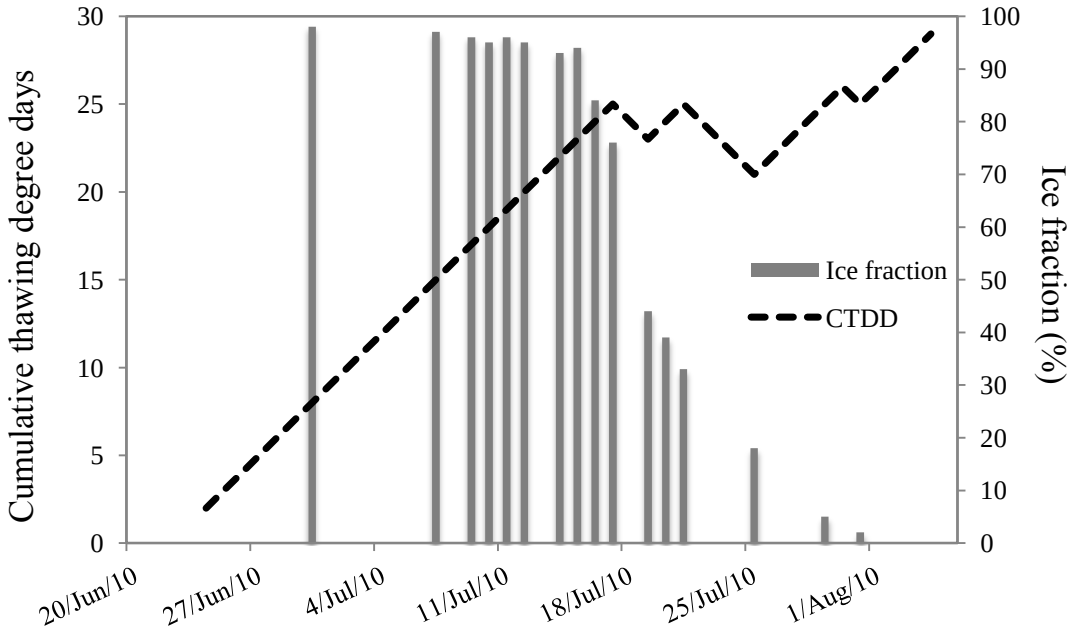

Figure 5.10: The cumulative thawing degree days and ice fraction for Lake Hazen during the 2010 break-up season.

The close relation between WCI dates and temperature was also associated with the 0° spring isotherm date (Bonsal et al., 2003; Duguay et al., 2006). This study shows that a correlation of R = 0.63 exists between the timing of WCI dates and the 0° spring isotherm date.

The greatest changes during the break-up season from 1997 through 2011 were recorded for lake L6 on Devon Island, Buchanan Lake, Eleanor Lake, and lake L7 on Bathurst Island. These lakes experienced earlier melt onset by 19.5-30 days, earlier ice minimum dates by 15-30 days and earlier WCI dates by 15-23.6 days. These extreme changes seem to be characteristic for smaller lakes located in polar oases environments.

Earlier ice break-up consequent to the loss of perennial ice has been observed for Lake Hazen as well but these changes are not statistically significant as they are for the smaller lakes in Arctic oases (earlier melt onset by 14 days, summer ice minimum and end of break-up earlier by 9 days). These findings suggest that due to their smaller surface area and possibly to smaller depths, small High Arctic lakes are prone to more dramatic changes than the larger and deeper lakes. Greater changes in the timing of the WCI date for these lakes are expected to occur as a result of increasing positive air temperature anomalies at these latitudes.

5.4.4 Lake ice and coupled atmosphere-land-ocean interactions

The Arctic cryosphere is a complex system driven by strong interactions among the atmosphere, land and ocean. Under projected amplified warming of polar regions, ice break-up of inland lakes will be prone to a greater change as ice decay is more responsive to changes in air temperature (Bonsal et al., 2006). Considering the dynamic nature of the ocean-atmosphere-land linkages, changes within the lake ice cover are likely to be more prominent and result in more extreme ice conditions associated with warmer events (e.g., extremely late freeze-up, extremely early break-up; Benson et al., 2011), and shift from perennial to seasonal ice cover.

The 1-km resolution combined Moderate Resolution Imaging Spectroradiometer (MODIS)-Aqua/Terra Land Surface Temperature (LST) maps represent a valuable tool in obtaining

consistent observations of “skin” temperature over land at high latitudes. MODIS observations acquired during the break-up season of two extreme years, 2004 (negative air temperature anomalies) and 2011 (positive air temperature anomalies) show up to 5°C differences in the mean JJA air temperatures of the two years, over all study sites (Figures 5.11, 5.12 and 5.13).

(a)

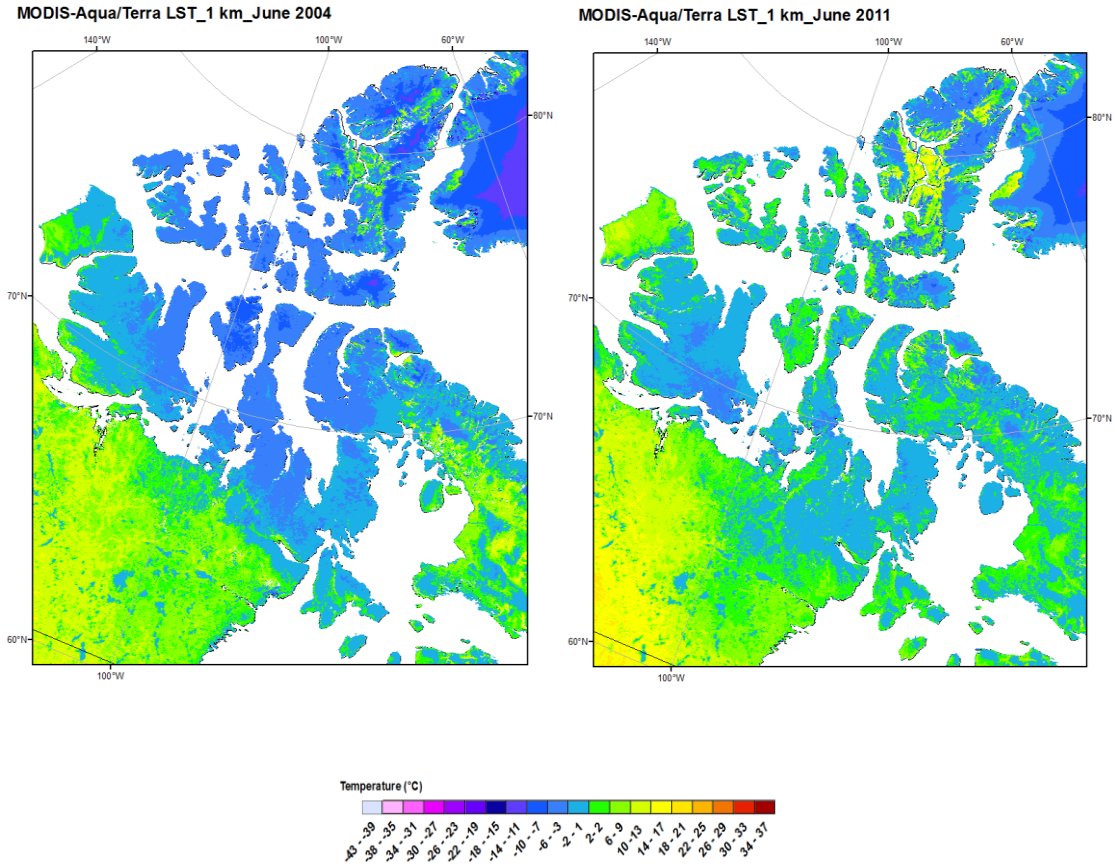

(b)

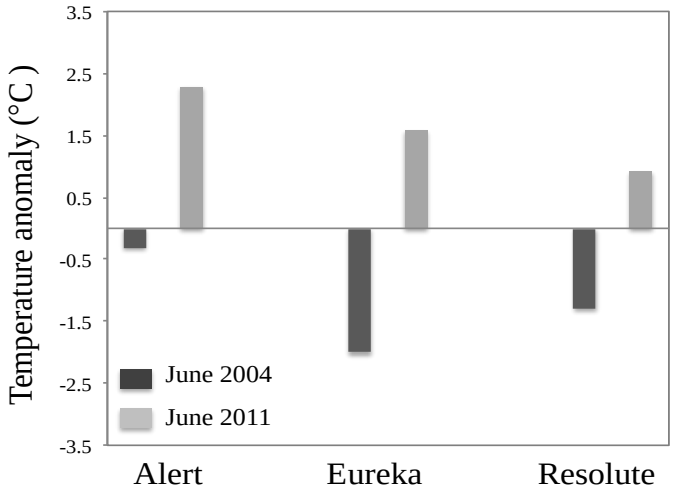

Figure 5.11: (a) Mean land surface temperature derived from MODIS-Aqua/Terra over the CAA during the month of June 2004 and 2011; (b) June air temperature anomalies for Alert, Eureka and Resolute compared to the 1997-2011 June mean air temperature.

Differences in the surface "skin" temperature (MODIS) discriminate the warmer land areas from the colder ones. During years with negative JJA air temperature anomalies, these differences range from 5°-15°C for the polar oases areas around Lake Hazen on Northern Ellesmere Island and Buchanan Lake on Axel Heidberg Island, and from 1°-4°C for the polar oases areas around lake L6 on Devon Island and lake L7 on Bathurst Island. The air temperature differences between the investigated polar oases and the surrounding areas during years with positive JJA air temperatures range from 10°-19°C around lake Hazen and Buchanan Lake and from 9°-16°C for areas around lakes L6 and L7.

In June 2004, the areas around Lake Hazen and Buchanan Lake experienced higher temperatures than the surrounding areas that are controlled by a typical polar desert climate by 5°-12°C. No air temperature difference was observed in the case of areas around lakes L6 and L7 during the same month. In 2011, the June air temperature differences between the warmer polar oases and surrounding areas ranged from 3°-4°C (lakes L6 and L7) and 10°-16°C (Lake Hazen and Buchanan Lake).

(a)

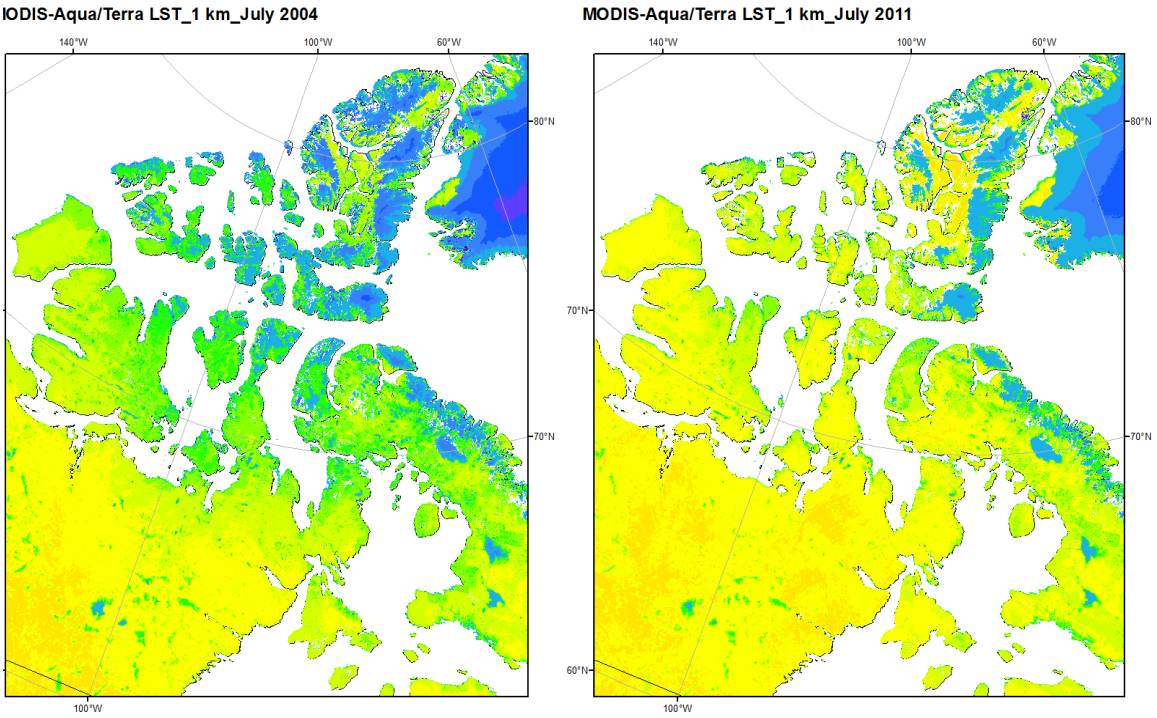
MODIS-Aqua/Terra LST_1 km_July 2004
MODIS-Aqua/Terra LST_1 km_July 2011
140°W
100°W
60°W
80°N
70°N
60°N

(b)

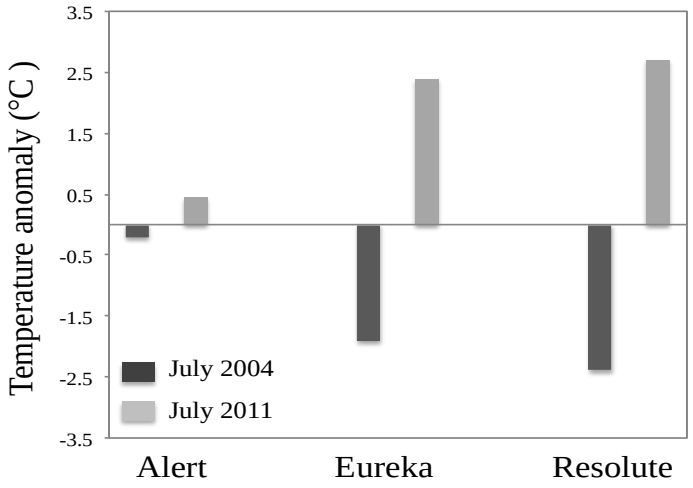
Temperature anomaly (°C)
3.5
2.5
1.5
0.5
-0.5
-1.5
-2.5
-3.5
July 2004
July 2011
Alert
Eureka
Resolute

Figure 5.12: (a) Mean land surface temperature derived from MODIS-Aqua/Terra over the CAA during the month of July 2004 and 2011; (b) July air temperature anomalies for Alert, Eureka and Resolute compared to the 1997-2011 July mean air temperature.

During the month of July, all areas around the investigated polar oases experienced higher air temperature than the surrounding areas. In 2004, these differences ranged from 3°-4°C (lakes L6 and L7) to 3°-11°C (Lake Hazen and Buchanan Lake). These differences were considerably higher in 2011 and ranged from 12°-15°C (lakes L6 and L7) to 9°-19°C (Lake Hazen and Buchanan Lake).

(a)

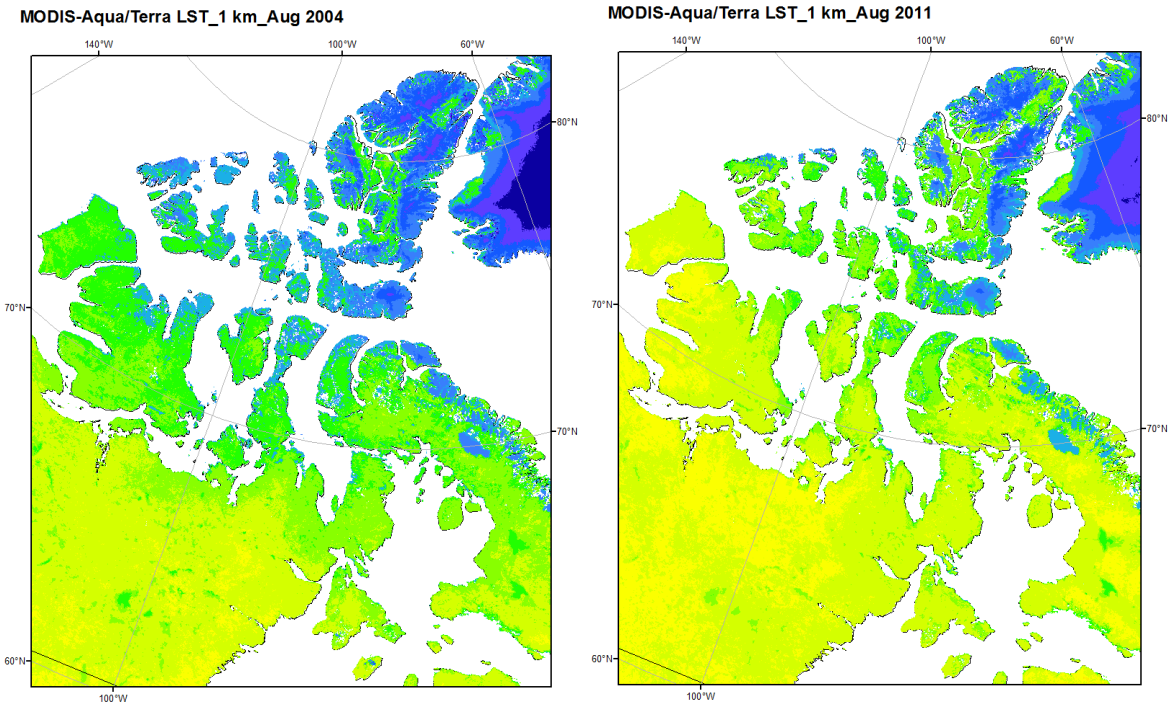

(b)

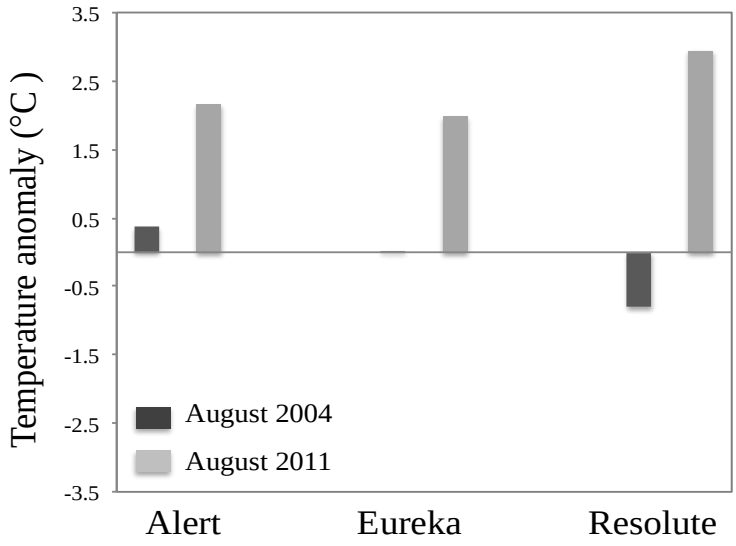

Figure 5.13: (a) Mean land surface temperature derived from MODIS-Aqua/Terra over the CAA during the month of August 2004 and 2011; (b) June air temperature anomalies for Alert, Eureka and Resolute compared to the 1997-2011 August mean air temperature.

During the month of August 2004 and 2011, no noticeable "skin" temperature differences were observed for areas around lakes L6 and L7 in comparison to the usually colder surrounding areas. Air temperatures around Lake Hazen and Buchanan Lake during the same month were higher than the neighbouring areas by 9°-12°C in 2004 and by 13°-16°C in 2011.

Analysis of MODIS data shows that the greatest differences in surface temperature of polar oases and those polar deserts locations investigated in the current study occur in June and July, with significant surface temperature differences during years with higher air temperature anomalies of the same month. Moreover, differences in surface temperature between polar oases and the surrounding polar desert environments is considerably higher around Lake Hazen on Northern Ellesmere Island and Buchanan Lake on Axel Heidberg Island, and less around lake L6 on Devon Island and lake L7 on Bathurst Island. In years with high positive air temperature anomalies, these polar 'hot spots' extend over larger areas and could be impacting

the otherwise typical polar desert climate of these areas (e.g., Craig Lake, located north-east of Lake Hazen).

Investigations of location of polar oases across the Canadian High Arctic have not been performed since 1997. Using the surface temperature compared to the neighbouring areas, through longer records, the MODIS LST product presents the potential to locate other polar oases that may not have been previously identified.

Analysis of air temperature as recorded at the weather stations with available data reveals that temperature anomalies during the same month of the two years are greatest during the month of June at all stations, and smallest in August. The smallest positive air temperature anomaly between 2004 and 2011 was recorded in July, at Alert (0.67°C) and the greatest positive anomaly was observed in July, at Resolute (5.09°C) (Figure 12). In 2004, delayed break-up dates were observed for most lakes, with Craig Lake, lake L11 on Baffin Island, lake L7 on Bathurst Island and Eleanor Lake experiencing the latest break-up dates during the 15-year record. Lake Hazen and lake L6 on Devon Island also maintained a perennial ice cover throughout the 2004 summer. Conversely, melt onset and break-up occurred earlier for most lakes in 2011, extreme earlier WCI dates were observed for Lake Buchanan, lakes L6, L7, Eleanor Lake, lakes L9 and L11. Perennial ice was not observed on any of the 11 lakes at the end of the 2010/11ice season.

Air temperatures at high latitudes are associated with changes in the coupled atmosphere-ocean system (Trenberth and Hurrell, 1994). Warmer air temperatures and a higher Arctic troposphere will continue to reduce the pressure gradient between northern and southern latitudes and will lead to substantial changes in atmospheric circulation patterns (Watanabe et al., 2006). Extreme phases of atmospheric circulation patterns, also known as teleconnections, have been shown to influence ice phenology of lakes in the northern hemisphere (Bonsal et al., 2006), such as the major shift in the Pacific Decadal Oscillation (PDO) in mid-1970s toward a positive phase when North-American lakes experienced earlier break-up and shorter ice seasons (Benson et al.,

2000) or the strong positive phase of El Niño Southern Oscillation (ENSO) in 1998 that resulted in extreme ice events for many of the lakes in the High Arctic and when none of the study lakes maintained a perennial ice cover. The North Atlantic Oscillation (NAO) and the Arctic Oscillation (AO), highly related to each other, also play a significant role in the winter (November-April) Arctic atmosphere.

The lack of a strong correlation between ice break-up of High Arctic lakes and teleconnections from 1997 through 2011 as indicated by a preliminary analysis (not shown) could be explained by the fact that neither PDO nor the NAO/AO has been in a phase to contribute to the Arctic warming during the past several years (AMAP, 2011). On a background of increased warming at higher latitudes, the previous strong correlation between AO and ice regimes of lakes north of 65° (Bonsal and Prowse, 2003) could weaken in the forthcoming decades. However, in order to determine the impact that atmospheric circulation patterns have had on ice phenology during recent years, a more comprehensive analysis is needed.

Recently observed warming of the Arctic (Overland and Wang, 2010; Serreze et al., 2011) has been largely attributed to summer sea ice loss (12% decade^{-1}) in September (NSIDC, 2011) and an ice-albedo feedback, resulting in amplified sensible and latent heat fluxes between the ocean and the Arctic atmosphere (Strey et al., 2010). Sea ice reduction is mostly noticeable during summer and autumn (Deser et al., 2010) but due to the extensive memory of the ocean, its effects are greatly influencing the winter climate and weather patterns of the northern high latitudes (Wu et al., 2006). While the current study does not focus on the analysis of sea ice conditions, a preliminary assessment of the historical total accumulated ice coverage (TAC) and mean air temperature from either weather station or ERA-Interim data in the Canadian Arctic between the weeks of 2 July-30 July is shown (Figure 5.14).

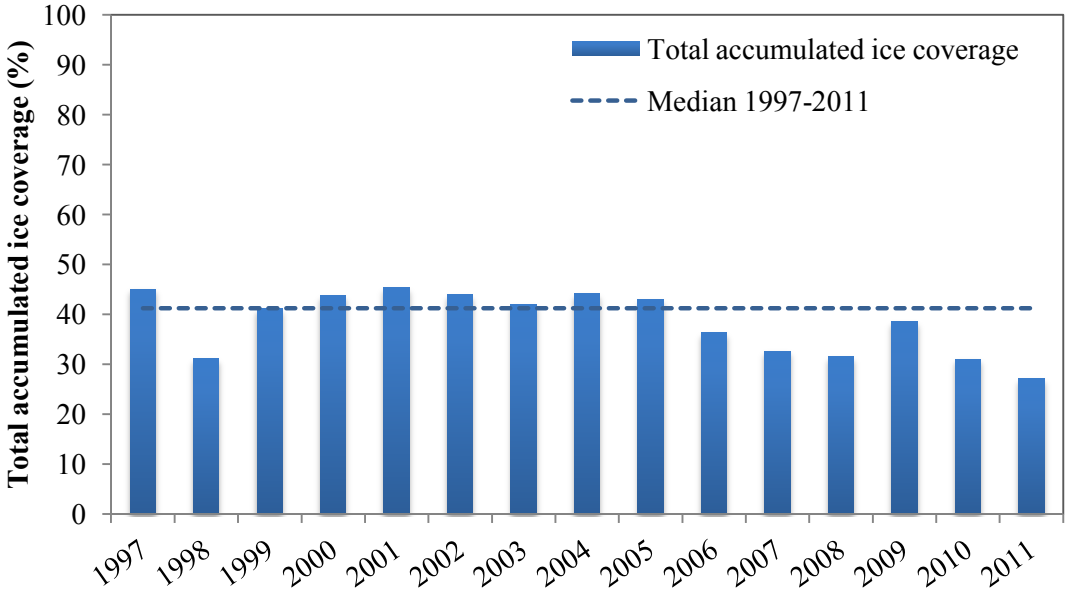

Figure 5.14: Historical total accumulated sea ice coverage in the Canadian Arctic for the weeks of 9 July-3 September, during the summer seasons of 1997-2011. Ice coverage fractions are courtesy of CIS.

Analysis indicates that accumulated July sea ice coverage correlates well with mean air temperatures during the same period (R = -0.72 for Eureka, R = -0.73 for Resolute, R = -0.61 for Somerset Island and R = -0.57 for Baffin Island). Spaceborne observations indicate earlier WCI dates for most lakes in years with lower percentages of total accumulated July sea ice coverage (e.g., 2010 and 2011, with the TAC from 2 July to 30 July of 47% and 43%, respectively). Mean air temperatures for 2010 ranged from 4.77°C (Eureka) to 9.41°C (Baffin Island). In 2011, mean air temperatures ranged from 7.22°C (Eureka) to 11.28°C (Baffin Island).

Conversely, in years when the TAC was higher (e.g., 64% in 2002) and mean air temperatures were lower (between 2.41°C and 6.78°C), delayed WCI dates were observed for many lakes (e.g., Lake Hazen, lake L6 on Devon Island, Eleanor Lake, lake L9 on Somerset Island).

Additionally, a few lakes also preserved a perennial ice cover (Lower Murray Lake and Stanwell Fletcher Lake).

Changes in the sea ice surface are well correlated with changes in the overlying atmosphere (Zhang et al., 2008), the latter strongly influencing surface temperature and large-scale atmosphere and ocean circulation patterns (Hall et al., 2004; Tivy et al., 2011). Sea ice retreat and atypical atmospheric flows are frequently associated with anomalous advection of warmer and moister air by transient winds (Stroeve et al., 2011), considered to be the main driver of high-latitude terrestrial warming (Deser et al., 2010). This anomalous poleward heat transport at the beginning of summer is likely to amply the effect of air temperature on the ice cover at the beginning of lake ice decay and result in extremely early melt onset. Consequent to changes in surface heating and distribution of the atmospheric pressure as a result of sea ice reduction, coastal terrestrial Arctic areas in particular experience higher summer temperatures, often associated with higher vegetation productivity. This relation weakens gradually with increasing distance from the coast (Bhatt et al., 2014).

These results provide an initial assessment of the relation between air temperature, sea ice coverage and lake ice phenology but for a better understanding of the strength of interactions between these components require a more detailed analysis looking at specific sectors of the Canadian Arctic Archipelago.

5.5 Summary and Conclusions

This study provides a robust assessment of lake ice conditions in the Canadian High Arctic, and reveals changes in the break-up dates and the summer ice cover that these lakes experienced between 1997-2011. Analysis of the available SAR and Landsat data from 1997 to 2011 indicates that the start of ice break-up is occurring by 14-39 days earlier for polar-oasis lakes and by 2.7-22.5 days earlier for polar-desert lakes. Changes were also observed in the summer

ice minimum, with ice generally disappearing earlier on all lakes, by 9-30 days earlier in polar oasis environments and by 1.5-18.8 earlier in polar desert environments. Timing of the WCI dates ranges from 9-23.6 days earlier in polar oasis environments and from 1.6-20 days earlier in polar desert environments. The only lake with later WCI dates is Lower Murray Lake (12.5 days).

During the 15-year period covered by this study, the melt onset and ice-off dates occurred earlier for all 11 lakes, with the exception of Lower Murray Lake on Northern Ellesmere Island that despite experiencing earlier melt onset, had an ice cover lasting longer into the summer or even occasionally persisting from one year to another. The lakes with the greatest changes in the timing of melt onset date were Buchanan Lake on Axel Heidberg Island (23.6 days early), Eleanor Lake on Cornwallis Island (20 days early), lake L7 on Bathurst Island (15 days early), Lake Hazen (9 days early) and lake L6 on Devon Island (8.4 days early). Earlier summer ice minimum was also observed on these lakes. Given that with the exception of Eleanor Lake, the lakes with the shortest ice seasons are located in polar oases areas, environments dominated by milder temperatures, comes to reinforce the strong relation between air temperature and lake ice break-up. The increasing positive air temperature anomalies are likely the cause of perennial ice loss for lakes. Lakes that preserved their ice cover from one season to another on a consistent basis (e.g., Lake Hazen, Stanwell Fletcher Lake) in previous decades are transitioning toward a seasonal ice cover, with sparse or no perennial ice seasons. Some of the lakes on Northern Ellesmere Island (i.e. Lake Hazen and Murray Lakes), along with lake L6 on Devon Island and Stanwell Fletcher Lake are the only lakes with observed occasional perennial ice. From 2007 to 2011, Lake Hazen and Murray Lakes were the only ones with observed perennial ice cover in 2009.

In an Arctic that has warmed during recent decades and that will likely continue to be driven by above-normal air temperatures, shorter ice seasons, with later freeze-up and earlier break-up dates, complete loss the perennial ice cover (Brown and Duguay, 2011) and major biological changes within the High Arctic lakes are predicted to persist in forthcoming decades.

Studies suggest that consequent to ice loss and longer growing seasons Arctic lakes and ponds have the potential to experience a large leap in productivity (Smol and Douglas, 2007; Paul et. al., 2010). A possible scenario consequent to a reduced ice cover involves abundance of peripytic diatoms in shallow lakes (Smol et al., 2005), diversification of the planktonic flora (Keatley et al., 2008) and an overall increase of the primary production rate (Smol et al., 2005). Lakes within the polar deserts may virtually start to respond and act like those within polar oases due to the changing climate conditions (Young and Abnizova, 2011). Studying the phenology of the lakes that are presently located in polar oases environments could provide an insight as to how the ice conditions of polar desert lakes may be in the near future.

The increasing positive air temperature anomalies recorded across the Arctic, sea ice reduction, the increased cloudiness over the Arctic consequent to longer summer seasons (AMAP, 2011), earlier snow melt and reduced snow extent at high latitudes (AMAP, 2011), the accelerated glacier melt in the Canadian Arctic, including the Devon Ice Cap (ACIA, 2011) have led to positive feedbacks within the Arctic system. However, given the complexity of the atmosphere-ocean-land interactions and the variability of the Arctic climate, linkages between these components and lake ice phenology require to be investigated in greater detail.

The results presented in this paper document changes in the ice cover of lakes in the Canadian High Arctic in recent years as observed by a combination of SAR and optical sensors, and present a preview of changes that Arctic lakes are likely to undergo in future decades. The combination of radar satellite missions, the recently launched (Sentinel-1a) and the forthcoming RADARSAT constellation, and the upcoming optical (Sentinel 2-a/b Multi-Spectral instrument), with frequent revisit times, will be invaluable tools that will enable consistent monitoring of High Arctic lakes in a dynamic and rapidly changing climate. The 15-year ice records for the observed 11 lakes in the CAA set the baseline for a long-term monitoring database for High Arctic lakes that can be consolidated through observations from future satellite missions.

5.6 Acknowledgements

This work was supported by a Discovery Grant from the Natural Sciences and Engineering Research Council of Canada (NSERC) to Claude Duguay. The authors would like to thank our colleague, Homa Kheyrollah Pour, for providing the MODIS LST maps. We are also grateful to Andrew Wong (University of Waterloo) for helping with processing the overwhelming amount of RADARSAT-1/2 data. We would like to extend our gratitude to Kevin Kang for sorting the RADARSAT data. Additionally, the authors would like to thank to Dr. Laura Brown (University of Toronto) for the personal notes exchanged and for kindly sharing her unpublished work results. We would like to extend our gratitude to the European Space Agency (ESA) for providing the ASAR data and to ESA's Grid Processing on Demand (GPOD) team led by Roberto Cuccu and Giovanni Sabatini for pre-processing the ASAR images. The RADARSAT-1/2 imagery was downloaded from the Polar Data Catalogue. RADARSAT-1 images are copyright the Canadian Space Agency (CSA) 1997-2010. The RADARSAT-2 images were provided by the Canadian Ice Service (CIS). RADARSAT-2 Data and Products, © MacDonald, Dettwiler and Associates Ltd., 2008-2011, all rights reserved. RADARSAT is an official trademark of the Canadian Space Agency. Landsat images were provided by the U.S. Geological Survey.

Chapter 6

General Conclusions

6.1 Overall Summary

The overall objective of this research was to provide a better understanding of the response of Arctic lake ice to recent climate conditions. This work is not only a contribution to Arctic research and freshwater studies in general but it also provides an overview of the implications related to changes in the ice cover of Arctic lakes. Furthermore, considering the extended time series of the analysis, this study also provides the basis of a lake-ice monitoring network that can be further built on in order to create a long-term record.

Chapters 1 and 2 covered the motivation and the research background required to understand the complex interactions between climate and lake ice cover, lake ice thermodynamics, spaceborne monitoring of lakes and lake ice, and lake ice modeling.

The first analysis of a 20-year time series of ERS-1/2 SAR images (1991-2011) investigating the evolution of grounded ice of shallow lakes on the North Slope of Alaska was presented in Chapter 3. Findings were also evaluated against model simulations of ice thickness. Moreover, in order to determine the long-term changes (1950-2011) in the ice cover of these lakes, model simulations of freeze-up and break-up dates, and ice thickness were also derived. The study revealed a trend toward floating ice covers (22% reduction in the grounded ice cover), thinner ice by 18-22 cm for the period of ERS-1/2 image analysis (1991-2011) and by 21-38 cm over the last six decades (1950-2011). Freeze-up occurred 5.9 days later and break-up 17.7-18.6 days earlier for the same time period (1950-2011).

Analysis of the temporal evolution of C-band backscatter from ASAR and RADARSAT-2 was employed to evaluate the potential of relatively high temporal frequency SAR to detect the timing of ice freeze and melt onset, and ice-off for shallow Alaskan lakes (2005-2011) with an accuracy of 2-5 days. Results presented in Chapter 4 showed that with some

limitations, particularly during the freeze onset, high temporal frequency SAR allows detection of important lake ice events. For the 2005-2011, the mean freeze onset date was 28 September (DOY271), mean melt onset date was 23 May (DOY143) and mean ice-off date was 10 July (DOY191). Comparison of SAR-observed dates with CLIMo simulations revealed similar lake ice events dates, in particular for SAR observations versus the outputs of the 53% snow depth scenario, and during years with more frequent SAR observations (2009-2011).

Chapter 5 documented ice conditions from the start to the end of the break-up season, including summer ice minimum and the presence/absence of perennial ice for 11 lakes in the Canadian Arctic Archipelago (1997-2011). The analysis of combined SAR and optical images showed not only that the investigated High Arctic lakes experienced earlier melt onset and ice-off dates, but also that the lakes have been experiencing advanced summer ice minimum dates that could result in the loss of perennial ice. This study showed that lakes located in polar oasis environments experienced greater changes in ice conditions than the polar desert lakes. Findings indicated that melt onset has been occurring earlier by 14-39 days for polar oases lakes and by 2.7-22.5 days for polar desert lakes. Timing of the ice-off date advanced by 9-23.6 days for lakes in polar oasis environments and by 1.6-20 days for lakes in a typical polar desert. With the occasional residual ice that persists throughout the summer for a few lakes, most lakes do not maintain a perennial ice cover from one ice season to the other.

This thesis investigated changes in the ice cover of North-American Arctic lakes over a two-decade period and thus provides a comprehensive monitoring record that can be further build on. Spaceborne observations were found to be an invaluable tool in documenting changes in the ice cover of remote Arctic lakes where consistent *in situ* observations are sparse or nonexistent. The use of C-band SAR images combined with optical imagery provided the opportunity to detect changes in the lake ice cover with a accuracy of 2-5 days for melt onset

and of 1-2 days for the end of break-up. The C-band backscatter from two different SAR sensors allowed detection of both freeze-up and break-up.

Lake ice has been shown to promptly reflect changes resulting from complex feedback processes and interactions between land, ocean and atmosphere. Lake ice response to a changing Arctic climate system is controlled by a multitude of parameters but identified short-term and long-term lake ice trends have been particularly associated with changes in air temperature, and snow depth and distribution. The assessment of spaceborne satellite observations of lake ice conditions against model simulations, air temperature data from weather stations, ERA-Interim and MODIS, and snow depth measurements reinforce the strong relationship between lake ice as well as regional and local climate conditions. Variations in air temperature are meaningful particularly for break-up. In a climate largely controlled by positive air temperature anomalies observed during the last decade, the lake ice cover of Arctic lakes is expected to undergo significant changes. Trends toward thinner ice covers, later freeze-up dates, earlier break-up dates, reduced late-winter grounded ice and the loss of the perennial ice cover at high latitudes have been observed and are expected to continue or even intensify in the future.

6.2 Limitations

The two most prominent drawbacks of this work are the temporal and the spatial resolution of the SAR sensors that were available. While revisit times range from 24 to 35 days, for both SAR and optical sensors, more frequent acquisitions are possible at higher latitudes. Considering that small lakes respond to synoptic weather conditions and that ice cover conditions could change within one day, spaceborne observations do not always manage to capture these daily changes. The combined use of SAR and optical sensors improves the accuracy of ice events timing, particularly during break-up when optical observations are not as hampered by the presence of clouds.

The medium resolution SAR data available for this thesis were a limiting factor for detection of melt onset on small lakes in particular. The 100-150 m spatial resolution does not always allow detection of small areas of open water, typically lateral, if only a few lake pixels are affected by melt. Landsat images, with a 30-m spatial resolution, present a valuable complimentary tool for break-up monitoring.

Freeze onset detection is complicated by the effect of wind speed and direction over open water on C-band co-pol (HH and VV) backscatter and that of similar radar returns from the newly formed ice and open water, resulting in high returns that may signal a false freeze onset. Detection of lake complete freeze over was not feasible because of the limited number of available images following freeze onset.

Image segmentation was performed in order to derive the grounded ice fraction versus that of floating ice using the MAGIC software (Chapter 3) or to determine the ice fraction of ice versus that of open water (Chapter 5). Algorithms used for image segmentation do not include automated labeling and thus a human operator was needed to visually inspect each segmented image and compare the segmentation results with the original image in order to determine class merging and perform labeling of each class.

Lack of weather station data in the High Arctic limits model simulations with parameters illustrative of local climate conditions. Considering this limitation, CLIMo results were not used for evaluating the observed ice conditions in the Canadian Arctic Archipelago presented in Chapter 4, as they would not have been always representative. Scarcity of weather station data limited the assessment of spaceborne detected changes in the lake ice cover against local climate conditions. Lack of air temperature records was supplemented with MODIS-Aqua/Terra LST data, also known to inherent a cold bias.

6.3 Future Directions

Documenting the response of Arctic lakes to changing climate conditions is limited by a declining, almost non-existent *in situ* lake ice monitoring network since the 1980s. This research demonstrates that historical C-band SAR and Landsat observations provide a practical alternative to documenting long-term changes in the ice cover of small lakes on the North Slope of Alaska or lakes of various sizes in the Canadian High Arctic. Moving forward, an important step in improving the monitoring record of lake ice phenology and improving the retrieval accuracy of changes in the lake ice cover mandates a multi-sensor approach, with higher temporal and spatial resolution. The recent launch of the Sentinel-1a mission, with a spatial resolution of 20 x 40 m in extra-wide swath mode and the upcoming RADARSAT constellation will not continue the C-band SAR operational applications but it will also increase the temporal frequency of observations and thus improve the detection accuracy of important lake ice events. Additionally, the future multi-spectral Sentinel-2a/b missions (planned for launch in 2015 and 2016, respectively) will provide high-resolution (10-20 m in the visible band) data that will increase the sampling density at northern latitudes – every 1-2 days in cloud-free conditions. Moreover, future missions such as Surface Water and Ocean Topography (SWOT) will enable accurate monitoring of water levels and thus contributing to a better understanding of lake conditions prior to freezing. Future work needs to continue the monitoring record of the lakes investigated in this research but also needs to document lake ice changes for a large number of lakes across the Arctic.

Regarding monitoring lake ice phonological events at the beginning of the ice season, freeze-up detection could benefit from the polarimetric observations of RADARSAT-2 that provide many additional parameters (Geldsetzer and van der Sanden, 2013).

With respect to image segmentation, automated labelling of MAGIC would greatly improve the segmentation process and would constitute a step forward toward development of an operational product.

Finally, assessment of changes in lake ice conditions would benefit from a greater availability of local weather data. Limited by substantial costs, installation of automated inland weather stations or buoys on lakes would provide at the very least accurate local air/water temperature.

References

ACIA. (2005). Impacts of a Warming arctic: arctic climate impact. *Cambridge University Press, New York*, 1042.

Adams, W. P. (1976). A classification of freshwater ice. *Musk-Ox, 18*, 99-102.

Adams, W. P., Doran, P. T., Ecclestone, M., Kingsbury, C. M., & Allan, C. J. (1989). A rare second year - lake ice cover in the Canadian High Arctic. *Arctic,* (42), 299-306.

Adams, W. P., & Prowse, T. D. (1981). Evolution and magnitude of spatial patterns in the winter cover of temperate lakes. *Fennia, 159*(2), 343-359.

Aiken, S. G., Dallwitz, M. G., Consaul, L. L., Mcjannet, C. L., Boles, R. L., Argus, G. W., Harris, J. G. (1999). Flora of the Canadian Arctic Archipelago: Descriptions, illustrations, identification, and information retrieval. Version:1, October 2005. http://www.mun.ca/biology/delta/arcticf/.

AMAP. (2011). *Snow, water, ice and permafrost in the arctic (SWIPA) 2011*. Oslo: Arctic Monitoring and Assessment Programme (AMAP).

Arp, C. D., Jones, B. M., & Grosse, G. (2013). Recent lake ice-out phenology within and among lake districts of Alaska, U.S.A. *Limnology and Oceanography, 58*(6), 2013-2028. doi: 10.4319/lo.2013.58.6.2013

Arp, C. D., Jones, B. M., Lu, Z., & Whitman, M. S. (2012). Shifting balance of thermokarst lake ice regimes across the Arctic Coastal Plain of Northern Alaska. *Geophysical Research Letters, 39*(L16503).

Arp, C. D., Jones, B. M., Urban, F. E. & Grosse, G. (2011). Hydrogeomorphic processes of thermokarst lakes with grounded-ice and floating-ice regimes on the Arctic coastal plain, Alaska. *Hydrological Processes, 25*(15), 2422-2438. doi: 10.1002/hyp.8019

Assel, R., Cronk, K., & Norton, D. (2003). Recent trends in Laurentian Great Lakes ice cover. *Climatic Change, 57*(1-2), 185-204.

Assel, R. A., & Robertson, D. M. (1995). Changes in winter air temperatures near Lake Michigan, 1851–1993, as determined from regional lake-ice records. *Limnology and Oceanography, 40*, 165-176. doi: 10.4319/lo.1995.40.1.0165

Belzile, C., Vincent, W. F., Gibson, J. A. E., & Van Hove, P. (2001). Bio-optical characteristics of the snow, ice, and water column of a perennially ice-covered lake in the High Arctic. *Canadian Journal of Fisheries and Aquatic Sciences, 58*(12), 2405-2418.

Bengtsson, L. (1986). Spatial variability of lake ice covers (Sweden). *Geografiska Annaler, Series A, 68 A*(1-2), 113-121.

Benson, B. J., Magnuson, J. J., Jacob, R. L., & Fuenger, S. L. (2000). Response of lake ice break-up in the Northern Hemisphere to the 1976 interdecadal shift in the North Pacific. *Verhandlungen Des Internationalen Verein Limnologie, Ver. 27*, 2770-2774.

Benson, B. J., Magnuson, J. J., Jensen, J. J., Card, O. P., Hodgkins, G., Korhonen, J., & Granin, N. G. (2011). Extreme events, trends, and variability in Northern Hemisphere lake-ice phenology (1855-2005). *Climatic Change,* 1-25.

Bhatt, U. S., Walker, D. A., Raynolds, M. K., Comiso, J. C., Epstein, H. E., Jia, G., Webber, P. J. (2010). Circumpolar Arctic tundra vegetation change is linked to sea ice decline. *Earth Interactions, 14*(8).

Bhatt, U. S., Walker, D. A., Walsh, J. E., Carmack, E. C., Frey, K. E., Meier, W. N., Moore, S. E., Parmentier, F. – J. W., Post, E., Romanovsky, V. E., and Simpson, W. R. (2014). Implications of Arctic sea ice decline for the Earth system. *Annu. Rev. Environ. Resour*., 39, 57-89. doi: 10.1146/annurev-environ-122012-094357

Bilello, M. A. (1980). Maximum thickness and subsequent decay of lake, river and fast sea ice in Canada and Alaska. *Cold Regions Research and Engineering Laboratory Report, 80*(6).

Bliss, L. C. (1977). Introduction. In: Truelove lowland, Devon Island, Canada: A High Arctic ecosystem. *Edmonton: University of Alberta Press,* 1-12.

Bolsenga, S. J. (1969). Total albedo of Great Lakes. *Water Resources Research, 5*(5), 1132-1133.

Bolsenga, S. J. (1977). Preliminary observations on the daily variation of ice albedo. *Journal of Glaciology, 18*(80), 517-521.

Bonsal, B. R., & Prowse, T. D. (2003). Trends and variability in spring and autumn 0°C-isotherm dates over Canada. *Climatic Change, 57*(3), 341-358.

Bonsal, B. R., Prowse, T. D., Duguay, C. R., & Lacroix, M. P. (2006). Impacts of large-scale teleconnections on freshwater-ice break/freeze-up dates over Canada. *Journal of Hydrology, 330*(1-2), 340-353.

Bowling, L. C., Kane, D. L., Gieck, R. E., Hinzman, L. D., & Lettenmaier, D. P. (2003). The role of surface storage in a low-gradient Arctic watershed. *Water Resources Research, 39*(4), SWC21-SWC213.

Brown, L. C. (2012). Modelling lake ice cover under contemporary and future climate conditions. *Doctoral Thesis, University of Waterloo*.

Brown, L. C., & Duguay, C. R. (2010). The response and role of ice cover in lake-climate interactions. *Progress in Physical Geography, 34*(5), 671-704.

Brown, L. C., & Duguay, C. R. (2011). A comparison of simulated and measured lake ice thickness using a shallow water ice profiler. *Hydrological Processes, 25*(19), 2932-2941.

Brown, L. C., & Duguay, C. R. (2011). The fate of lake ice in the North American Arctic. *The Cryosphere, 5*, 869-892. doi: 10.5194/tc-5-869-2011

Brown, R., Derksen, C., & Wang, L. (2007). Assessment of spring snow cover duration variability over northern Canada from satellite datasets. *Remote Sensing of Environment, 111*(2-3), 367-381.

Brown, R., Derksen, C., & Wang, L. (2010). A multi-data set analysis of variability and change in Arctic spring snow cover extent, 1967-2008. *Journal of Geophysical Research D: Atmospheres, 115*(16).

Callaghan, T. V., Johansson, M., Prowse, T., Olsen, M. S., & Reiersen, L. -. (2012). Arctic cryosphere: Changes and impacts. *Ambio, 40*(S1), 3-5. doi:10.1007/s13280-011-0210-0

Callaghan, T. V., Johansson, M., Brown, R. D., Groisman, P. Y., Labba, N., Radionov, V., Wood, E. F. (2011). Multiple effects of changes in Arctic snow cover. *Ambio, 40*(SUPPL. 1), 32-45.

Cheng, B., Vihma, T., Rontu, L., Kontu, A., Kheyrollah Pour, H., Duguay, C. R., & Pulliainen, J. (2014). Evolution of snow and ice temperature, thickness and energy

balance in Lake Orajärvi, northern Finland. *Tellus Series A*: *Dynamic Meteorology and Oceanography, 66* (21564), http://dx.doi.org/10.3402/tellusa.v66.21564

Clausi, A., Qin, A. K., Chowdhury, M. S., Yu, P., & Maillard, P. (2010). MAGIC: Map-guided ice classification system. *Canadian Journal of Remote Sensing, 36*(SUPPL.), S13-S25.

Coakley, J. P., & Rust, B. R. (1968). Sedimentation in an Arctic lake. *Journal of Sedimentary Petrology, 38*, 1290-1300.

Comiso, J. C., Parkinson, C. L., Gersten, R., & Stock, L. (2008). Accelerated decline in the Arctic sea ice cover. *Geophysical Research Letters, 35*(1).

Cook, T. L., & Bradley, R. S. (2010). An analysis of past and future changes in the ice cover of two High-Arctic lakes based on synthetic aperture radar (SAR) and Landsat imagery. *Arctic, Antarctic, and Alpine Research, 42*(1), 9-18.

Courtin, G. M., & Labine, C. L. (1977). Microclimatological studies on Truelove Lowland . *In Bliss, L. C. (Ed.), Truelove Lowland, Devon Island, Canada: A High Arctic Ecosystem. University of Alberta Press, Edmonton,* 73-106.

Dee, D. P., Uppala, S. M., Simmons, A. J., Berrisford, P., Poli, P., Kobayashi, S., Vitart, F. (April 2011 A). The ERA-Interim reanalysis: Configuration and performance of the data assimilation system. *Quarterly Journal of the Royal Meteorological Society, 137*, 553-597.

Derksen, C., Smith, S. L., Sharp, M., Brown, L., Howell, S., Copland, L., Walker, A. (2012). Variability and change in the Canadian cryosphere. *Climatic Change, 115*(1), 59-88. doi: 10.1007/s10584-012-0470-0

Deser, C., Tomas, R., Alexander, M., & Lawrence, D. (2010). The seasonal atmospheric response to projected Arctic sea ice loss in the late twenty-first century. *Journal of Climate, 23*(2), 333-351.

Dickson, R. R., Osborn, T. J., Hurrell, J. W., Meincke, J., Blindheim, J., Adlandsvik, B., Maslowski, W. (2000). The Arctic Ocean response to the North Atlantic Oscillation. *Journal of Climate, 13*(15), 2671-2696.

Doran, P. T., McKay, C. P., Adams, W. P., English, M. C., Wharton Jr., R. A., & Meyer, M. A. (1996). Climate forcing and thermal feedback of residual lake-ice covers in the High Arctic. *Limnology and Oceanography, 41*(5), 839-848.

Dufresne, J. -., Foujols, M. -., - Denvil, S., Caubel, A., Marti, O., Aumont, O, B., Y., Viovy, N. (2013). Climate change projections using the IPSL-CM5 Earth system model: From CMIP3 to CMIP5. *Climate Dynamics, 40*(9-10), 2123-2165.

Duguay, C., Brown, L., Kang, K. -., & Kheyrollah Pour, H. (2012). [The Arctic] Lake ice, in "State of the climate in 2011". *Bulletin of the American Meteorological Society, 93*(7), S152-S154.

Duguay, C., Brown, L., Kang, K. -., & Kheyrollah Pour, H. (2014). [The Arctic] Lake ice, in "State of the climate in 2013". *Bulletin of the American Meteorological Society, 95*(7), S138-S139.

Duguay, C. R., Flato,G. M., Jeffries, M. O., Ménard, P., Morris, K., & Rouse, W. R. (2003). Ice-cover variability on shallow lakes at high latitudes: Model simulations and observations. *Hydrological Processes, 17*, 3465-3483.

Duguay, C. R., & Lafleur, P. M. (2003). Determining depth and ice thickness of shallow subarctic lakes using spaceborne optical and SAR data. *International Journal of Remote Sensing, 24*(3), 475-489.

Duguay, C. R., Prowse, T. D., Bonsal, B. R., Brown, R. D., Lacroix, M. P., & Ménard, P. (2006). Recent trends in Canadian lake ice cover. *Hydrological Processes, 20*(4), 781-801.

Duguay, C. R., Pultz, T. J., Lafleur, P. M., & Drai, D. (2002). RADARSAT backscatter characteristics of ice growing on shallow sub-arctic lakes, Churchill, Manitoba, Canada. *Hydrological Processes, 16*(8), 1631-1644.

Duguay, C. R., Rouse, W. R., Lafleur, P. M., & Boudreau, L. D. (1999). Radiation balance of wetland tundra at northern treeline estimated from remotely sensed data. *Climate Research, 13*(1), 77-90.

Duguay, C. R., Soliman, A., Hachem, S., & Saunders, W. (2012). Circumpolar and regional land surface temperature (LST) with links to geotiff images and netCDF files. *University of Waterloo, Canada,* doi:10.1594/PANGAEA.775962. PANGAEA: Data Publisher for Earth & Environmental Science.

Edlund, S. A., & Alt, B. T. (1989). Regional congruence of vegetation and summer climate patterns in the Queen Elizabeth Islands, Northwest Territories, Canada. *Arctic, 42*, 3-23.

Eerola, K., Rontu, L., Kourzeneva, E., & Shcherbak, E. (2010). A study on effects of lake temperature and ice cover in HIRLAM. *Boreal Environment Research, 15*, 130-142.

Elachi, C., Bryan, M. L., & Weeks, W. F. (1976). Imaging radar observations of frozen Arctic lakes. *Remote Sensing of Environment, 5*(C), 169-175.

Engram, M., Anthony, K. W., Meyer, F. J., & Grosse, G. (2013). Characterization of L-band synthetic aperture radar (SAR) backscatter from floating and grounded lake ice in Arctic Alaska. *The Cryosphere, 7*, 1741-1752.

Environment Canada.National. (2011). Climate data and information archive. Retrieved from http://climate.weatheroffice.gc.ca/climate_normals.

Flato, G. M., & Brown, R. D. (1996). Variability and climate sensitivity of landfast Arctic sea ice. *Journal of Geophysical Research, 101*(C10), 25767-25777.

France, R. L. (1993). The Lake Hazen trough: A late winter oasis in a polar desert. *Biological Conservation, 63*, 149-151.

Freedman, B., Svoboda, J., & Henry, G. H. R. (1994). Alexandra Fiord: An ecological oasis in the polar desert. In: Svoboda, J., and Freedman, B., eds. Ecology of a polar oasis: Alexandra Fiord, Ellesmere Island, Canada. *Toronto: Captus University Publications*, 1-12.

Futter, M. N. (2003). Patterns and trends in southern Ontario lake ice phenology. *Environmental Monitoring and Assessment, 88*, 431-444.

Gao, S., & Stefan, H. G. (2004). Potential climate change effects on ice covers of five freshwater lakes. *Journal of Hydrologic Engineering, 9*(3), 226-234.

Geldsetzer, T., & Van Der Sanden, J. J. (2013). Identification of polarimetric and nonpolarimetric C-band SAR parameters for application in the monitoring of lake ice freeze-up. *Canadian Journal of Remote Sensing, 39*(3), 263-275.

Geldsetzer, T., Van Der Sanden, J., & Brisco, B. (2010). Monitoring lake ice during spring melt using RADARSAT-2 SAR. *Canadian Journal of Remote Sensing, 36*(SUPPL. 2), S391-S400.

Ghanbari, R. N., Bravo, H. R., Magnuson, J. J., Hyzer, W. G., & Benson, B. J. (2009). Coherence between lake ice cover, local climate and teleconnections (Lake Mendota, Wisconsin). *Journal of Hydrology, 374*(3-4), 282-293.

Grosswald, M. G., Hughes, T. J., & Lasca, N. P. (1999). Oriented lake-and-ridge assemblages of the Arctic coastal plains: Glacial landforms modified by thermokarst and solifluction. *Polar Record, 35*(194), 215-230.

Guirguis, K., Gershunov, A., Schwartz, R., & Bennett, S. (2011). Recent warm and cold daily winter temperature extremes in the Northern Hemisphere. *Geophysical Research Letters, 38*(17).

Hall, D. K. (1998). Remote sensing of snow and ice using imaging radar. In Henderson, F. M., and Lewis, A. J. (eds.). Principles and applications of imaging radar. *New York: John Wiley and Sons, Inc.,* 677-698.

Hall, D. K., Key, J. R., Casey, K. A., Riggs, G. A., & Cavalieri, D. J. (2004). Sea ice surface temperature product from MODIS. *IEEE Transactions on Geoscience and Remote Sensing, 42*(5), 1076-1087.

Hall, D. K., Fagre, D. B., Klasner, F., Linebaugh, G., & Liston, G. E. (1994). Analysis of ERS 1 synthetic aperture radar data of frozen lakes in northern Montana and implications for climate studies. *Journal of Geophysical Research, 99*(C11), 22,473-22,482.

Hartmann, B., & Wendler, G. (2005). The significance of the 1976 Pacific climate shift in the climatology of Alaska. *Journal of Climate, 18*(22), 4824-4839.

Hattersley-Smith, G. (1974). North of latitude eighty. *Defence Research Board.*

Heron, R., & Woo, M. -. (1994). Decay of a high Arctic lake-ice cover: Observations and modelling. *Journal of Glaciology, 40*(135), 283-292.

Hinkel, K. M., Jones, B. M., Eisner, W. R., Cuomo, C. J., Beck, R. A., & Frohn, R. C. (2007). Methods to assess natural and anthropogenic thaw lake drainage on the western Arctic Coastal Plain of northern Alaska. *Journal of Geophysical Research, 112*(F02S16) doi: 10.1029/2006JF000584

Hinkel, K. M., Nelson, F. E., Klene, A. F., & Bell, J. H. (2003). The urban heat island in winter at Barrow, Alaska. *International Journal of Climatology, 23*, 1889-1905.

Hinkel, K. M., Frohn, R. C., Nelson, F. E., Eisner, W. R., & Beck, R. A. (2005). Morphometric and spatial analysis of thaw lakes and drained thaw lake basins in the western Arctic Coastal Plain, Alaska. *Permafrost and Periglacial Processes, 16*(4), 327-341.

Hinkel, K. M., Zheng, L., Yongwei, S., & Evan, A. (2012). Regional lake ice meltout patterns near Barrow, Alaska. *Polar Geography, 35*, 1-18.

Hodgkins, G. A., James, I. C., & Huntington, T. G. (2002). Historical changes in lake ice-out dates as indicators of climate change in New England, 1850-2000. *International Journal of Climatology, 22*(15), 1819-1827.

Hostetler, S. W., Bates, G. T., & Giorgi, F. (1993). Interactive coupling of a lake thermal model with a regional climate model. *Journal of Geophysical Research, 98*(D3), 5045-5052.

Howell, S. E. L., Brown, L. C., Kang, K. -., & Duguay, C. R. (2009). Variability in ice phenology on Great Bear Lake and Great Slave Lake, Northwest Territories, Canada, from SeaWinds/QuikSCAT: 2000-2006. *Remote Sensing of Environment, 113*(4), 816-834.

Hurrell, J. W. (1996). Influence of variations in extra-tropical wintertime teleconnections on Northern Hemisphere temperature. *Geophysical Research Letters, 23*(6), 665-668.

IPCC. (2013). Climate change 2013: The physical science basis. Contribution of working group I to the fifth assessment report of the Intergovernmental Panel on Climate Change [stocker, T.F., D. Qin, G.-K. Plattner, M. Tignor, S.K. Allen, J. Boschung, A. Nauels, Y. Xia, V. Bex and P.M. Midgley (eds.)]. *Cambridge University Press, New York*, 1535 pp. doi: 10.1017/CBO9781107415324

IGOS. (2007). Integrated Global Observing Strategy Cryosphere Theme Report - For the Monitoring of our Environment from Space and from Earth. Geneva, *World Meteorological Organization*, WMO/TD-No. 1405, 100 pp.

Jeffries, M., Morris, K., & Liston, G. (1996). ERS-1 SAR monitoring of ice growth on shallow lakes to determine water depth and availability in N.W. Alaska. *European Space Agency, (Special Publication) ESA SP,* (391), 177-182.

Jeffries, M. O., & Krouse, H. R. (1985). Isotopic and chemical investigations of two stratified lakes in the Canadian Arctic. *Zeitschrift Für Gletscherkunde Und Glazialgeologie, 21*, 71-78.

Jeffries, M. O., & Morris, K. (2007). Some aspects of ice phenology on ponds in central Alaska, USA. *Annals of Glaciology, 46*, 397-403.

Jeffries, M. O., Morris, K., & Duguay, C. R. (1996). Lake ice and river ice. in satellite image atlas of glaciers of the world - review of the state of the Earth's cryosphere. edited by R.S. Williams, Jr. and J.G. Ferrigno . *U.S. Geological Survey Professional Paper,* 1386-A.

Jeffries, M. O., Morris, K., & Kozlenko, N. (2005). Ice characteristics and processes, and remote sensing of frozen rivers and lakes. In Duguay, C. R., and Pietroniro, A. (eds.), *Remote Sensing in Northern Hydrology: Measuring Environmental Change. Washington: American Geophysical Union,* 63-90.

Jeffries, M. O., Morris, K., & Liston, G. E. (1996). A method to determine lake depth and water availability on the North Slope of Alaska with spaceborne imaging radar and numerical ice growth modelling. *Arctic, 49*(4), 367-374.

Jeffries, M. O., Morris, K., Weeks, W. F., & Wakabayashi, H. (1994). Structural and stratigraphic features and ERS 1 synthetic aperture radar backscatter characteristics of ice growing on shallow lakes in NW Alaska, winter 1991-1992. *Journal of Geophysical Research, 99*(C11), 22,459-22,471.

Jeffries, M. O., Morris, K., Weeks, W. F., & Wakabayashi, H. (1994). Structural and stratigraphic features and ERS 1 synthetic aperture radar backscatter characteristics of ice growing on shallow lakes in NW Alaska, winter 1991-1992. *Journal of Geophysical Research, 99*(C11), 22459-22471.

Jeffries, M. O., Zhang, T., Frey, K., & Kozlenko, N. (1999). Estimating late-winter heat flow to the atmosphere from the lake-dominated Alaskan North Slope. *Journal of Glaciology, 45*(150), 315-324.

Jensen, O. P., Benson, B. J., Magnuson, J. J., Card, V. M., Futter, M. N., & Soranno, P. A. (2007). Spatial analysis of ice phenology trends across the Laurentian Great Lakes region during a recent warming period. *Limnology and Oceanography, 52*, 2013-2026.

Jones, B. M., Grosse, G., Arp, C. D., Jones, M. C., Walter, A. K. M., & Romanovsky, V. E. (2011). Modern thermokarst lake dynamics in the continuous permafrost zone, northern Seward Peninsula. *Journal of Geophysical Research, 16*(G00M03).

Jones, B. M., Gusmeroli, M. A., Arp, C. D., Strozzi, T., Grosse, G., Gaglioti, B. V., & Whitman, B. S. (2013). Classification of freshwater ice conditions on the Alaskan Arctic Coastal Plain using ground penetrating radar and TSX satellite data. *International Journal of Remote Sensing, 34*, 8253-8265.

Jones, B. M., Arp, C. D., Hinkel, K. M., Beck, R. A., Schmutz, J. A., & Winston, B. (2009). Arctic lake physical processes and regimes with implications for winter water availability and management in the National Petroleum Reserve Alaska. *Environmental Management, 43*(6), 1071-1084.

Karlsson, J. M., Bring, A., Peterson, G. D., Gordon, L. J., & Destouni, G. (2011). Opportunities and limitations to detect climate-related regime shifts in inland Arctic ecosystems through eco-hydrological monitoring. *Environmental Research Letters, 6*(1).

Kaufman, D. S., Schneider, D. P., McKay, N. P., Ammann, C. M., Bradley, R. S., Briffa, K. R., Thomas, E. (2009). Recent warming reverses long-term Arctic cooling. *Science, 325*(5945), 1236-1239.

Keatley, B. E., Douglas, M. S. V., & Smol, J. P. (2007). Limnological characteristics of a High Arctic oasis and comparisons across Northern Ellesmere Island. *Arctic, 60*(3), 294-308.

Keatley, B. E., Douglas, M. S. V., & Smol, J. P. (2008). Prolonged ice cover dampens diatom community responses to recent climatic change in High Arctic lakes. *Arctic, Antarctic, and Alpine Research, 40*(2), 364-372.

Kheyrollah Pour, H., Duguay, C. R., Martynov, A., & Brown, L. C. (2012). Simulation of surface temperature and ice cover of large northern lakes with 1-D models: A comparison with MODIS satellite data and in-situ measurements. *Tellus A, 64*(17614) doi: 10.3402/tellusa.v64i0.17614

Kheyrollah Pour, H., Duguay, C. R., Solberg, R., & Rudjord, Ø. (2014). Impact of satellite-based lake surface observations on the initial state of HIRLAM. part I: Evaluation of remotely-sensed lake surface water temperature observations. *Tellus A, 66* doi: 10.3402/tellusa.v66.21534

Koenigk, T., Brodeau, L., Graversen, R. G., Karlsson, J., Svensson, G., Tjernström, M., & Willén, K. (2013). Arctic climate change in 21st century CMIP5 simulations with EC-earth. *Climate Dynamics, 40*, 2719-2743.

Korhonen, J. (2006). Long-term changes in like ice cover in Finland. *Nordic Hydrology, 37*(4-5), 347-363.

Labrecque, S., Lacelle, D., Duguay, C. R., Lauriol, B., & Hawkings, J. (2009). Contemporary (1951-2001) evolution of lakes in the Old Crow basin, northern Yukon, Canada: Remote sensing, numerical modeling, and stable isotope analysis. *Arctic, 62*(2), 225-238.

Latifovic, R., & Pouliot, D. (2007). Analysis of climate change impacts on lake ice phenology in Canada using the historical satellite data record. *Remote Sensing of Environment, 106*(4), 492-507.

Leconte, R., & Klassen, P. D. (1991). Lake and river ice investigations in northern Manitoba using airborne SAR imagery. *Arctic, 44*(Suppl. 1), 153-163.

Lee, J. -. (1980). Digital image enhancement and noise filtering by use of local statistics. *IEEE Transactions on Pattern Analysis and Machine Intelligence, 2*(2), 165-168. doi: 10.1109/TPAMI.1980.4766994

Lenormand, F., Duguay, C. R., & Gauthier, R. (2002). Development of a historical ice database for the study of climate change in Canada. *Hydrological Processes, 16*(18), 3707-3722.

Li, S., Jeffries, M., & Morris, K. (2000). Mapping the bathymetry of shallow tundra lakes using INSAR techniques. *International Geoscience and Remote Sensing Symposium (IGARSS), 5* 2230-2232.

Ling, F., & Zhang, T. (2003). Numerical simulation of permafrost thermal regime and talik development under shallow thaw lakes on the Alaskan Arctic Coastal Plain. *Journal of Geophysical Research, 108*(D16, 27) doi: 10.1029/2002JD003014

Liston, G. E., & Hall, D. K. (1995). An energy-balance model of lake-ice evolution. *Journal of Glaciology, 41*(138), 373-382.

Liston, G. E., & Sturm, M. (2002). Winter precipitation patterns in Arctic Alaska determined from a blowing-snow model and snow-depth observations. *Journal of Hydrometeorology, 3*(6), 646-659.

Livingstone, D. M. (1997). Break-up dates of alpine lakes as proxy data for local and regional mean surface air temperatures. *Climatic Change, 37*(2), 407-439.

Livingstone, D. M. (1999). Ice break-up on southern Lake Baikal and its relationship to local and regional air temperatures in Siberia and to the North Atlantic Oscillation. *Limnology and Oceanography, 44*(6), 1486-1497.

Magnuson, J. J., Robertson, D. M., Benson, B. J., Wynne, R. H., Livingstone, D. M., Arai, T., Vuglinski, V. S. (2000). Historical trends in lake and river ice cover in the Northern Hemisphere. *Science, 289*(5485), 1743-1746.

Martynov, A., Sushama, L., & Laprise, R. (2010). Simulation of temperate freezing lakes by one-dimensional lake models: performance assessment for interactive coupling with regional climate models. *Boreal Environment Research, 15*, 143-164.

Mellor, J. (1982). Bathymetry of Alaskan Arctic lakes: A key to resource inventory with remote sensing methods. *Ph.D. Thesis, Institute of Marine Science, University of Alaska.*

Ménard, P., Duguay, C. R., Flato, G. M., & Rouse, W. R. (2002). Simulation of ice phenology on Great Slave Lake, Northwest Territories, Canada. *Hydrological Processes, 16*(18), 3691-3706.

Mendez, J., Hinzman, L. D., & Kane, D. L. (1998). Evapo-transpiration from a wetland complex on the Arctic Coastal Plain of Alaska. *Nordic Hydrology, 29*, 303-330.

Mishra, V., Cherkauer, K. A., Bowling, L. C., & Huber, M. (2011). Lake ice phenology of small lakes: Impacts of climate variability in the Great Lakes region. *Global and Planetary Change, 76*(3-4), 166-185.

Morris, K., Jeffries, M., & Duguay, C. (2005). Model simulation of the effects of climate variability and change on lake ice in central Alaska, USA. *Annals of Glaciology, 40*, 113-118.

Morris, K., Jeffries, M. O., & Weeks, W. F. (1995). Ice processes and growth history on Arctic and sub-arctic lakes using ERS-1 SAR data. *Polar Record, 31*(177), 115-128.

Mueller, D. R., Van Hove, P., Antoniades, D., Jeffries, M. O., & Vincent, W. F. (2009). High arctic lakes as sentinel ecosystems: Cascading regime shifts in climate, ice cover, and mixing. *Limnology and Oceanography, 54*(6, Part 2), 2371-2385.

Nakamura, N., & Oort, A. H. (1988). Atmospheric heat budgets of the polar regions. *Journal of Geophysical Research, 93*(D8), 9510-9524.

National Snow and Ice Data Center. (2011). Average Arctic sea ice extent for September. retrieved from http://nsidc.org/arcticseaicenews.

Nghiem, S. V., & Leshkevich, G. A. (2007). Satellite SAR remote sensing of Great Lakes ice cover, part 1. Ice backscatter signatures at C-band. *Journal of Great Lakes Research, 33*, 722-735. doi: 10.3394/ 0380-1330(2007)33[722:SSRSOG]2.0.CO;2

Noguchi, K., Gel, Y. R., & Duguay, C. R. (2011). Bootstrap-based test for trends in hydrological times series, with application to ice phenology data. *Journal of Hydrology, 410*(3-4), 150-161.

Ochilov, S., Svacina, N. A., Duguay, C. R., & Clausi, D. A. (2010). Towards an automated lake ice monitoring system for SAR imagery. *American Geophysical Union,* abstract #C51A-0474.

Overland, J. E., Spillane, M. C., Percival, D. B., Wang, M., & Mofjeld, H. O. (2004). Seasonal and regional variation of pan-arctic surface air temperature over the instrumental record. *Journal of Climate, 17*, 3263-3282.

Overland, J. E., Wang, M., & Bond, N. A. (2002). Recent temperature changes in the western Arctic during spring. *Journal of Climate, 15*, 1702-1716.

Overland, J. E., Wang, M., Walsh, J. E., Christensen, J. H., Kattsov, V. M., & Chapman, W. L. (2011). Chapter 3: Climate model projections for the Arctic, *Snow, Water, Ice and Permafrost in the Arctic (SWIPA), Oslo, Arctic Monitoring and Assessment Programme (AMAP)*.

Overland, J. E., & Wang, M. Y. (2010). Large-scale atmospheric circulation changes are associated with the recent loss of Arctic sea ice. *Tellus, Series A, 62*, 1-9.

Overland, J. E., Adams, J. M., & Bond, N. A. (1997). Regional variation of winter temperatures in the Arctic. *Journal of Climate, 10*(5), 821-837.

Palecki, M. A., & Barry, R. G. (1986). Freeze-up and break-up of lakes as an index of temperature changes during the transition seasons: A case study for Finland. *Journal of Climate & Applied Meteorology, 25*(7), 893-902.

Paul, C. A., Douglas, M. S. V., & Smol, J. P. (2010). Diatom-inferred holocene climatic and environmental changes in an unusually subsaline High Arctic Nunatak pond on Ellesmere Island (Nunavut, Canada). *Journal of Paleolimnology, 44*(4), 913-929.

Perren, B. B., Bradley, R. S., & Francus, P. (2003). Rapid lacustrine response to recent High Arctic warming: A diatom record from Sawtooth Lake, Ellesmere Island, Nunavut. *Arctic, Antarctic, and Alpine Research, 35*(3), 271-278.

Petoukhov, V., & Semenov, V. A. (2010). A link between reduced Barents-Kara sea ice and cold winter extremes over northern continents. *Journal of Geophysical Research D: Atmospheres, 115*(21).

Prowse, T., Alfredsen, K., Beltaos, S., Bonsai, B. R., Bowden, W. B., Duguay, C. R., Weyhenmeyer, G. A. (2011). Effects of changes in Arctic lake and river ice. *Ambio, 40*(Suppl. 1), 63-74. doi: 10.1007/s13280-011-0217-6

Prowse, T. D., Furgal, C., Melling, H., & Smith, S. L. (2009). Implications of climate change for northern Canada: The physical environment. *Ambio, 38*(5), 266-271.

Prowse, T. D. (2009). Introduction: Hydrologic effects of a shrinking cryosphere. *Hydrological Processes, 23*(1), 1-6.

Radionov , V. F., Aleksandrov, E. I., Bayborodova, V. R., Bryazgin, N. N., & Dement'ev, A. A. (2004). Long-term changes of snow cover period in the Arctic. *Data of Glaciological Studies, 97*, 136-142, (in Russian with English summary).

Reed, B., Budde, M., Spencer, P., & Miller, A. E. (2009). Integration of MODIS-derived metrics to assess interannual variability in snowpack, lake ice, and NDVI in southwest Alaska. *Remote Sensing of Environment, 113*(7), 1443-1452.

Riordan, B., Verbyla, D., & McGuire, A. D. (2006). Shrinking ponds in subarctic Alaska based on 1950-2002 remotely sensed images. *Journal of Geophysical Research G: Biogeosciences, 111*(4) doi: 10.1029/2005JG000150

Robertson, D. M., Ragotzkie, R. A., & Magnuson, J. J. (1992). Lake ice records used to detect historical and future climatic changes. *Climatic Change, 21*(4), 407-427.

Romanovsky, V. E., Smith, S. L., & Christiansen, H. H. (2010). Permafrost thermal state in the polar Northern Hemisphere during the international polar year 2007-2009: A synthesis. *Permafrost and Periglacial Processes, 21*(2), 106-116.

Rouse, W. R., Blanken, P. D., Bussières, N., Oswald, C. J., Schertzer, W. M., Spence, C., & Walker, A. E. (2008). An investigation of the thermal and energy balance regimes of Great Slave and Great Bear Lakes. *Journal of Hydrometeorology, 9*(6), 1318-1333.

Rovansek, R. J., Hinzman, L. D., & Kane, D. L. (1996). Hydrology of a tundra wetland complex in the Alaskan Arctic Coastal Plain, U.S.A. *Arctic and Alpine Research, 28*, 311-317.

Rowland, J. C., Jones, C. E., Altmann, G., Bryan, R., Crosby, B. T., Geernaert, G. L., Wilson, C. J. (2010). Arctic landscapes in transition: Responses to thawing permafrost. *Eos, 91*(26), 229-230.

Ruhland, K., Patterson, A. M., & Smol, J. P. (2008). Hemispheric-scale patterns of climate-related shifts in planktonic diatoms from North American and European lakes. *Global Change Biology, 14*, 1-15.

Schindler, D. W., Beaty, K. G., Fee, E. J., Cruikshank, D. R., DeBruyn, E. R., Findlay, D. L., Turner, M. A. (1990). Effects of climatic warming on lakes of the central boreal forest. *Science, 250*(4983), 967-970.

Schindler, D. W., & Smol, J. P. (2006). Cumulative effects of climate warming and other human activities on freshwaters of Arctic and subarctic North America. *Ambio, 35*(4), 160-168.

Screen, J. A., & Simmonds, I. (2010). The central role of diminishing sea ice in recent Arctic temperature amplification. *Nature, 464*(7293), 1334-1337.

Sellmann, P. V., Brown, J., Lewellen, H., McKim, H., & Merry, C. (1975). The classification and geomorphic implications of thaw lakes found in Arctic Alaska. *U.S. Cold Regions Research and Engineering Laboratory, Research Report 344*.

Sellmann, P. V., Weeks, W. F., & Campbell, W. J. (1975). Use of side-looking airborne radar to determine lake depth on the Alaskan North Slope. *CRREL Special Report (US Army Cold Regions Research and Engineering Laboratory),* (230).

Sen, P. K. (1968). Estimates of the regression coefficient based on Kandall's tau. *Journal of American Statistical Association, 63*, 1379-1389.

Serreze, M. C., Walsh, J. E., Chapin III, F. S., Osterkamp, T., Dyurgerov, M., Romanovsky, V., Barry, R. G. (2000). Observational evidence of recent change in the northern high-latitude environment. *Climatic Change, 46*, 159-207.

Serreze, M. C., Barrett, A. P., & Cassano, J. J. (2011). Circulation and surface controls on the lower tropospheric air temperature field of the Arctic. *Journal of Geophysical Research D: Atmospheres, 116*(7).

Serreze, M. C., Barrett, A. P., Stroeve, J. C., Kindig, D. N., & Holland, M. M. (2009). The emergence of surface-based Arctic amplification. *Cryosphere, 3*(1), 11-19.

Serreze, M. C., & Barry, R. G. (2011). Processes and impacts of Arctic amplification: A research synthesis. *Global and Planetary Change, 77*(1-2), 85-96.

Serreze, M. C., Holland, M. M., & Stroeve, J. (2007). Perspectives on the Arctic's shrinking sea-ice cover. *Science, 315*(5818), 1533-1536.

Serreze, M. C. (2005). In Barry R. G. (Ed.), *The arctic climate system*. Cambridge, UK; New York: Cambridge University Press.

Sharp, M., Burgess, D. O., Cogley, J. G., Ecclestone, M., Labine, C., & Wolken, G. J. (2011). Extreme melt on Canada's Arctic ice caps in the 21st century. *Geophysical Research Letters, 38*(LI1501) doi: 10.1029/2011GL047381

Smith, L. C., Sheng, Y., MacDonald, G. M., & Hinzman, L. D. (2005). Disappearing Arctic lakes. *Science, 308*(1429).

Smith, S. L., Burgess, M. M., Riseborough, D., & Nixon, F. M. (2005). Recent trends from Canadian permafrost thermal monitoring network sites. *Permafrost and Periglacial Processes, 16*(1), 19-30.

Smith, S. L., Romanovsky, V. E., Lewkowicz, A. G., Burn, C. R., Allard, M., Clow, G. D., Throop, J. (2010). Thermal state of permafrost in North America: A contribution to the international polar year. *Permafrost and Periglacial Processes, 21*(2), 117-135.

Smol, J. P., & Douglas, M. S. V. (2007). Crossing the final ecological threshold in High Arctic ponds. *Proceedings of the National Academy of Sciences of the United States of America, 104*(30), 12395-12397.

Smol, J. P., Wolfe, A. P., Birks, H. J. B., Douglas, M. S. V., Jones, V. J., Korhola, A., Weckström, J. (2005). Climate-driven regime shifts in the biological communities of Arctic lakes. *Proceedings of the National Academy of Sciences of the United States of America, 102*(12), 4397-4402.

Sobiech, J., & Dierking, W. (2013). Observing lake- and river-ice decay with SAR: Advantages and limitations of the unsupervised K-means classification approach. *Annals of Glaciology, 54*(62) doi: 10.3189/2013AoG62A037

Soliman, A., Duguay, C. R., Saunders, W., & Hachem, S. (2012). Pan-arctic land surface temperature from MODIS and AATSR: Product development and inter-comparison. *Remote Sensing, 4*, 3833-3856. doi: 10.3390/rs4123833

Stephenson, S. R., Smith, L. C., & Agnew, J. A. (2011). Divergent longterm trajectories of human access to the arctic. *Nature Climate Change, 1*, 156-160. doi: 10.1038/NCLIMATE112

Stewart, K. A., Lamoureux, S. F., & Finney, B. P. (2008). Multiple ecological and hydrological changes recorded in varved sediments from Sanagak Lake, Nunavut, Canada. *Journal of Paleolimnology, 40*(1), 217-233.

Strey, S. T., Chapman, W. L., & Walsh, J. E. (2010). The 2007 sea ice minimum: Impacts on the Northern Hemisphere atmosphere in late autumn and early winter. *Journal of Geophysical Research D: Atmospheres, 115*(23).

Stroeve, J. C., Serreze, M. C., Holland, M. M., Kay, J. E., Malanik, J., & Barrett, A. P. (2011). The Arctic's rapidly shrinking sea ice cover: A research synthesis. *Climatic Change,* 1-23.

Sturm, M., Holmgren, J., König, M., & Morris, K. (1997). The thermal conductivity of seasonal snow. *Journal of Glaciology, 43*(143), 26-41.

Sturm, M., & Liston, G. E. (2003). The snow cover on lakes of the Arctic Coastal Plain of Alaska, U.S.A. *Journal of Glaciology, 49*(166), 370-380.

Surdu, C. M., Duguay, C. R., Brown, L. C., & Fernández Prieto, D. (2014). Response of ice cover on shallow lakes of the North Slope of Alaska to contemporary climate conditions (1950-2011): Radar remote sensing and numerical modeling data analysis. *The Cryosphere, 8*(1), 167-180.

Svoboda, J., & Freedman, B. (1981). Ecology of a High Arctic lowland oasis Alexandra fiord (78° 53' N, 75° 55' W), Ellesmere Island, NWT, Canada. *University of Toronto, Department of Botany, Toronto, Canada.*

Thomas, E. K., & Briner, J. P. (2009). Climate of the past millennium inferred from varved proglacial lake sediments on northeast Baffin Island, Arctic Canada. *Journal of Paleolimnology, 41*(1), 209-224.

Thompson, W. (1994). Climate. in: Resource description and analysis: Ellesmere island, National Park Reserve, chapter 5. *Winnipeg, Manitoba: National Resource Conservation Section, Prairie and Northern Region, Parks Canada, Department of Canadian Heritage,* 1-78.

Tisler, P., Vihma, T., Müller, G., & Brümmer, B. (2008). Modelling of warm-air advection over Arctic sea ice. *Tellus, 60A*, 775-788.

Tivy, A., Howell, S. E. L., Alt, B., McCourt, S., Chagnon, R., Crocker, G., & Yackel, J. J. (2011). Trends and variability in summer sea ice cover in the Canadian Arctic based on the Canadian Ice Service digital archive, 1960-2008 and 1968-2008. *Journal of Geophysical Research C: Oceans, 116*(3).

Todd, M. C., & Mackay, A. W. (2003). Large-scale climatic controls on Lake Baikal ice cover. *Journal of Climate, 16*(19), 3186-3199.

Tomkins, J. D., Lamoureux, S. F., Antoniades, D., & Vincent, W. F. (2009). Sedimentology of perennial ice-covered, meromictic lake A, Ellesmere Island, at the northern extreme of Canada. *Canadian Journal of Earth Sciences, 46*(2), 83-100.

Trenberth, K. E. (1990). Recent observed interdecadal climate changes in the Northern Hemisphere. *Bulletin - American Meteorological Society, 71*(7), 988-993.

Trenberth, K. E., & Hurell, J. W. (1994). Decadal atmosphere-ocean variations in the Pacific. *Climate Dynamics, 9*(6), 303-319.

Turner, J., Overland, J. E., & Walsh, J. E. (2007). An Arctic and Antarctic perspective on recent climate change. *International Journal of Climatology, 27*(3), 277-293.

U!aby, F. T., Moore, R. K., & Fung, A. K. (1986). Microwave Remote Sensing: Active and Passive, vol III, *Addison-Wesley-Longman Reading, Mass.*

Vavrus, S. J., Wynne, R. H., & Foley, J. A. (1996). Measuring the sensitivity of southern Wisconsin lake ice to climate variations and lake depth using a numerical model. *Limnology and Oceanography, 41*(5), 822-831.

Vincent, A. C., Mueller, D. R., & Vincent, W. F. (2008). Simulated heat storage in a perennially ice-covered High Arctic lake: Sensitivity to climate change. *Journal of Geophysical Research C: Oceans, 113*(4).

Walsh, S. E., Vavrus, S. J., Foley, J. A., Fisher, V. A., Wynne, R. H., & Lenters, J. D. (1998). Global patterns of lake ice phenology and climate: Model simulations and observations. *Journal of Geophysical Research D: Atmospheres, 103*(D22), 28825-28837.

Walter, K. M., Zimov, S. A., Chanton, J. P., Verbyla, D., & Chapin III, F. S. (2006). Methane bubbling from Siberian thaw lakes as a positive feedback to global warming. *Nature, 443*, 71-75.

Walter, K. M., Engram, M., Duguay, C. R., Jeffries, M. O., & Chapin III, F. S. (2008). The potential use of synthetic aperture radar for estimating methane ebullition from Arctic lakes. *Journal of the American Water Resources Association, 44*(2), 305-315.

Wang, J., Zhang, J., Watanabe, E., Ikeda, M., Mizobata, K., Walsh, J. E., Wu, B. (2009). Is the dipole anomaly a major driver to record lows in Arctic summer sea ice extent? *Geophysical Research Letters, 36*(5).

Watanabe, E., Wang, J., Sumi, A., & Hasumi, H. (2006). Arctic dipole anomaly and its contribution to sea ice export from the Arctic Ocean in the 20th century. *Geophysical Research Letters, 33*(23).

Weeks, W. F., Fountain, A. G., Bryan, M. L., & Elachi, C. (1978). Differences in radar returns from ice-covered North Slope lakes. *Journal of Geophysical Research, 83*, 4069-4073.

Weyhenmeyer, G. A., Livingstone, D. M., Meili, M., Jensen, O., Benson, B., & Magnuson, J. J. (2011). Large geographical differences in the sensitivity of ice-covered lakes and rivers in the northern hemisphere to temperature changes. *Global Change Biology, 17*(1), 268-275.

Weyhenmeyer, G. A., Meili, M., & Livingstone, D. M. (2004). Nonlinear temperature response of lake ice break-up. *Geophysical Research Letters, 31*(7), L07203 1-4.

White, D. M., Prokein, P., Chambers, M. K., Lilly, M. R., & Toniolo, H. (2008). Use of synthetic aperture radar for selecting Alaskan lakes for winter water use. *Journal of the American Water Resources Association, 44*(2), 276-284.

Williams, S. G., & Stefan, H. G. (2006). Modeling of lake ice characteristics in North America using climate, geography, and lake bathymetry. *Journal of Cold Regions Engineering, 20*(4), 140-167.

Williamson, C. E., Dodds, W., Kratz, T. K., & Palmer, M. A. (2008). Lakes and streams as sentinels of environmental change in terrestrial and atmospheric processes. *Frontiers in Ecology and the Environment, 6*(5), 247-254.

Woo, M. -., & Guan, X. J. (2006). Hydrological connectivity and seasonal storage change of tundra ponds in a polar oasis environment, Canadian High Arctic. *Permafrost and Periglacial Processes, 17*, 309-323.

Woo, M. -., & Young, K. L. (1996). Summer solar radiation in the Canadian High Arctic. *Arctic, 49*, 170-180.

Woo, M. -., & Young, K. L. (1997). Hydrology of a small drainage basin with polar oasis environment, Fosheim Peninsula, Ellesmere Island, Canada. *Permafrost and Periglacial Processes, 8*(3), 257-277.

Wu, B., Wang, J., & Walsh, J. E. (2006). Dipole anomaly in the winter Arctic atmosphere and its association with sea ice motion. *Journal of Climate, 19*(1), 210-225.

Young, K. L., & Woo, M. K. (2000). Hydrological response of a patchy High Arctic wetland. *Nordic Hydrology, 31*, 317-338.

Young, K. L., & Abnizova, A. (2011). Hydrologic thresholds of ponds in a polar desert wetland environment, Somerset Island, Nunavut, Canada. *Wetlands, 31*(3), 535-549. doi: 10.1007/s13157-011-0172.9

Yu, P., Clausi, D. A., & Qin, K. (2012). Unsupervised polarimetric SAR image segmentation and classification using region growing with edge penalty, *IEEE Transactions on Geoscience and Remote Sensing, 50*(4), 1302 – 1317. doi: 10.1109/TGRS.2011.2164085

Zhang, T., & Jeffries, M. O. (2000). Modeling interdecadal variations of lake ice thickness and sensitivity to climatic change in northernmost Alaska. *Annals of Glaciology, 31*, 339-347.

Zhang, X., Sorteberg, A., Zhang, J., Gerdes, R., & Comiso, J. C. (2008). Recent radical shifts of atmospheric circulations and rapid changes in Arctic climate system. *Geophysical Research Letters, 35*(22).